

AD-A070 183

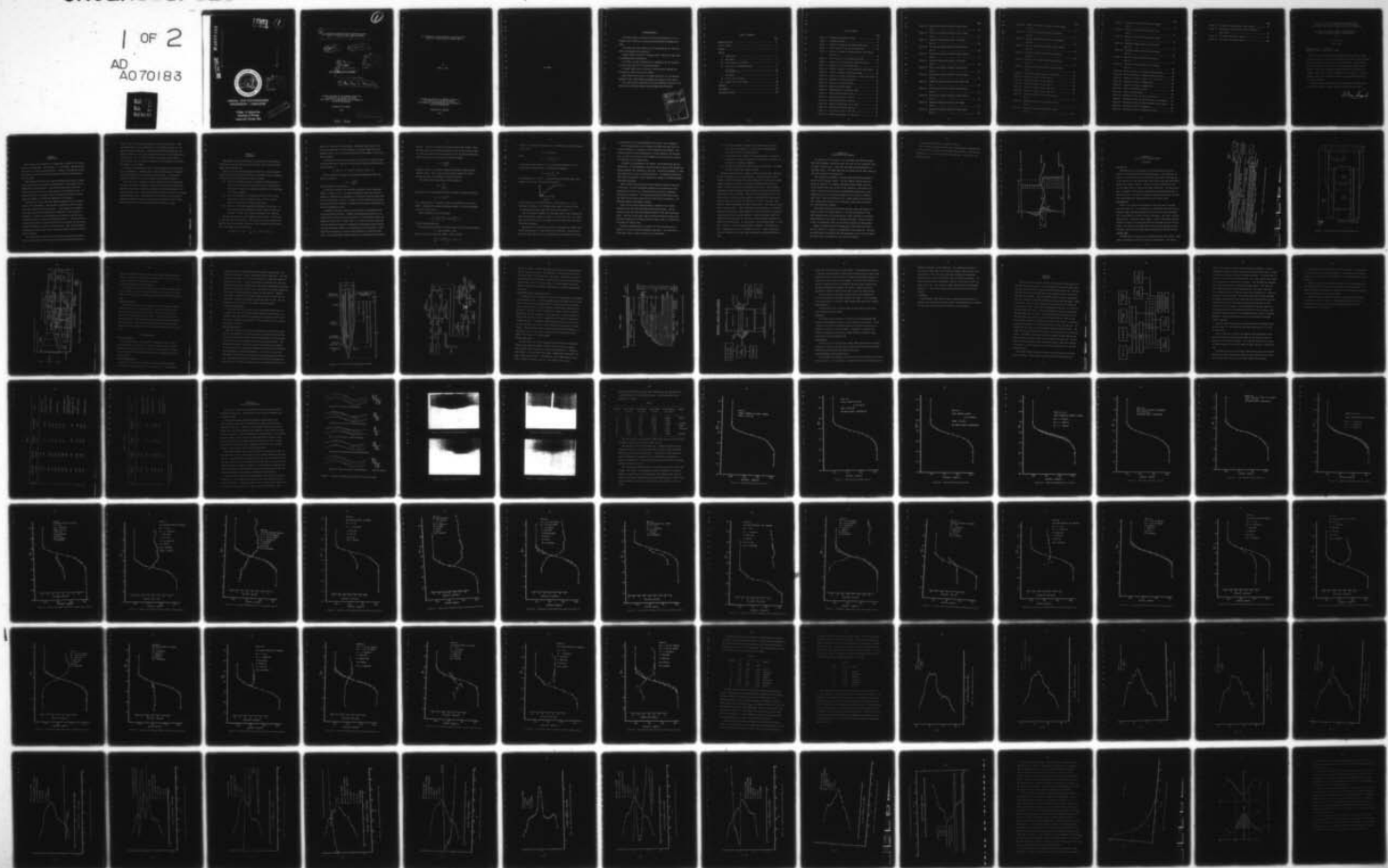
FLORIDA UNIV GAINESVILLE COASTAL AND OCEANOGRAPHIC --ETC F/6 8/10
AN EXPERIMENTAL INVESTIGATION OF INTERFACIAL WAVES GENERATED BY--ETC(U)
1975 I B CHOU N00014-68-A-0173

UNCLASSIFIED

NL

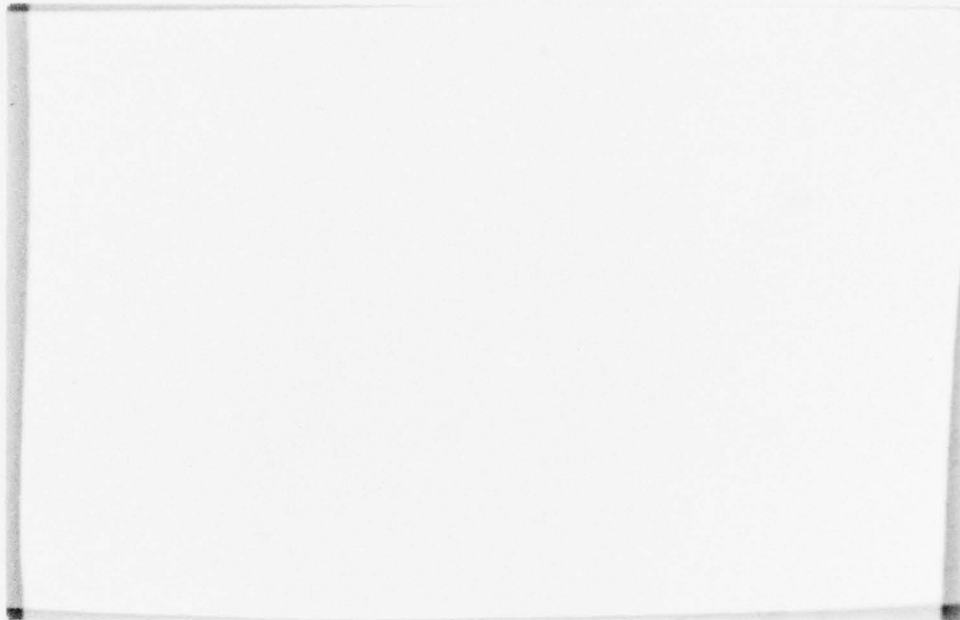
1 OF 2

AD
A070183

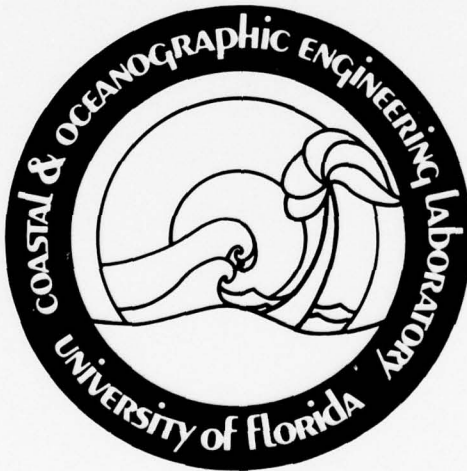


AD A070183

LEVEL



DDC FILE COPY



DDC
RECEIVED
JUN 15 1979
[Signature]

COASTAL AND OCEANOGRAPHIC
ENGINEERING LABORATORY

College of Engineering
University of Florida
Gainesville, Florida 32611

This document has been approved
for public release and sale; its
distribution is unlimited.

79 05 14 182

1

6 AN EXPERIMENTAL INVESTIGATION OF INTERFACIAL WAVES
GENERATED BY LOW FREQUENCY INTERNAL WAVES.

11 1975

12 116 p.

10 BY
IVAN B. CHOU

DDO
RECEIVED
JUN 15 1979
RECEIVED
C

15
Contract ~~NO0014-68-A-0173-0016~~

408 006

9 Master's thesis

A THESIS PRESENTED TO THE GRADUATE COUNCIL OF
THE UNIVERSITY OF FLORIDA IN PARTIAL
FULFILLMENT OF THE REQUIREMENTS FOR THE DEGREE OF
MASTER OF ENGINEERING

UNIVERSITY OF FLORIDA

1975

This document has been approved
for public release and sale; its
distribution is unlimited.

408 006

elt

AN EXPERIMENTAL INVESTIGATION OF INTERFACIAL WAVES
GENERATED BY LOW FREQUENCY INTERNAL WAVES

BY

IVAN B. CHOU

A THESIS PRESENTED TO THE GRADUATE COUNCIL OF
THE UNIVERSITY OF FLORIDA IN PARTIAL
FULFILLMENT OF THE REQUIREMENTS FOR THE DEGREE OF
MASTER OF ENGINEERING

UNIVERSITY OF FLORIDA

1975

to Penny

ACKNOWLEDGEMENTS

The author wishes to express his sincere gratitude to Dr. D. M. Sheppard for his patience, guidance and perseverance throughout this study.

The author also gives thanks to Dr. Yu-Hwa Wang and Dr. Fearn for their encouragement and consulting.

Special thanks are due Mr. Tomasello and Mr. Powell for their help in performing these experiments.

The author is deeply indebted to Dr. Doddington for the excellent circuit design used for the conductivity meter.

A special thanks goes to Ricardo A. Blue and Bruce Frendahl for drafting the figures used in this thesis.

Words cannot fully express the appreciation felt for the patience rendered by Mrs. Kathy Menezes throughout the typing of this thesis.

This work has been supported by the Fluid Mechanics Division of the Office of Naval Research under Contract N00014-68-A-0173-0016.

Accession For	
NTIS GEM&I	<input checked="" type="checkbox"/>
DDC TAB	<input type="checkbox"/>
Unannounced	<input type="checkbox"/>
Justification	<i>Added on file</i>
By	
Distribution/	
Availability Codes	
Dist	Avail and/or special
<i>A</i>	

TABLE OF CONTENTS

	Page
ACKNOWLEDGEMENTS	iv
LIST OF FIGURES	v
ABSTRACT	x
CHAPTER	
I. INTRODUCTION	1
II. BACKGROUND	3
III. DESCRIPTION OF THE PROBLEM	9
IV. FACILITIES AND INSTRUMENTATION	12
Facilities	12
Instrumentation	16
V. PROCEDURES	25
VI. RESULTS AND DISCUSSION	31
VII. ASPECTS FOR FUTURE STUDIES	88
APPENDIX	90
BIBLIOGRAPHY	101
BIOGRAPHICAL SKETCH	103

LIST OF FIGURES

	Page
Figure 1. Diagram of Wave Number Vector	6
Figure 2. Definition Sketch	11
Figure 3. Schematic Drawing of the Internal Wave Tank	13
Figure 4. Cross-section of the Internal Wave Tank	14
Figure 5. Schematic Drawing of the North End of the Internal Wave Tank	15
Figure 6. Cross-section of the Conductivity Probe	18
Figure 7. Circuit of the Conductivity Probe Electronics	19
Figure 8. Drawing of the Internal Wave Gage	21
Figure 9. Schematic Drawing of the Internal Wave Gage System .	22
Figure 10. Schematic Drawing of Measuring System	26
Figure 11. Sketch of Periodical Occurrence of Interfacial Waves	32
Figure 12. Formation of Interfacial Waves	33
Figure 13. Roll-up of Interfacial Waves	33
Figure 14. Trapped Interfacial Waves	34
Figure 15. Disappearance of Interfacial Waves	34
Figure 16. Initial Density Profile, Run #1	36
Figure 17. Final Density Profile, Run #5	37
Figure 18. Final Density Profile, Run #8	38
Figure 19. Comparison Among Runs #1, 5, and 8	39
Figure 20. Final Density Profile, Run #14	40
Figure 21. Final Density Profile, Run #19	41
Figure 22. Comparison Among Runs #9, 14 and 19	42

	Page
Figure 23. Density and Velocity Profiles at Wave Crest, Run #2	43
Figure 24. Density and Velocity Profiles at Wave Trough, Run #2	44
Figure 25. Comparison Between Wave Crest and Trough, Run #2	45
Figure 26. Density and Velocity Profiles at Wave Crest , Run #4	46
Figure 27. Density and Velocity Profiles at Wave Trough, Run #4	47
Figure 28. Comparison Between Wave Crest and Trough, Run #4	48
Figure 29. Density and Velocity Profiles at Wave Crest, Run #6	49
Figure 30. Density and Velocity Profiles at Wave Trough, Run #6	50
Figure 31. Comparison Between Wave Crest and Trough, Run #6	51
Figure 32. Density and Velocity Profiles at Wave Crest, Run #9	52
Figure 33. Density and Velocity Profiles at Wave Trough, Run #9	53
Figure 34. Comparison Between Wave Crest and Trough, Run #9	54
Figure 35. Density and Velocity Profiles at Wave Crest, Run #11	55

	Page
Figure 36. Density and Velocity Profiles at Wave Trough, Run #11	56
Figure 37. Comparison Between Wave Crest and Trough, Run #11	57
Figure 38. Density and Velocity Profiles at Wave Crest, Run #15	58
Figure 39. Density and Velocity Profiles at Wave Trough, Run #15	59
Figure 40. Comparison Between Wave Crest and Trough, Run #15	60
Figure 41. Density and Velocity Profile at Wave Crest, Run #17	61
Figure 42. Density and Velocity Profile at Wave Trough, Run #17	62
Figure 43. Comparison Between Wave Crest and Trough	63
Figure 44. Natural Frequency Profile, Run #1	66
Figure 45. Natural Frequency Profile, Run #5	67
Figure 46. Natural Frequency Profile, Run #8	68
Figure 47. Natural Frequency Profile, Run #14	69
Figure 48. Natural Frequency Profile, Run #19	70
Figure 49. Richardson Number Profile at Wave Crest, Run #2	71
Figure 50. Richardson Number Profile at Wave Trough, Run #2	72
Figure 51. Richardson Number Profile at Wave Crest, Run #4	73

	Page
Figure 52. Richardson Number Profile at Wave Trough, Run #4	74
Figure 53. Richardson Number Profile at Wave Crest, Run #6	75
Figure 54. Natural Frequency Profile at Wave Trough, Run #6	76
Figure 55. Richardson Number Profile at Wave Crest, Run #11	77
Figure 56. Richardson Number Profile at Wave Trough, Run #11	78
Figure 57. Natural Frequency Profile at Wave Crest, Run #15	79
Figure 58. Richardson Number Profile at Wave Trough, Run #15	80
Figure 59. Energy Transfer vs. Minimum Richardson Number	82
Figure 60. Definition Sketch of Trapped Interfacial Waves	83
Figure 61. Temperature Profiles, Runs # 1, 5, 14 and 19	85
Figure 62. Temperature Effect on Conductivity	86
Figure 63. Temperature Effect on Conductivity	87
Figure 64. Taylor and Goldstein's Model	90
Figure 65. Hazel's Numerical Model	91
Figure 66. Calibration Curve for Position Indicator	92
Figure 67. Calibration Curve for Hot-film Probe in Fresh Water ..	93
Figure 68. Calibration Curves for Hot-film Probe in Salt Water ..	94
Figure 69. Calibration Curve for Thermistor	95
Figure 70. Calibration Curve for Conductivity Probe	96

	Page
Figure 71. Pre-amplifier and Low-Pass Filter Circuit	97
Figure 72. Determination of Wave Height from X-Y Plotter Graph Paper	98
Figure 73. Visicorder Chart Paper, Run #4	99
Figure 74. Visicorder Chart Paper, Run #11	100

Abstract of Thesis Presented to the Graduate Council
of the University of Florida in Partial Fulfillment
of the Requirements for the Degree of Master of Engineering

AN EXPERIMENTAL INVESTIGATION OF INTERFACIAL WAVES
GENERATED BY LOW FREQUENCY INTERNAL WAVES

by

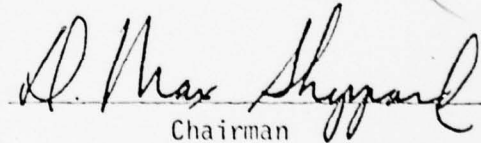
Ivan B. Chou

March, 1975

Chairman: Dr. D. M. Sheppard
Major Department: Engineering Sciences

ABSTRACT
In the density transition layer between salt and fresh water high frequency interfacial waves can be generated by the shear stresses created by finite amplitude internal waves at this interface. The conditions under which these waves occur are experimentally investigated in this thesis. Instantaneous Richardson number profiles at the crests and troughs of the finite amplitude internal waves were measured. The low frequency waves were mechanically generated by a hydraulically driven horizontal diaphragm.

The experiments were performed in an internal wave facility with a test section eighty feet long, four feet high and two feet wide.


Chairman

CHAPTER I INTRODUCTION

Mass density stratification in a fluid plays an essential role in the gravity wave phenomenon. As stated by C. S. Yih (1965), "wave motion can only exist in a stably stratified fluid". Indeed, a free surface is just an extreme case of density stratification with a density discontinuity at the surface.

From a physical point of view, the oscillatory wave motion is caused by the restoring force acting on a fluid particle as the particle is displaced from its mean position. The restoring force which causes the particle to seek its way to its mean position is the buoyancy force. So buoyancy forces are the primary forces associated with internal gravity waves that appear at the interface between two fluid layers.

Internal waves are a common and important phenomenon in the ocean as well as in the atmosphere. They can have a significant effect on both fixed and floating submarine structures. Internal waves are thought to be a major source for the production of turbulence in the oceans and atmosphere. Theoretical investigations have shown that internal waves can be generated by a number of difference mechanisms. Under certain conditions shear flows in a stratified fluid can be unstable, and the growth of this instability can result in internal waves. Once finite amplitude internal waves exist, they in turn can generate higher frequency internal waves as follows.

In internal wave motion the fluid particle velocity above the interface is in the opposite direction to the particle velocity below the in-

terface, thus a large velocity gradient occurs at the interface. This can provide the necessary conditions for a disturbance to grow, i.e. an unstable region in the flow. J. D. Woods (1973) observed such wave induced disturbances in the ocean and referred to them as wave-induced shear instabilities. This is similar to those observed by Thorpe (1969) in the laboratory, and the clear-air turbulence in the atmosphere identified by Gossard, et. al. (1970).

In previous experimental studies of the mixing due to internal waves, by D. M. Sheppard, T. Tomasello, and I. Chou, high frequency disturbances (or interfacial waves) were observed at the interface. The disturbed region was confined to a thin layer with clearly defined boundaries.

This shear flow is unsteady and the interfacial waves that have been observed are finite in amplitude. There has been very little theoretical work done on non-linear stability in general, and to the knowledge of the author, no theoretical investigation done on non-linear stability of unsteady stratified shear flows. The objective of this thesis is then to obtain information about the physical processes that take place in this complex flow using the results of the linear stability theory as a guide.

CHAPTER II BACKGROUND

Hydrodynamic stability has become a large branch of fluid dynamics. Stability of parallel flow of inviscid fluid was first studied by Helmholtz, Kelvin and Rayleigh.

There are several different modes of instability. Brooks Benjamin (1963) has classified unstable differences in flexible surfaces bounding inviscid flows into three different types as follows:

- (1). Class "A" instability results in Tollmien-Schlichting waves. The presence of this type instability causes a dissipation of energy of the system in an amount proportional to the amplitude of the waves squared.
- (2). Class "B" instability is identified with free surface waves. The presence of this instability causes a raise in energy level, as in the case of wind generated waves.
- (3). Class "C" is the well known Kelvin-Helmholtz instability. It is a consequence of conservative forces acting on a small disturbance. It leads to a violent breakdown at the interface.

The stability problem is most readily treated in terms of the theory of small amplitude perturbations. The linearized stability equation for parallel flows of homogeneous fluids was first derived by Orr and Sommerfeld. This equation can be written as

$$(u-c)(\phi'' - k^2\phi) - u''\phi = -\frac{i}{\alpha R} (\phi'''' - 2k^2\phi'' + k^4\phi),$$

where u is the primary flow velocity, c the complex wave speed, ϕ the cross-flow dependence of the disturbance, k the wave number and R the Reynolds number. The primes denote derivatives with respect to the cross-flow coordinate.

The linearized governing equation for the stability of inviscid, density stratified shear flows was first derived by Taylor and Goldstein and can be written as

$$\phi'' - [(u-c)^{-1} u'' + (u-c)^{-2} (u')^2 R_j + k^2] \phi = 0.$$

Here the stability parameter is the gradient Richardson number, R_j , which is defined as

$$R_j \equiv - \frac{\rho' g}{\rho (u')^2}.$$

The mass density is denoted by ρ .

A sufficient condition for stability according to Miles and Howard (1966), is that $R_j > 1/4$. It should be emphasized that this criterion applies to infinitesimal disturbances in a parallel stratified shear flow of an inviscid fluid. Woods, in a series of field investigations, found that transition from turbulent to laminar flow occurred at Richardson numbers of approximately unity.

A number of analytical studies have been made using hypothetical velocity and density profiles. Examples include Howard and Drazin's sinusoidal flow in which the velocity profile is a sine function; Taylor and Goldstein's shear layer in which there is a linear variation of velocity with the vertical coordinate; and Holmboe's discontinuous density profile in which the density profile is a step function at the interface. Hazel (1972) did some numerical studies of the stability of stratified shear flows. He used hyperbolic tangent functions for the density and velocity

profiles. The error function shear layer has also been studied. Most of these results are presented as neutral curves in the k - J plane, where k is the wave number of the disturbance and J is the overall Richardson number based on the total density and velocity changes

$$J = \frac{g(\Delta\rho/\rho)h}{(\Delta u)^2}$$

A neutral curve is a line which separates the stable region from the unstable region. Some of the results of these theoretical investigations are given in the appendix (Figures 64 and 65).

The gradient Richardson number can be written as

$$R_i = \frac{N^2}{\left(\frac{\partial u}{\partial z}\right)^2}$$

where N is the so called Brunt-Väisälä or buoyancy frequency defined by

$$N = \left(-\frac{g}{\rho} \frac{\partial \rho}{\partial z} \right)^{1/2}$$

This frequency plays an important role in the stability of stratified fluids. Note that the gradient Richardson number is a ratio of buoyancy forces to inertia forces.

Phillips (1969) derived the equation

$$\frac{\partial^2}{\partial t^2} \left(\frac{\partial^2 w}{\partial x^2} + \frac{\partial^2 w}{\partial z^2} \right) + N^2(z) \frac{\partial^2 w}{\partial z^2} = 0$$

from the momentum equations.

For small disturbances the vertical velocity w can be found by taking

$$w = W(z) \exp\{i(kx - nt)\}$$

where k is the horizontal wave number. Then it follows

$$\frac{d^2 W}{dz^2} + \left\{ \frac{N^2(z)}{n^2} - k^2 \right\} W = 0$$

If $n > N$, W is a monotonic function of z , the only modes are surface waves.

If $n < N$, then

$$W = \bar{w} \exp(imz)$$

where

$$m = k \left(\frac{N^2 - n^2}{n^2} \right)^{1/2}$$

is the vertical wave number. W is an oscillatory function of z , it corresponds to internal waves. From the above equation,

$$n = N \left(\frac{k^2}{k^2 + m^2} \right)^{1/2}.$$

The denominator $(k^2 + m^2)^{1/2}$ is the resultant of the wave number components in the x and z direction (see Figure 1).

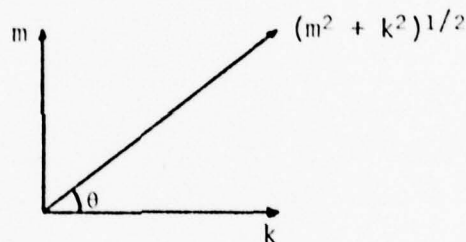


Figure 1

So the frequency of the internal wave $n = N \cos \theta$ where $|\theta| \leq 1/2 \pi$.

This shows that when $n < N$, internal waves travel at an angle θ from the horizontal direction, until they reach a level where $n = N$.

Thus the buoyancy frequency N is the upper limit of the frequency for which internal wave motions can exist in a stratified fluid. In a fluid with variable N , waves will be trapped within the layer where N exceeds the imposed frequency.

The passage of an internal wave along a sharp interface between stratified layers produces a vortex sheet at the interface. When the wave period is long compared to the time needed for any disturbance to grow,

an instability of the Kelvin-Helmholtz (K-H) type is to be expected.

If the energy supply to the internal wave mode continues after the critical minimum R_i is attained, a local instability may develop. The energy acquired by these disturbances is at the expense of the internal wave, so that the occurrence of an instability of this kind can restrict the amplitude of the internal wave.

In general the breakdown has two effects, one destabilizing and one stabilizing. If the breakdown is severe, mixing can occur which reduces the density gradient thus destabilizes the flow. The velocity gradient is likewise reduced but this has a stabilizing effect. It should be pointed out that stability parameter is more sensitive to changes in velocity gradient than density gradient.

Woods (1969) observed the same laminar-turbulent-laminar transition in the ocean. He also represented schematically the evolution of the spontaneous K-H billows in a thermocline sheet and their subsequent transition to turbulence. The density and velocity differences across the sheet did not change during the life time of the disturbances. The mechanism could be described as follows.

After the K-H billow formed and broke, turbulence in the sheet entrained water from above and below thickening the sheet. But the turbulent sheet died when the Richardson number of the sheet approached unity. Then the current shear above and below the sheet entrains water from the thickened but no longer turbulent sheet so that it slowly thins and reverts to laminar flow.

Yih-Ho Pao (1969) measured the spectra of internal waves and turbulence in a stably stratified atmosphere and ocean. He classified internal waves into 3 ranges according to the wave number.

- 1). At low wave numbers, buoyancy forces dominate over inertial forces and the disturbance is in the form of internal waves. Pao called this the internal subrange.
- 2). At intermediate wave number, the buoyancy effect is strong but inertial forces are also important and turbulence can exist. He called this the buoyancy subrange.
- 3). At high wave numbers the inertial forces are dominant. He called this the inertial and viscous subrange.

Although a great number of analytic studies have been made, few experimental investigations have been conducted. Scotti and Corcos (1971) created a stably stratified shear layer within the test section of a wind tunnel by merging two streams of air after uniformly heating the top stream. The two streams were accelerated side by side. Small periodic disturbances were introduced upstream of the test section by a fine wire oscillating in the thermocline. The critical R_i was found as 0.22. The growth rate is a function of wave number. Wang (1972) first used fresh water and dyed salt water to form two layers of fluid in a tank. Shear flow was induced by pumping the fluid in both layers. The velocity in the lower layer was larger. Small disturbances were generated by a vibrating ribbon at the interface. Wang compared his results with Hazel's numerical analysis which showed good confirmation. Browand and Winant (1972) conducted the same experiment in a two layer system, and they observed the growth of the disturbance. At the upstream, the Richardson number is small ($R_i = 0.02$ at $x = 0.394$ in) and the waves collapsed. The Richardson number is approximately 0.4 at a distance of 23.6 in. Further downstream, the waves decayed and the shear layer approached an undisturbed laminar flow.

CHAPTER III DESCRIPTION OF THE PROBLEM

The objective of this thesis is to investigate the conditions under which high frequency interfacial waves will occur in the interfacial layer of longer internal waves. Long waves were generated mechanically in a two layer system. The upper layer was fresh water and the lower layer was salt water, dyed with red food color.

The interface is defined as the level where the density gradient is maximum in the two-layer system. The wave induced velocity above and below the interface is in opposite directions thus causing a high velocity gradient (and shear stress) at the interface. According to the linear, inviscid stability theory, the Richardson number (R_i), as defined earlier, is the stability parameter for an inviscid, stratified shear flow. From the definition of R_i , a large density stratification has a stabilizing influence on the flow and a large velocity gradient has a destabilizing influence.

The velocity gradient is maximum at the wave crests and troughs so these are points of minimum stability. In order to determine if the high frequency waves can be generated by a shear instability, Richardson number profiles at the crests and troughs are needed. Velocity, conductivity, and temperature profiles must then be measured at these points.

Energy is transferred from the long waves to the interfacial waves and this results in a reduction in amplitude of the long waves. The long wave amplitude is monitored during the experiments to see if this transfer of energy can be correlated with the stability parameter.

A flow definition sketch is given in Figure 2.

Two coordinate systems are used, one (z , the vertical coordinate) has its origin fixed to the bottom of the tank and the other (ξ , the vertical coordinate) has its origin attached to the interface. Both z and ξ are positive upward.

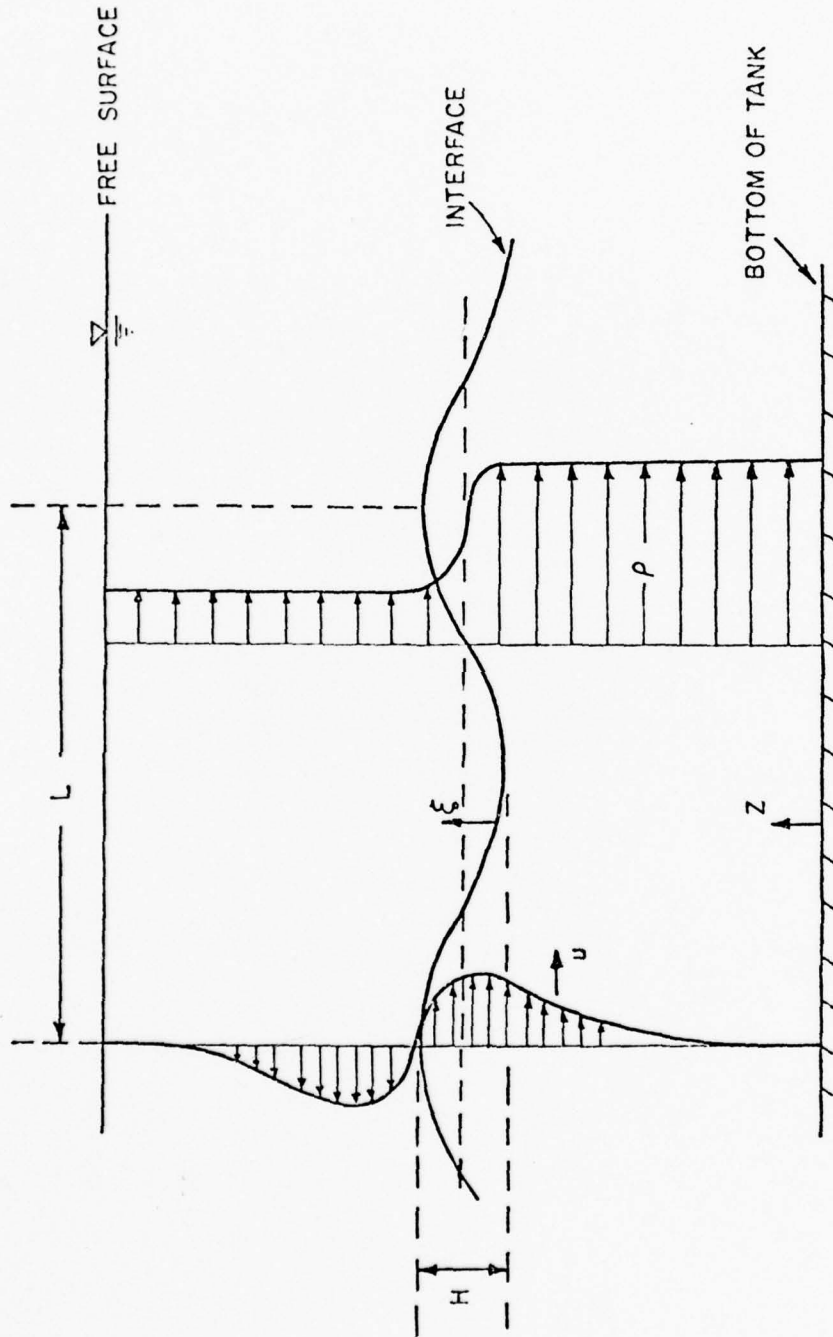


Figure 2. Definition Sketch

CHAPTER IV FACILITIES AND INSTRUMENTATION

Facilities

Test Section

The experiments were conducted in the internal wave tank in the Coastal and Oceanographic Engineering Laboratory, at the University of Florida. The test section of the tank is 80 feet long, 6 feet high and 2 feet wide in the lower portion and 3 feet wide in the upper wind tunnel section (see Figures 3 and 4). The tank is lined on both sides with 1/2 inch glass panels to facilitate visual observation. The entire wave tank is elevated 18 inches above the ground to provide bottom access to the test section. The tank is capable of generating wind waves and shear flows and mechanically generating surface and internal waves.

Wave Generator

There is an internal wave generator at the north end of the wave tank (see Figure 5). It is comprised of a horizontal 38 inch by 38 inch neoprene rubber diaphragm attached to the walls at its outer perimeter, and is activated by a vertical shaft at the center. The shaft is driven hydraulically. A hydraulic power supply is used in conjunction with the hydraulic actuator and associated electronic equipment to drive the diaphragm. The frequency and amplitude of the waves are adjusted by a Low Frequency Signal Generator Model 202A, manufactured by Hewlett Packard.

Storage Tanks

Two 4000 gallon storage tanks are located outside the building. These tanks are connected to the wave tank by 4 inch PVC pipe. The storage

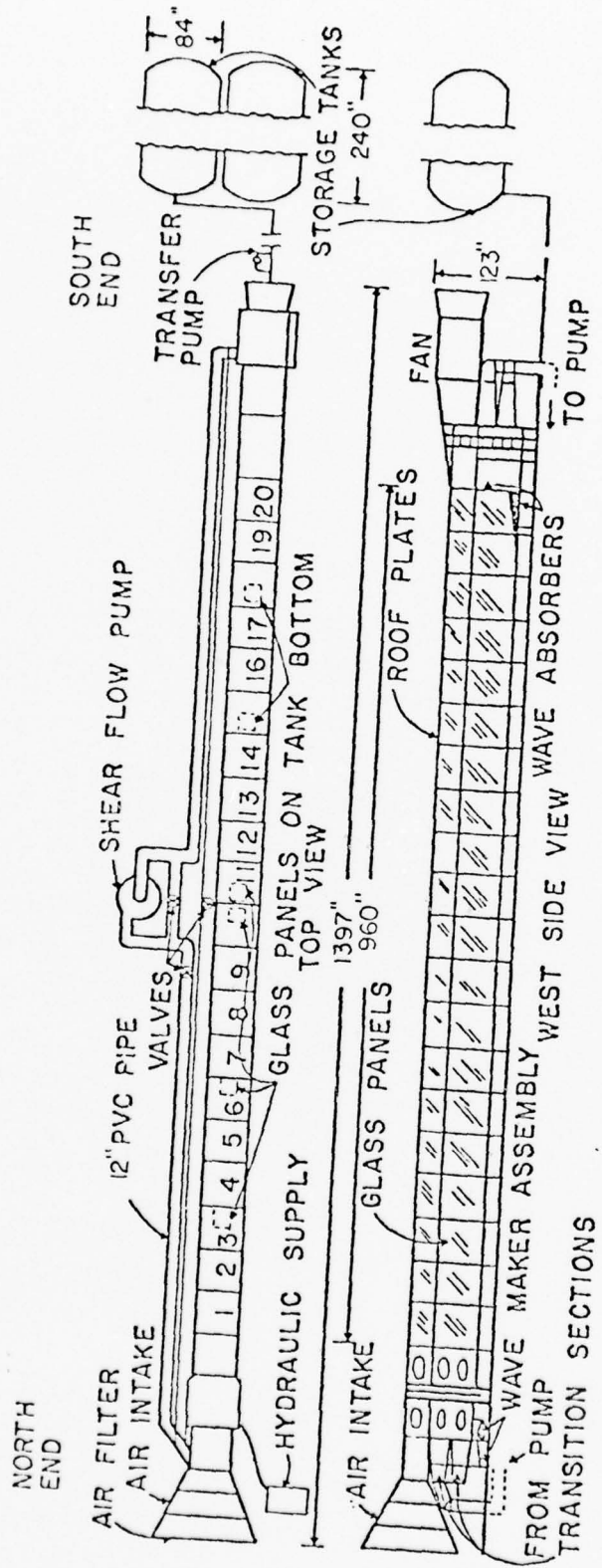


Figure 3. Schematic Drawing of the Internal Wave Tank

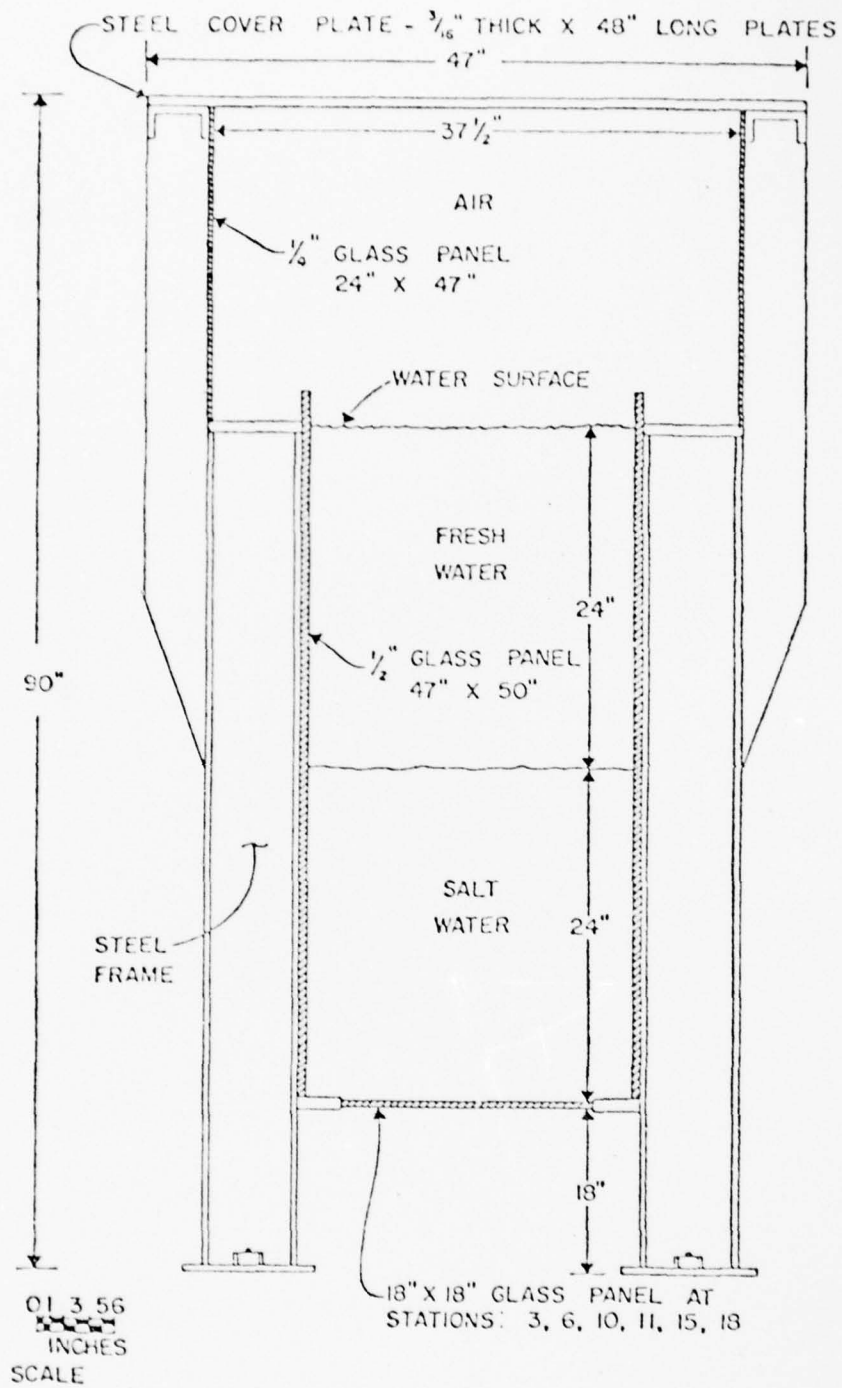


Figure 4. Cross-section of the Internal Wave Tank

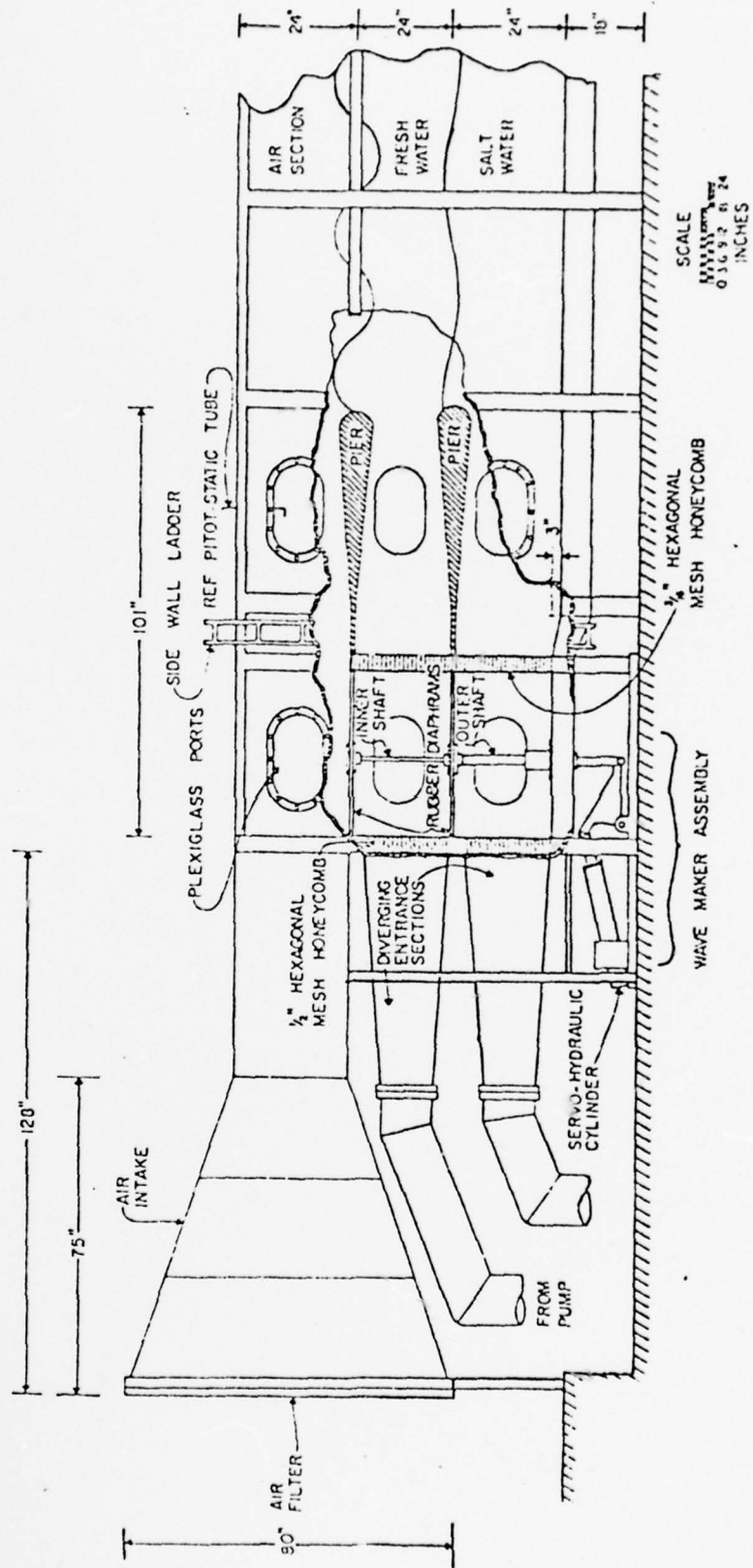


Figure 5. Schematic Drawing of the North End of the Internal Wave Tank

tanks are elevated so the wave tank can be filled from these tanks by gravity. A gear pump powered by a 5 horsepower electric motor is used to pump the water back into the storage tanks.

Tow Tank for Hot-Film Probe Calibration

A 112 inch by 13 inch by 12 inch tow tank is used to calibrate the hot-film probe. The tank is made of plexiglass. A 1/8 horsepower variable speed motor is used to drive the carriage which holds the hot-film probe.

Traverse Mechanism

The traversing mechanism is comprised of a 1/2 horsepower variable speed D.C. motor, a gear reduction box, a stainless steel tube with a gear rack and a motor controller system. The traverse speed can be varied from approximately zero to 6 in/sec. The direction of the traverse shaft can be switched manually or can be made to shuttle between any two positions. The velocity probe, temperature probe, and conductivity probe were mounted at the same level on the bottom of the traverse tube.

Instrumentation

Position Indicator

The traverse drives a ten-turn, 10 K potentiometer when it moves. The potentiometer is part of a D.C. circuit designed to give a linear output voltage proportional to the position of the traverse (see Figure 66 in the appendix). The vertical position can be measured accurately to 0.025 inch.

Velocity Measurements

Velocity of the fluid is measured by a Constant Temperature Hot-Film Anemometer, manufactured by Thermo-Systems, Inc.. The anemometry

system consisted of a Model 1051 Monitor and Power Supply module, two Model 1050 Anemometer modules, and two Model 1055 Linearizers. The probe which was mounted on the tip of the traverse was a wedge-type Model 1233 NaCl hot-film sensor. The hot-film probe was calibrated in a tow tank. Calibration curves were attained for several salt concentrations (specific gravities ranging from 1.00 to 1.03). The change in the probe output over this range of concentrations was found to be less than 2%. Problems with bubble formation on the probe at lower velocities in the salt solutions were overcome by lowering the over-heat ratio to 1.05. The calibration curves are shown in the appendix (Figure 67 and 68).

Temperature Measurements

Temperature was measured with a glass encapsulated thermistor, experimental Type 08127401, manufactured by Keystone Carbon Company. A constant temperature bath with a thermometer that could be read to 0.1°F was used to calibrate the thermistor. The calibration curve is shown in the appendix (Figure 69).

Density Measurements

Density stratification in these experiments was achieved by varying the salt concentration. Since the electrical conductivity and mass density of a salt solution varies with salt concentration, the mass density of the solution can be determined from conductivity measurements. The conductivity measuring system used in these experiments was developed for this work by Drs. Sheppard and Doddington (submitted for publication in the Review of Scientific Instruments). It consists of a two electrode probe (see Figure 6 and 7) and a constant peak-to-peak current supply. The fluid being measured is drawn into the probe through the horizontal slit at the bottom, through the 0.012 inch diameter hole and into

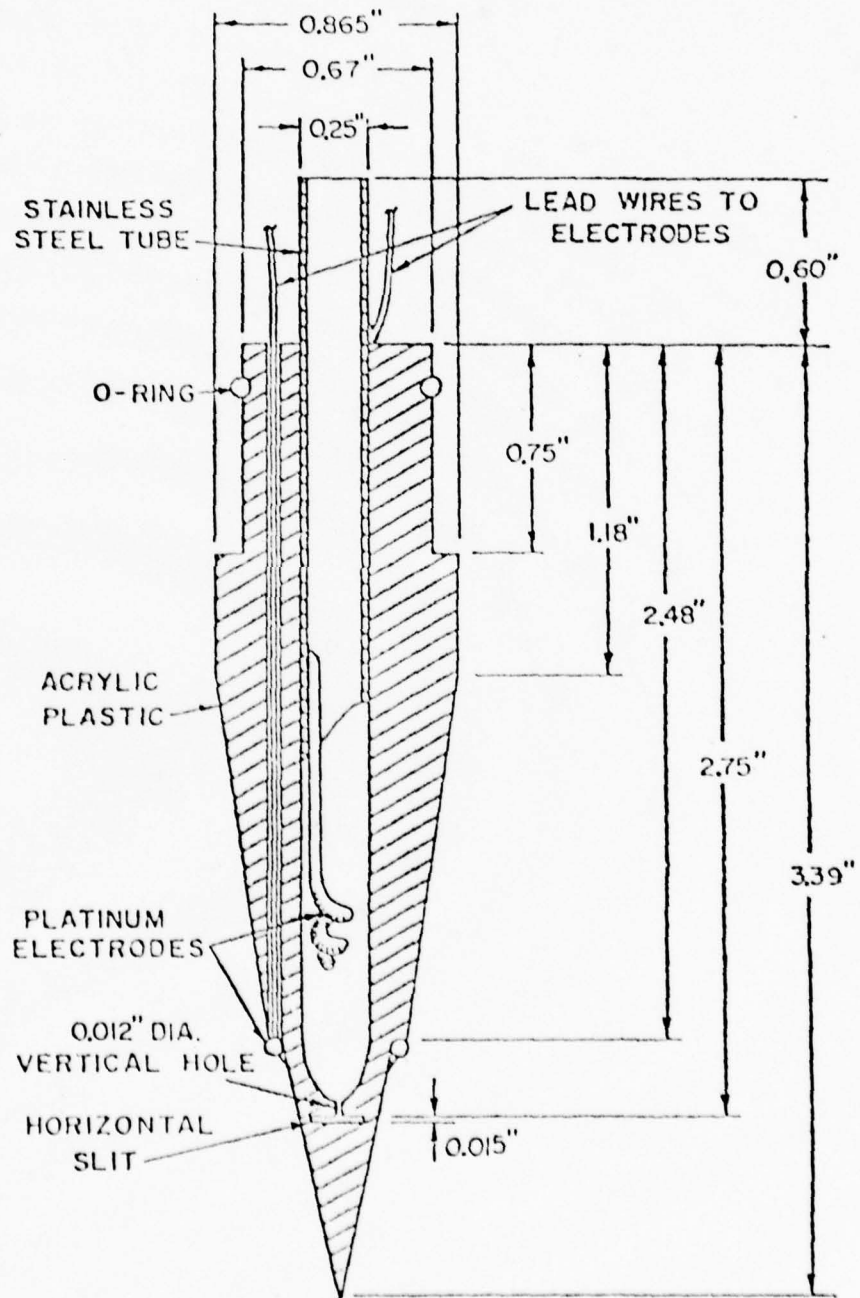


Figure 6. Cross-section of the Conductivity Probe

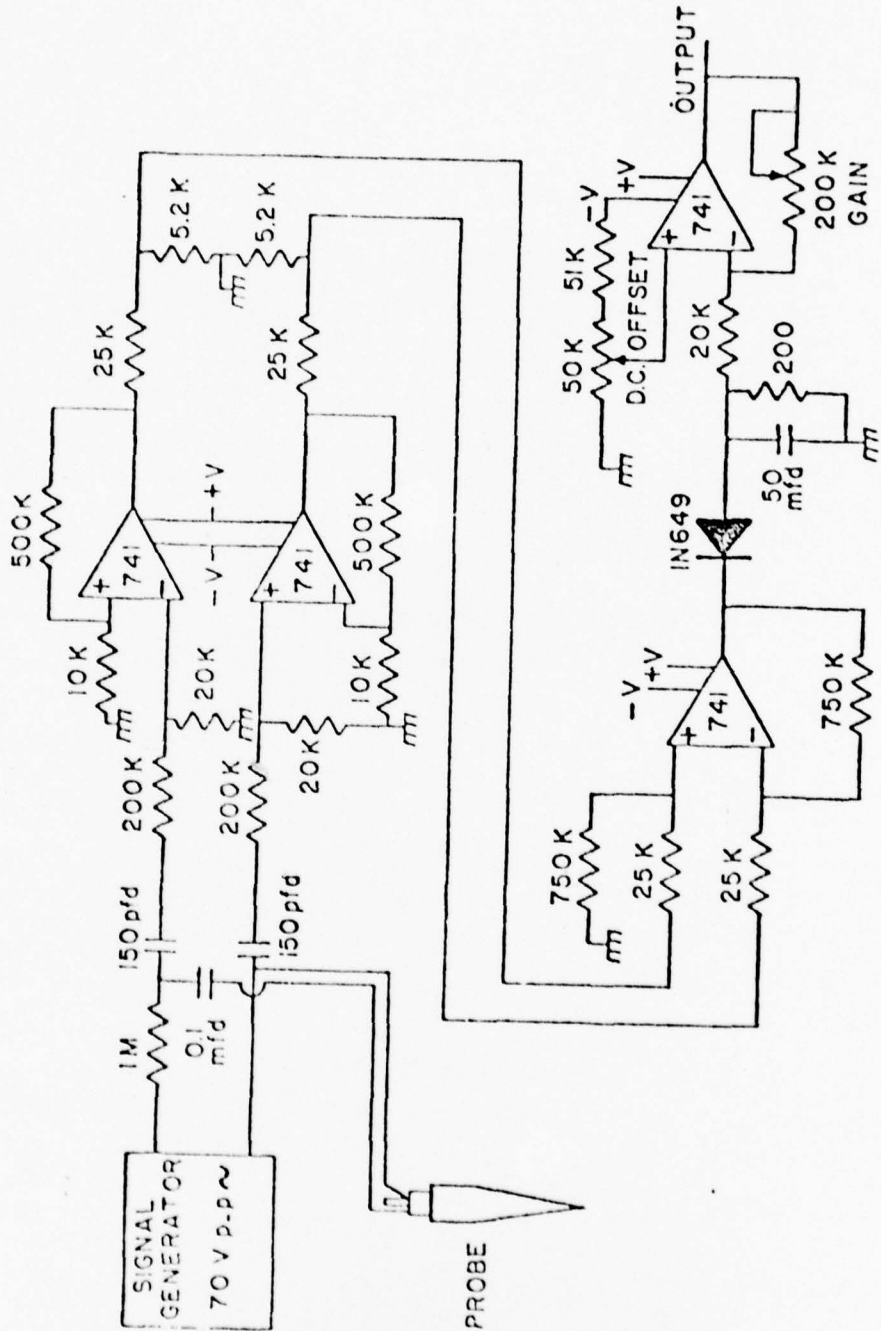


Figure 7. Circuit of the Conductivity Probe Electronics

the inner cavity. The fluid then goes out the top of the probe through plastic tubing to the pump. One electrode is located in the inner cavity and the other on the exterior of the probe. The electrical current density between the electrodes is small except in the 0.012 inch diameter vertical hole, where it is quite large. Thus the conductivity of the fluid in this hole at any instant determines the resistance between the electrodes.

Calibration of the Conductivity Probe

To minimize error, calibration is done in the tank under the conditions present during a test. A siphoning probe with a horizontal slot very similar to that in the conductivity probe is mounted on the traverse shaft at the same elevation as the other probes (conductivity, thermistor and hot-film). The tank is then filled in such a manner that the interface between the salt and fresh water is very diffused. At several points in the interfacial layer, fluid is siphoned from the tank and conductivity readings recorded. A hydrometer (with 0.0001 divisions) is used to measure the specific gravity and a mercury thermometer to measure the temperature. The temperature in the tank is measured with the thermistor. A calibration curve for the range of salinities of interest can then be plotted (see Figure 70 in the appendix).

Internal Wave Gages

The wave gages used in this experiment were designed to monitor the motion of the interface between the fresh and dyed salt water layers. The measuring system consists of a line voltage regulator, a collimated light source, a custom built light sensor, a Wheatstone bridge with a D.C. power supply and a recorder. The back edge of the light sensor is parabolic in shape (see Figure 8 and 9). All surfaces on the sensor

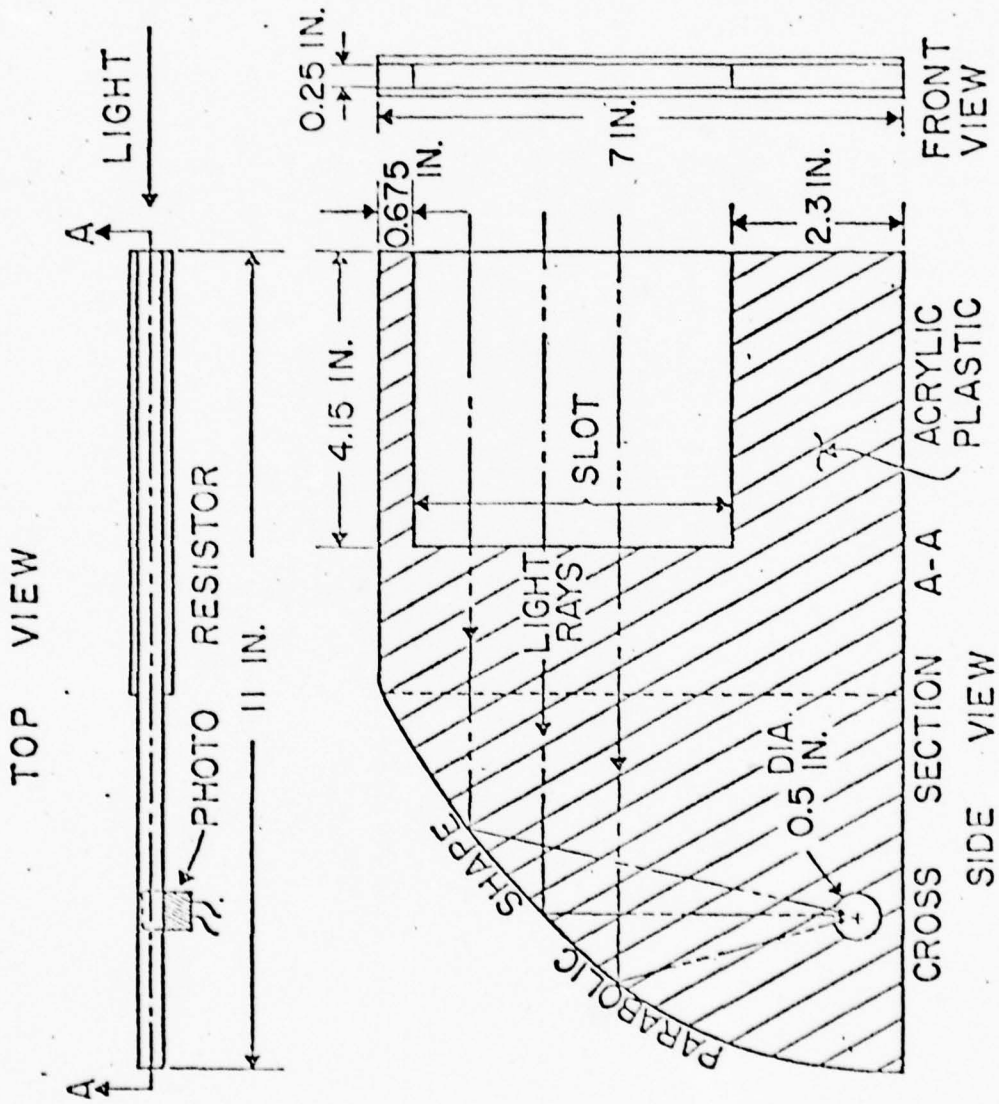
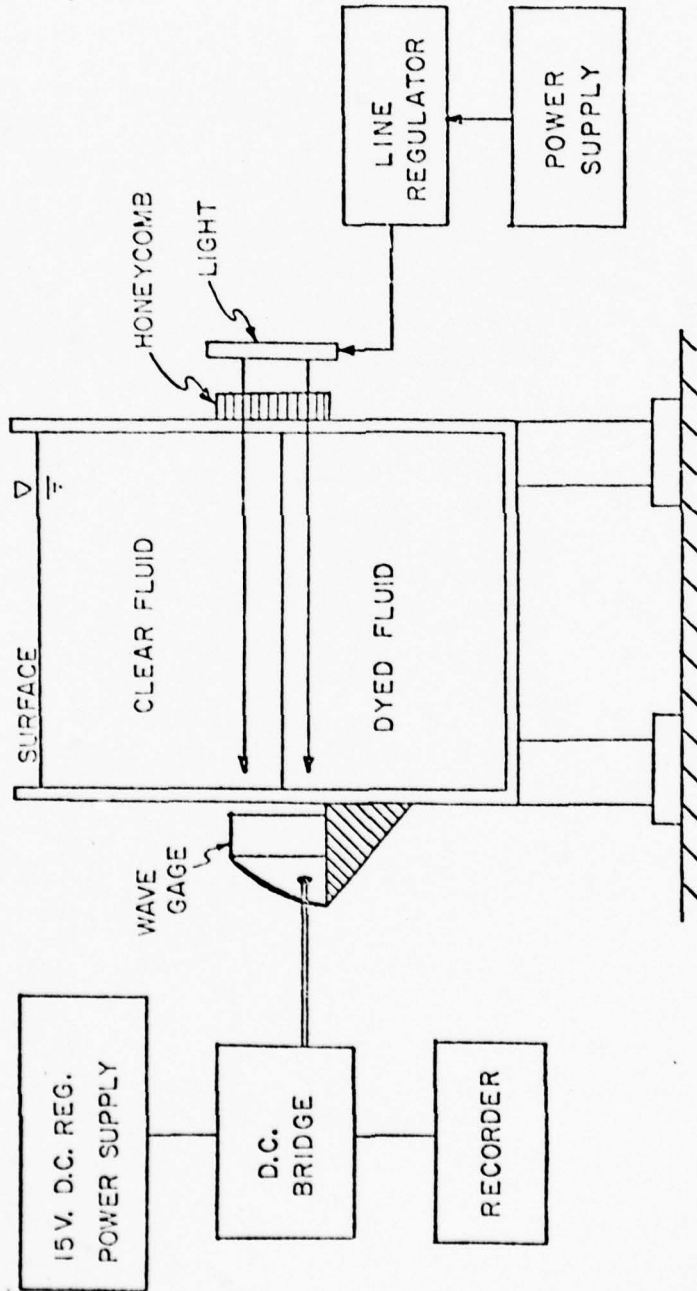


Figure 8. Drawing of the Internal Wave Gage

INTERNAL WAVE GAGE SYSTEM



CROSS SECTION

Figure 9. Schematic Drawing of Internal Wave Gage System

except the front and back are painted black. The parabolic back surface is polished and coated with a highly reflective paint and the front light admitting surface is just polished. A cadmium sulfide photo resistor is placed on the focal point of the parabola. The light source which is a vertical fluorescent lamp is centered at the undisturbed interface and projects through the wave tank to the sensor as shown in Figure 9. Honeycomb is placed in front of the lamps to make the light parallel.

The salt water is dyed with red food color to take advantage of the low sensitivity of the photo sensor to red light. As the interface moves up and down, the amount of light striking the light sensor changes proportionately.

In these experiments, the wave gages are only used to measure the wave frequency and wave length.

Visicorder

All signals were recorded on a Visicorder Oscillograph Model 906A, manufactured by Honeywell as well as on a magnetic tape recorder. It has a built-in Time Line System which provides accurately spaced pulses at intervals of 0.01, 0.1 and 1.0 second. It contains 17 channels and records on photographic paper with a high intensity ultraviolet light reflected by the galvanometer mirror.

Tape Recorder

A four-channel, FM tape recorder, Model 3960A, manufactured by Hewlett Packard was used to record the output voltage from the position indicator, thermistor, hot-film probe and conductivity probe.

The Pre-Amplifier and Low-Pass Filter

A four-channel pre-amplifier and low-pass filter is placed in series with the four sensors. This amplifier is designed to filter out electrical noise

induced by equipment in the laboratory. The amplifiers were used to increase the probe output to the maximum allowable input voltage of the tape recorder. This unit has a high input-impedance and low output-impedance which isolates the sensors from the recording equipment. The filter is fourth-order, Butterworth, low-pass filter with a cutoff frequency of 16.7 Hz. The circuit is shown schematically in the Appendix (Figure 71). The low-pass filter was not used in the hot-film probe circuit.

X-Y Plotter

An Omnigraphic 2000 Recorder, type 6, manufactured by Houston Instruments was used during the tests to plot the conductivity vs. position. This was used to locate the probe relative to the interface.

CHAPTER V PROCEDURE

Initially the wave tank was filled with 24 inches of fresh water from the fresh water storage tank. Salt was dissolved in the salt water storage tank until the specific gravity of the fluid was about 1.03. Red food color was used to dye the salt water, and compressed air was used to mix the salt, dye and water. After the fresh water was filled, the dyed salt water was allowed to flow into the tank very slowly from the bottom. After 6 to 7 hours, the salt water reached the desired depth of 24 inches and the valve was closed. This slow filling procedure resulted in a sharp interface between the fluids. After the conductivity probe was calibrated, the experimentation was begun. The conductivity probe, thermistor, and hot-film probe were mounted at the same elevation on the traverse shaft thus allowing continuous simultaneous measurement of salinity, temperature, velocity and position. The measurement system is shown in Figure 10. The signals from the probe were fed into the 4-channel amplifier-filter. The filter can be switched out of the circuit and was not used for the velocity signal. The output signals were fed to a 4-channel FM tape recorder and along with two wave gage outputs to a six-channel pre-amplifier. The outputs from the pre-amplifier were fed into an optical strip chart recorder (visicorder). An X-Y plotter was used to plot conductivity vs. position during the test.

An initial traverse was made to obtain the initial density and temperature profiles. The mechanical wave generator was then started and

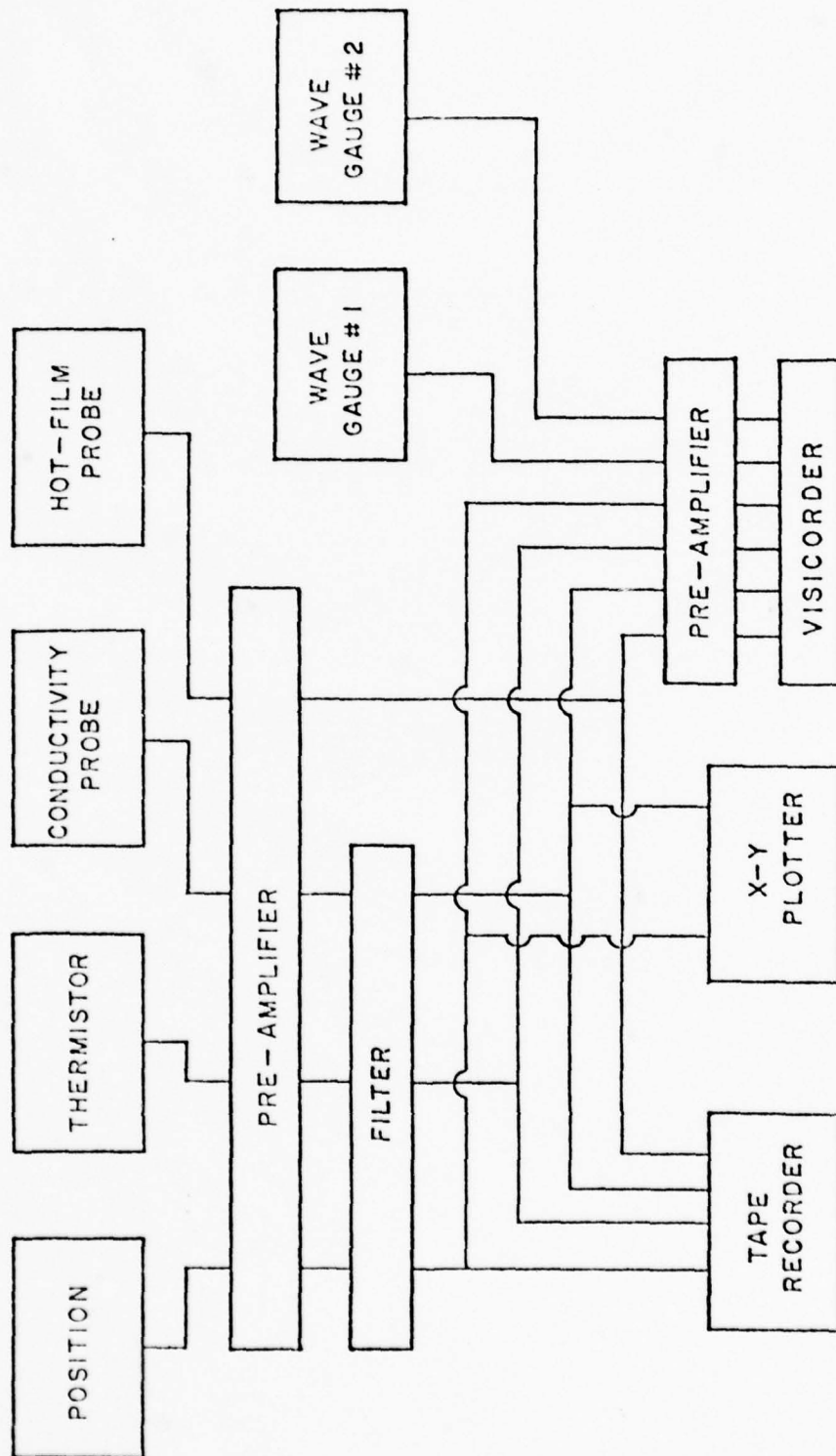


Figure 10. Schematic Diagram of Measuring System

waves of the desired frequency and amplitude were generated. Since instantaneous profiles could not be made with our measuring system, "average" profiles were measured using the following procedures. The probes were positioned at one point while approximately 3 to 5 waves passed, then lowered to a new position for the next 3 to 5 waves. This procedure was repeated until the vertical field of interest had been covered. The signal outputs varied periodically with the wave motion. The point of maximum S.G. indicated the S.G. at the wave crest, and the minimum S.G. indicated the S.G. at the wave trough. So the velocity at the crest was obtained by reading the velocity at the instant when the specific gravity was the maximum and similarly the trough velocities were taken at the point where the S.G. was a minimum. Since the wedge type hot-film probe used in these experiments can only measure velocities in one direction, only velocities in the direction of the propagating waves could be accurately obtained. Thus only profiles below the crests and above the troughs could be measured.

Specific gravity profiles were constructed from the averaged values at each point; i.e. the average of the values measured for 3 to 5 consecutive waves.

Due to a high noise level on the magnetic tape (attributed to the use of old tape) the various outputs could not be plotted on the X-Y plotter as was originally planned. The visicorder (optical strip chart recorder) output had to be used, making the data reduction a tedious process.

The output from two of the optical internal wave gages were recorded. Knowing the spacing between these gages and the approximate wave length of the waves, the celerity and exact wave lengths were obtained.

Several amplitudes were examined for each frequency. This was accomplished without stopping the wave generator. The generator was stopped, however, when the frequency was changed and a continuous traverse made at that time.

Attempts were made to record the frequencies of the trapped waves at the interface but this information was lost due to the noisy tape. A spectral analysis to determine the amplitudes of the frequencies present had been planned but now must be postponed.

A table listing the sequence of the various runs and the duration of each test is given in Table 1. Throughout the experiment, visual observations were made and recorded and photographs were taken of shadow-graphs of the interface.

TABLE 1

Run No.	Time Start (P.M.)	Time Stop (P.M.)	Frequency (Hz)	Wave Height* (in.)	Remark
1	1:26	1:27			Initial profile
2	1:45	1:53	0.1	1 1/16	Waves start at 1:40 p.m.
3	2:04	2:09	0.1	1 1/16	Frequency analysis
4	2:13	2:23	0.1	2 1/4	
5	2:33	2:34	0.1	2 1/4	Final profile
6	2:48	2:59	0.1	3 1/2	
7	3:03	3:08	0.1	3 1/2	Frequency analysis
8	3:23	3:24			Final profiles, waves stop at 3:10 p.m.
9	3:33	3:42	0.15	7/8	Waves start at 3:30 p.m.
10	3:44	3:50	0.15	7/8	Frequency analysis
11	3:50	4:00	0.15	1 3/8	
12	4:10	4:17	0.15	1 3/8	Frequency analysis

TABLE 1 - continued

Run No.	Time Start (P.M.)	Time Stop (P.M.)	Frequency (Hz)	Wave Height* (in.)	Remarks
13	4:21	4:29	0.15	1 3/8	
14	4:44	4:45			Final profile, waves stop at 4:31 p.m.
15	5:00	5:09	0.2	5/8	Waves start at 4:55 p.m.
16	5:17	5:24	0.2	5/8	Frequency analysis
17	5:28	5:40	0.2	1 1/4	
18	5:45	5:50	0.2	1 1/4	Frequency analysis
19	6:09	6:10			Final profile, waves stop at 5:52

* Initial Wave Height

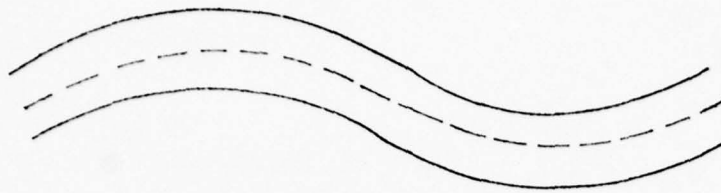
CHAPTER VI RESULTS AND DISCUSSION

Two types of results are presented here, visual observation and experimental measurements. A description of the visual observations will be presented first.

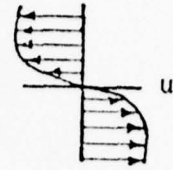
It was observed that mechanically-generated internal waves with small steepness ratios (H/L) maintained their smooth sinusoidal shape both in time and space. However, as the steepness ratio was increased beyond some value, high frequency waves appeared in the interfacial layer. Upon the formation of these interfacial waves the amplitude of the internal wave was reduced. After a period of time the interfacial waves ceased to exist and the internal wave amplitude increased once again. A short time later the interfacial waves reappeared and the cycle was repeated. Figure 11 shows sketches of this observed phenomenon.

These high frequency waves were confined to the interfacial layer, i.e. the transition layer for the density, by very distinct boundaries (see Figure 14). The interface was completely filled with waves which from time to time would roll up, break and appear to cause substantial mixing in the interfacial layer (see Figures 13 and 14). The measurements proved this not to be true, however, since only minor changes in the density profiles were observed even after several hours of performing the experiments.

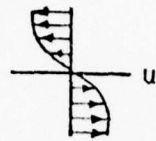
To aid in the discussion of this phenomenon, the following terminology will be used. If no interfacial waves occur the long internal waves are said to be stable. If interfacial waves occur but only after a long period of time this will be referred to as the transition conditions. Waves



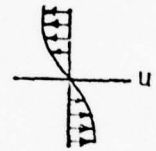
No interfacial waves, Large amplitude



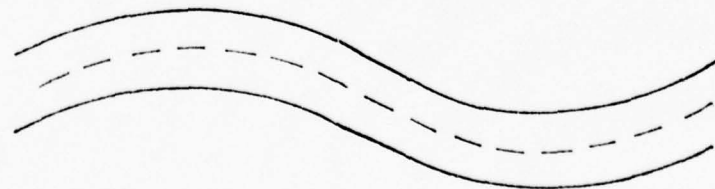
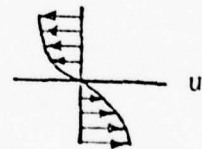
Interfacial waves occur, Reduced amplitude



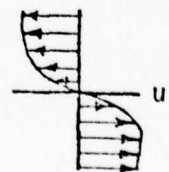
More interfacial waves, Small amplitude



Interfacial waves reduced, Increased amplitude



Interfacial waves disappear, Large amplitude



Velocity Profile

Figure 11. Sketch of Periodical Occurrence of Interfacial Waves

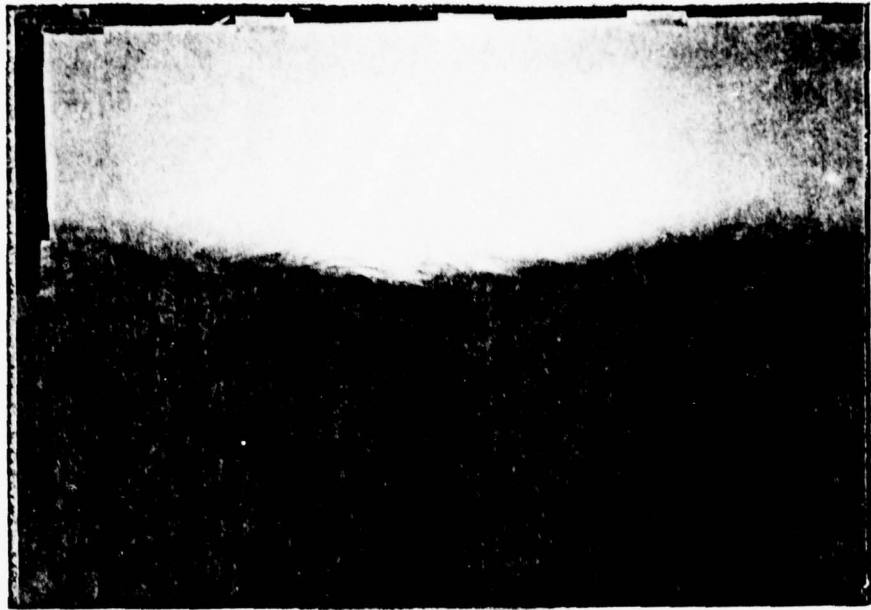


Figure 12. Formation of Interfacial Waves

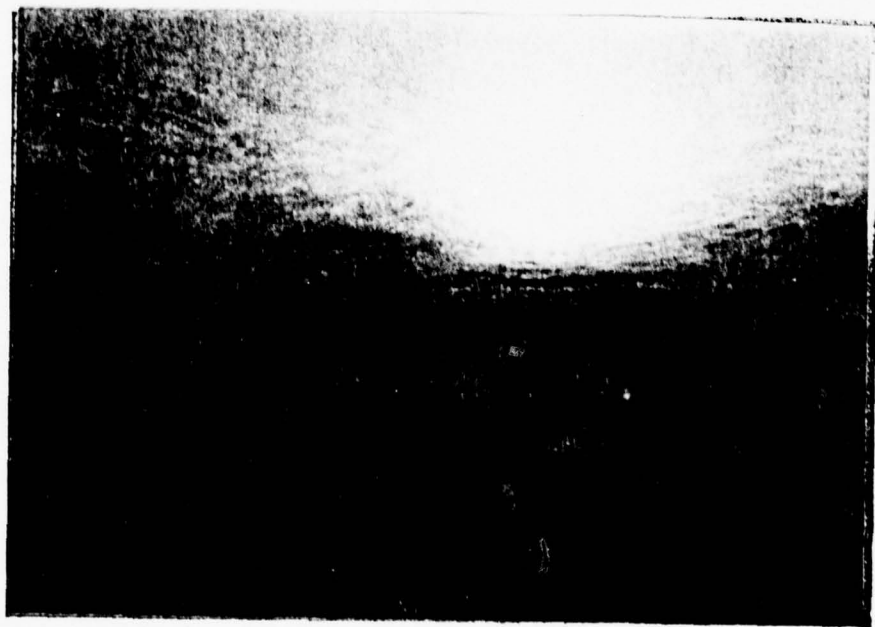


Figure 13. Roll-up of Interfacial Waves

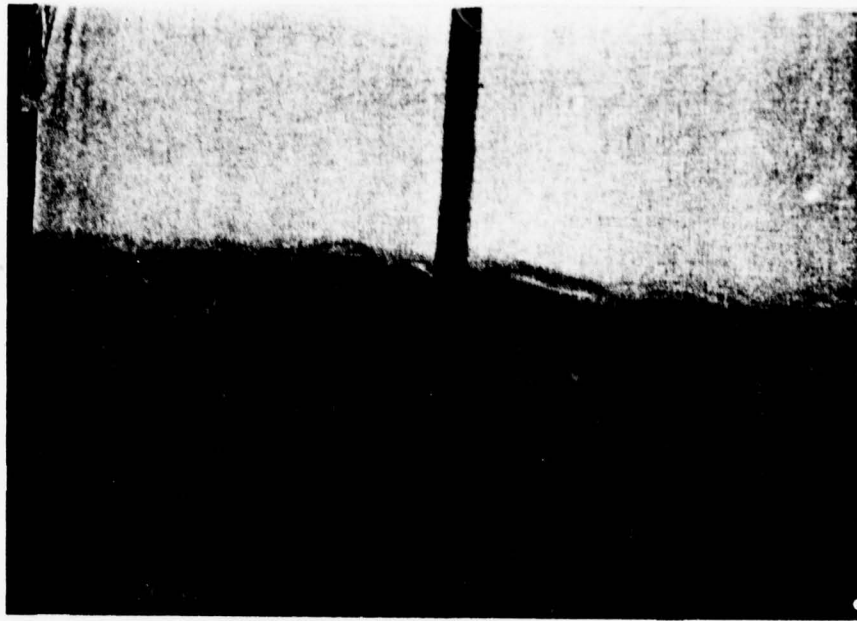


Figure 14. Trapped Interfacial Waves

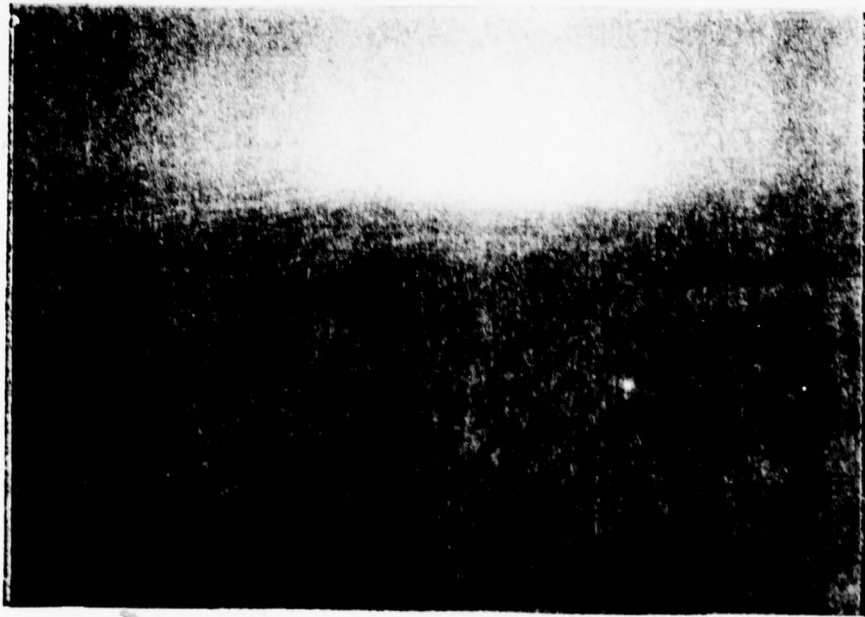


Figure 15. Disappearance of Interfacial Waves

that have high frequency internal waves appearing at the interface after a short time will be called unstable waves. The observed results are summarized in Table 2.

TABLE 2

Run No.	Wave Length L (in.)	Wave Height H_t (in.)	Wave Period T (sec)	Wave Steepness H/L (10^{-2})	Remark
2	117.7	1.05	10.15	0.8936	Stable
4	111.2	1.8	10.15	1.6187	
6	108.0	2.75	10.15	2.5463	Unstable
9	52.47	0.7	6.85	1.334	Stable
11	52.5	1.2	6.85	2.785	Transition
15	40.06	0.35	5.23	0.8737	
17	28.62	0.85	5.23	2.0369	Unstable

The wave heights, H_t , presented in Table 2 were measured after allowing sufficient time for the interfacial waves to form.

The experimental data is presented next. Complete conductivity and temperature profiles were measured with the wave maker turned off before and after each sequence of experiments. The results of these traverses which are denoted as run numbers 1, 5, 8, 14 and 19 are presented in Figures 16 through 21. For comparison purposes these profiles are plotted together in Figures 19 and 22.

The velocity and density profiles were measured at the wave crests and troughs. The results are presented in Figures 23 through 43. Velocity profiles at wave crests were obtained below the interface only, and profiles at wave troughs were obtained above the interface only. Some of the velocity profiles were lost due to the chart paper jamming in the visi-corder.

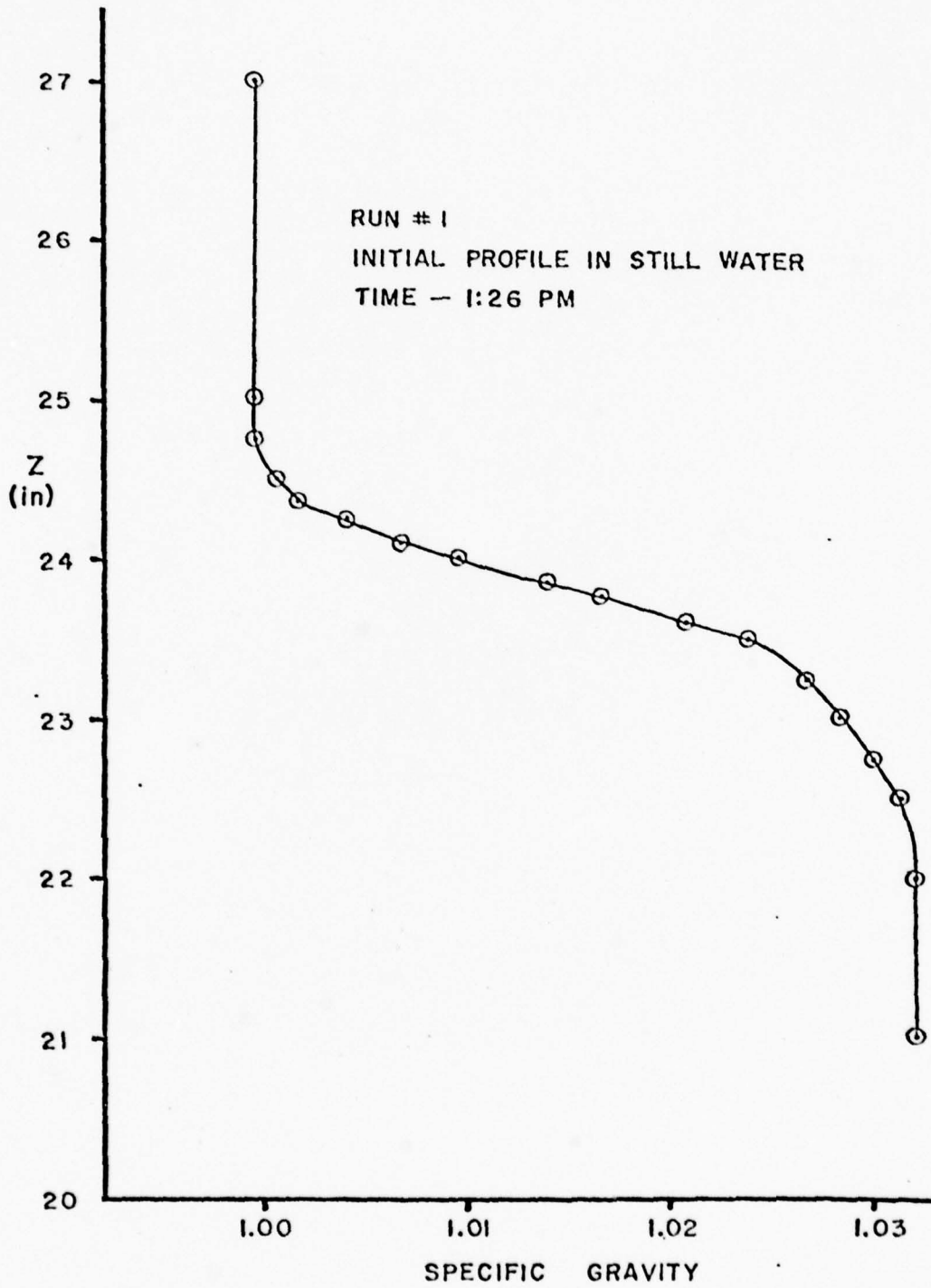


Figure 16. Initial Density Profile, Run #1

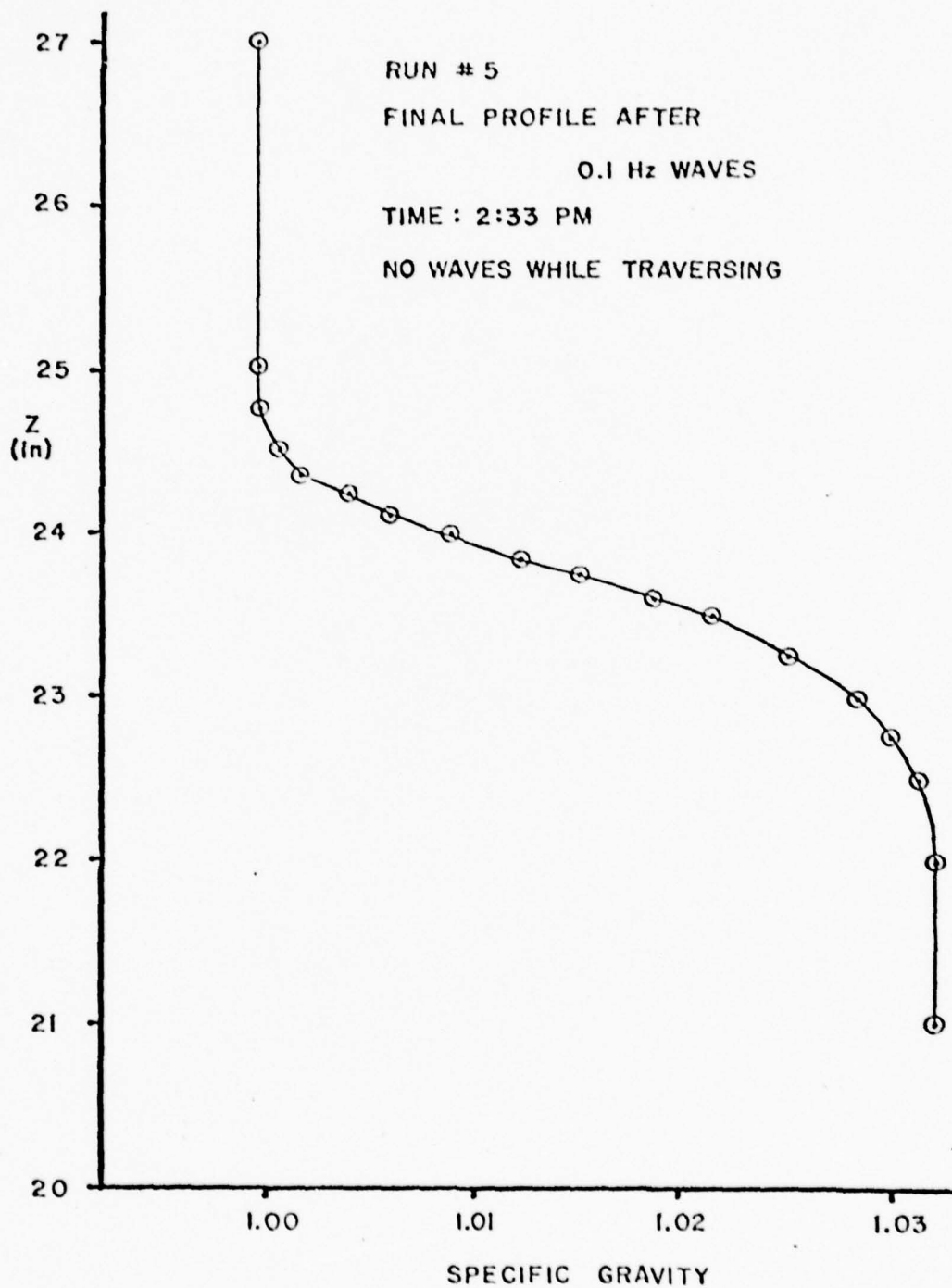


Figure 17. Final Density Profile, Run #5

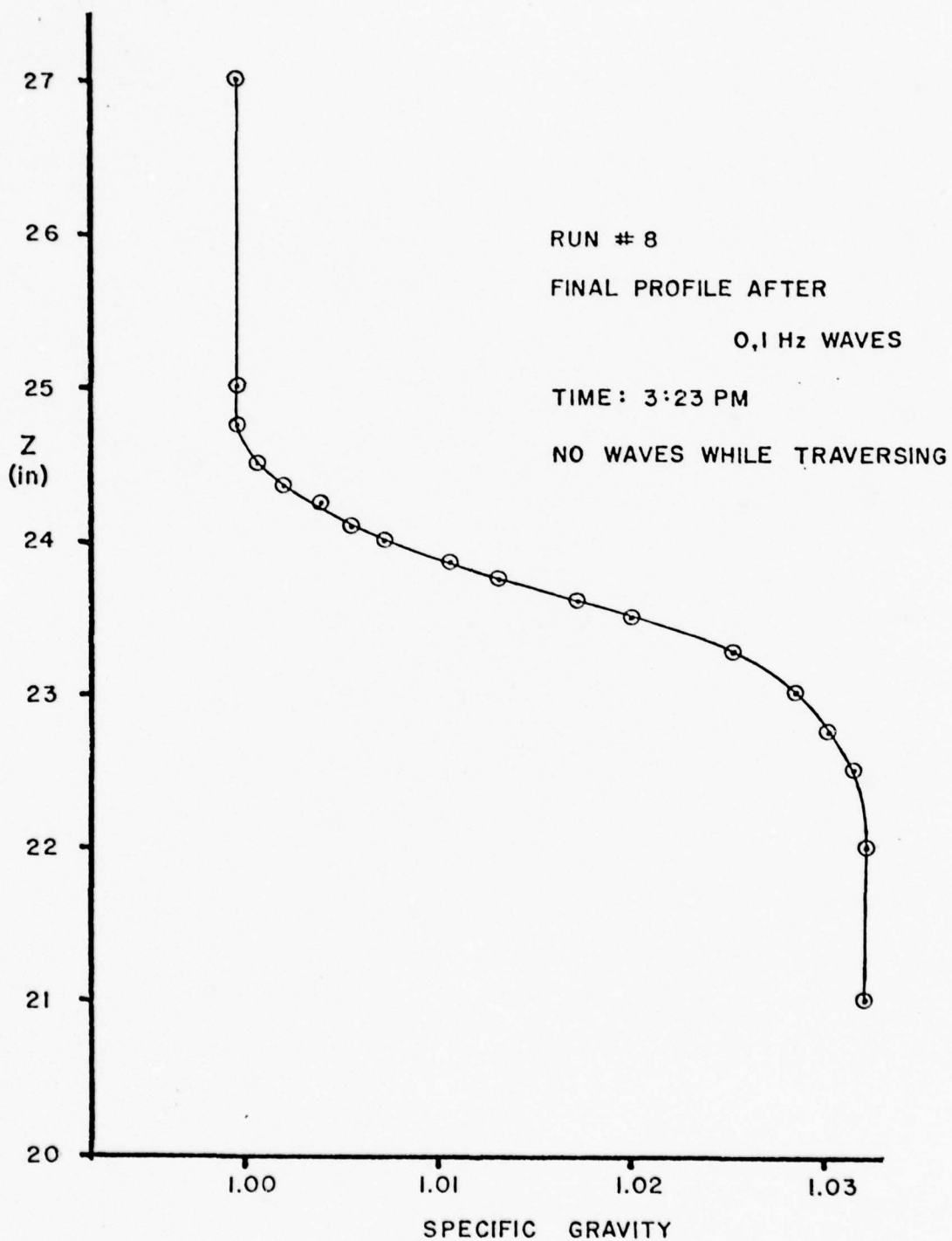


Figure 18. Final Density Profile, Run #8

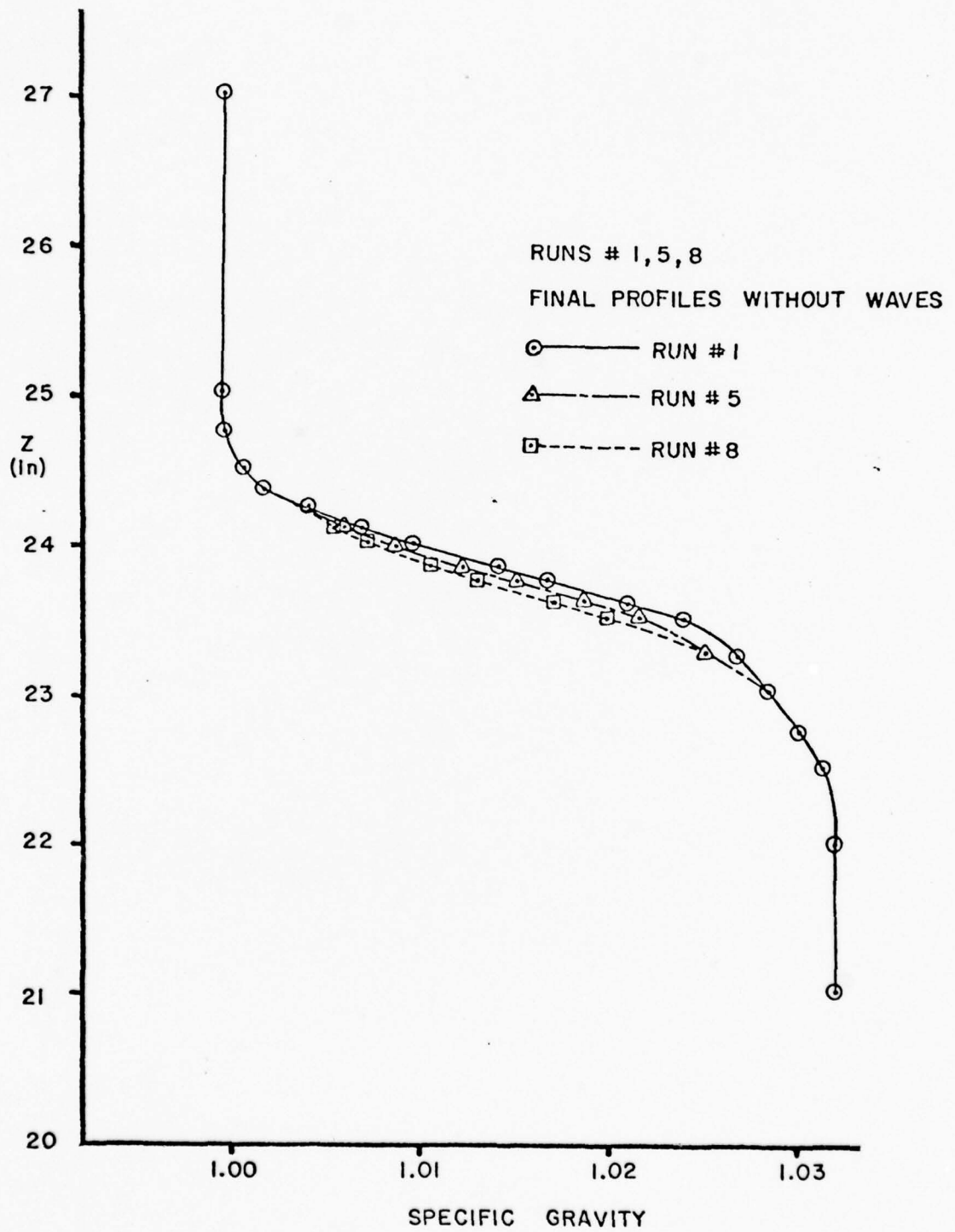


Figure 19. Comparison Among Runs #1, 5, and 8

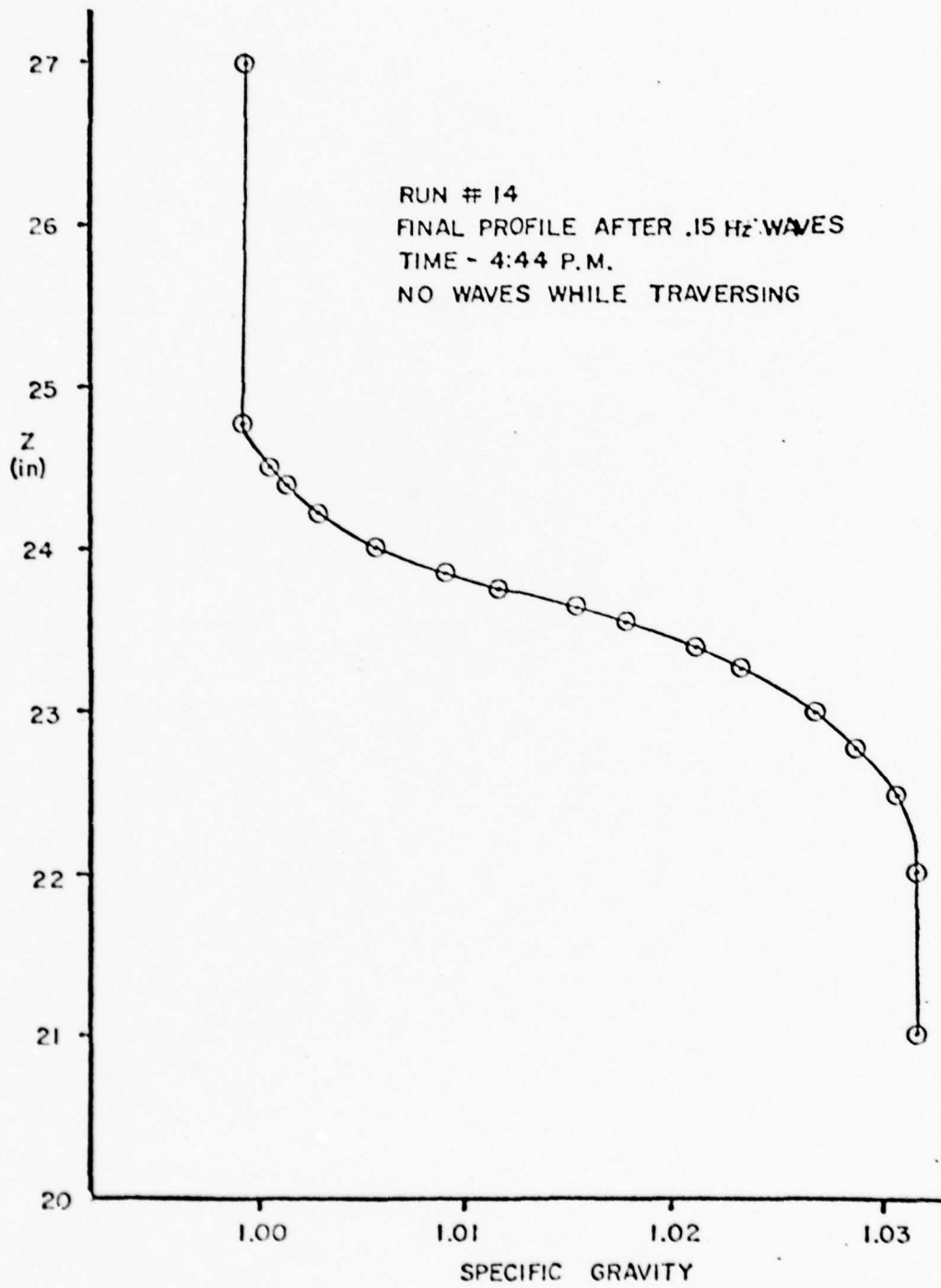


Figure 20. Final Density Profile, Run #14

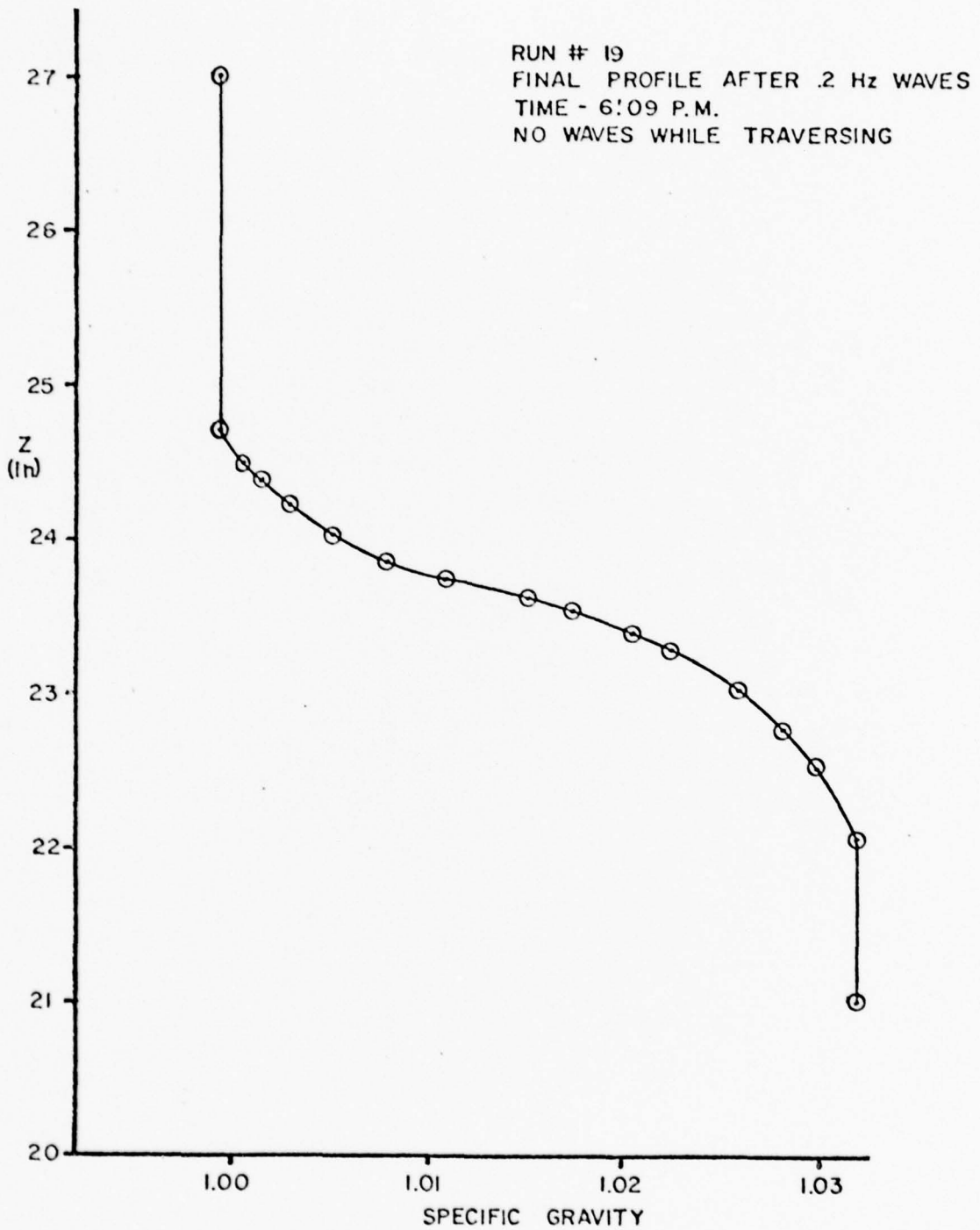


Figure 21. Final Density Profile, Run #19

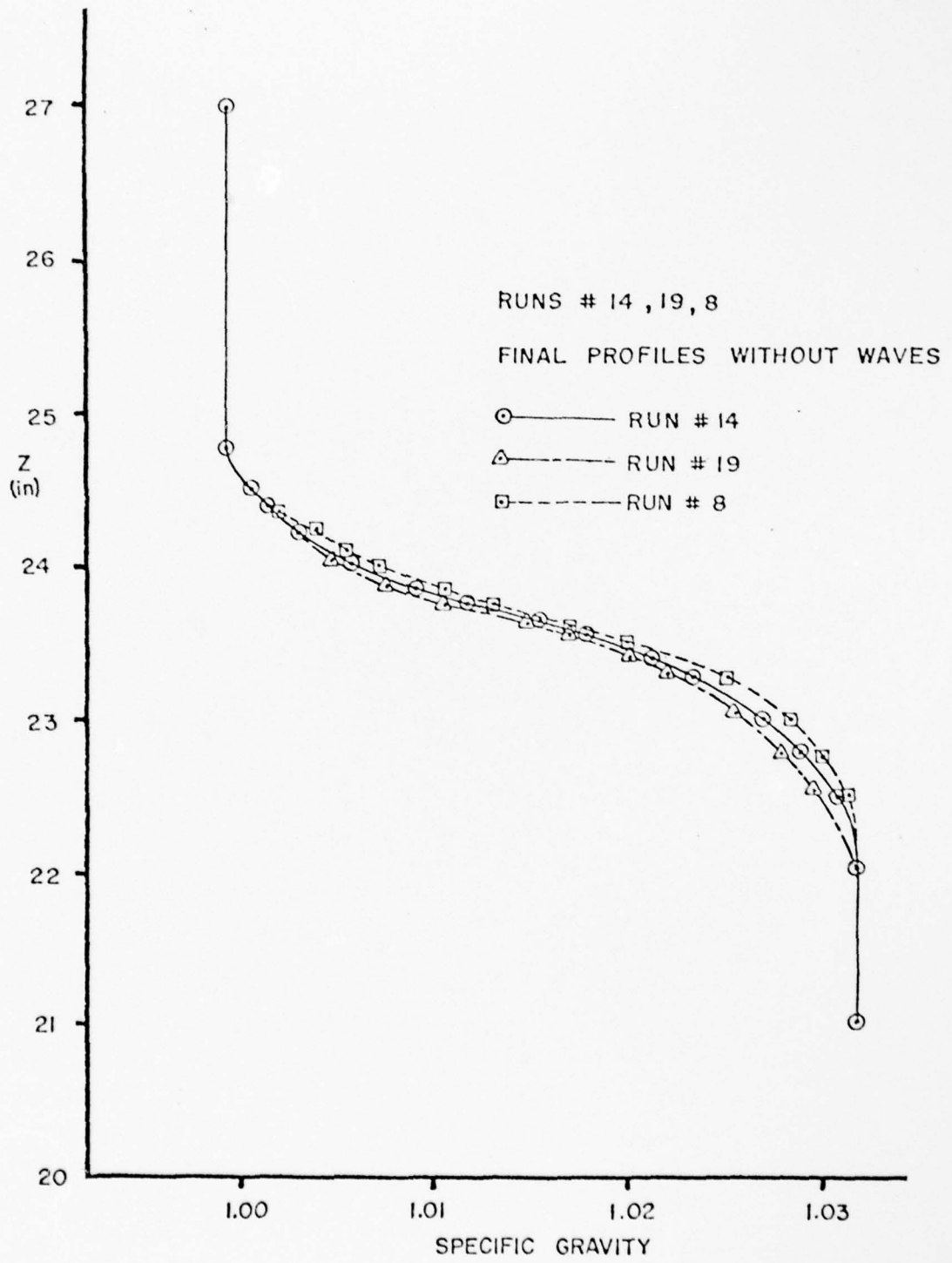


Figure 22. Comparison Among Runs #8, 14, and 19

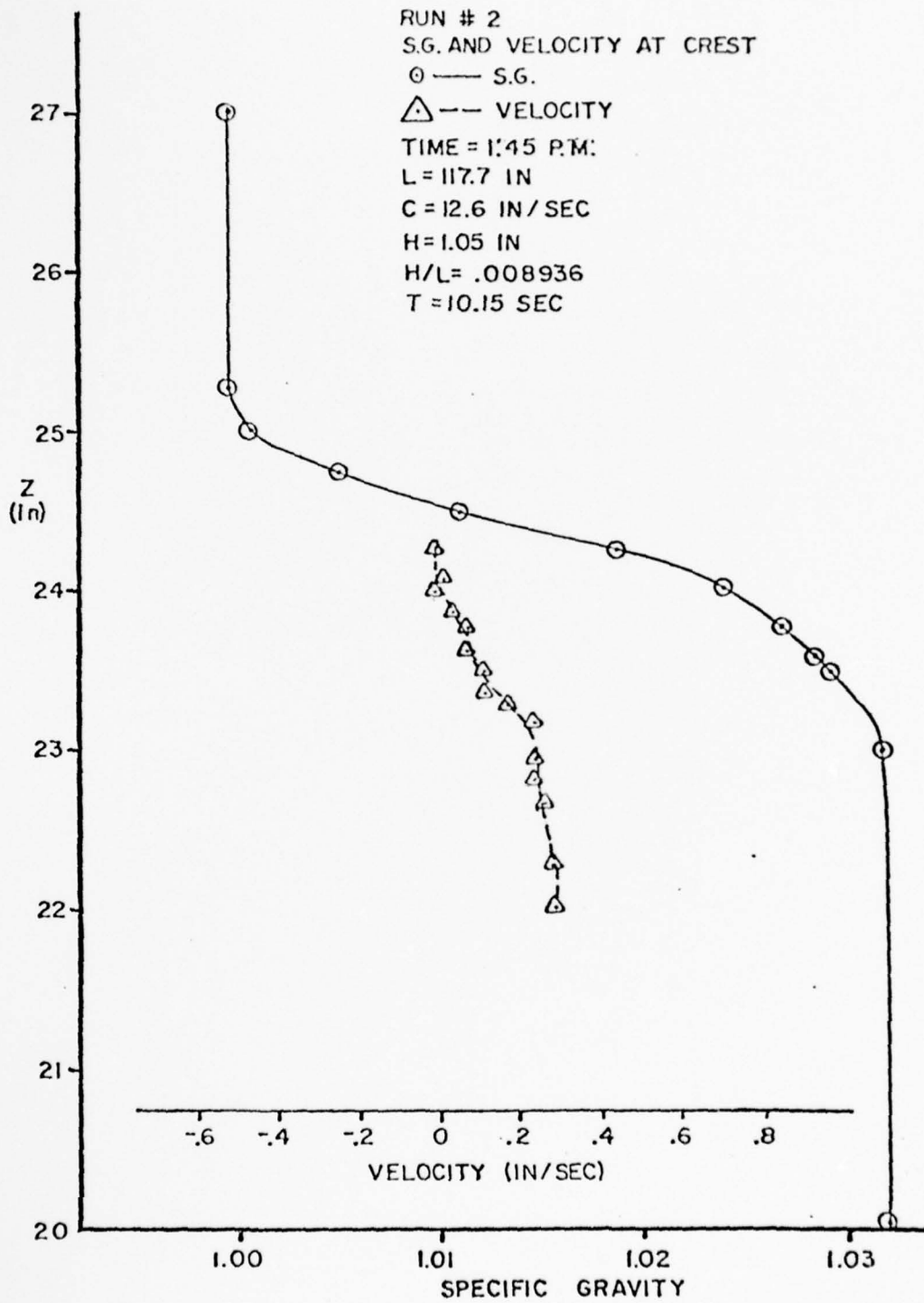


Figure 23. Density and Velocity Profiles at Wave Crest, Run #2

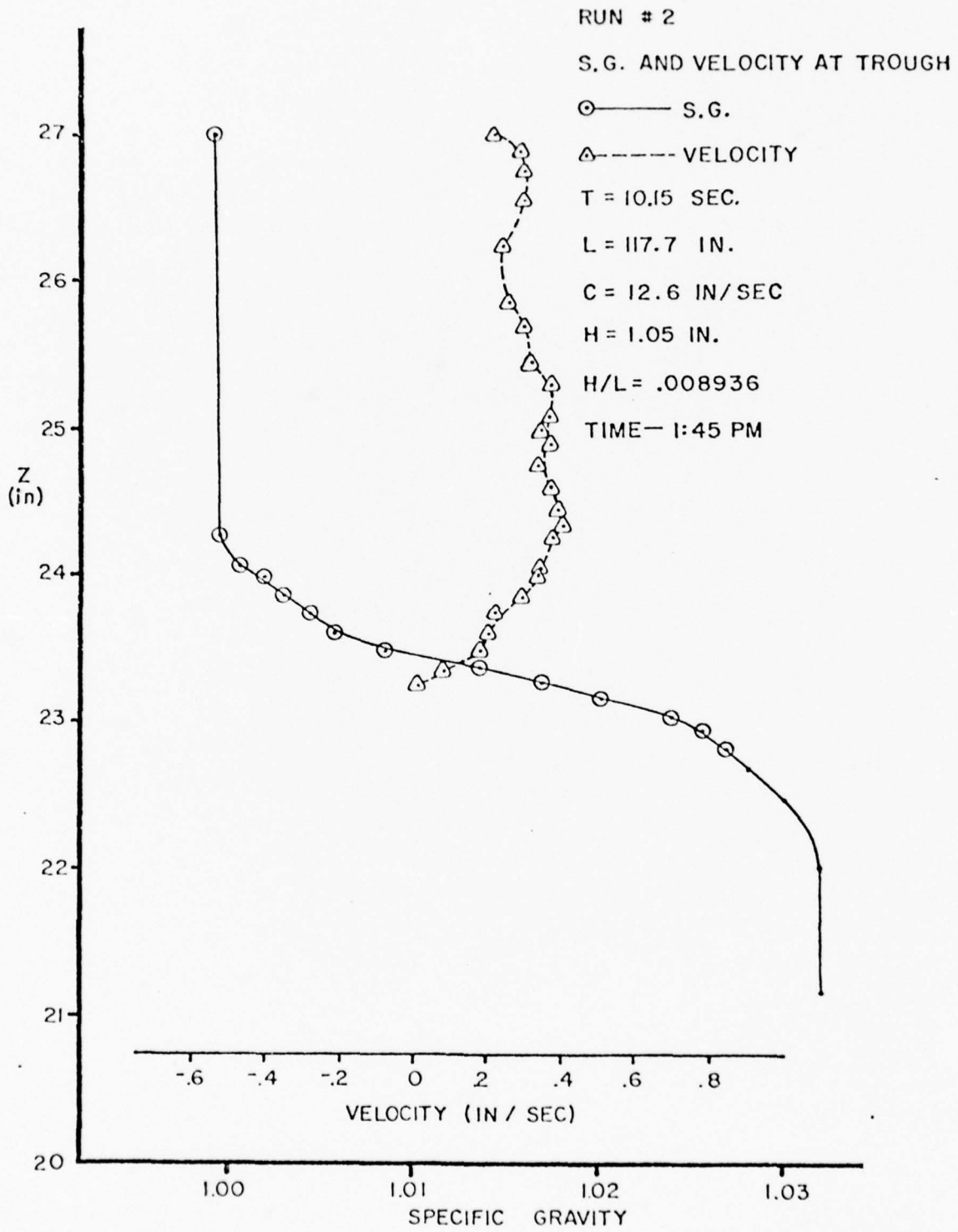


Figure 24. Density and Velocity Profiles at Wave Trough, Run #2

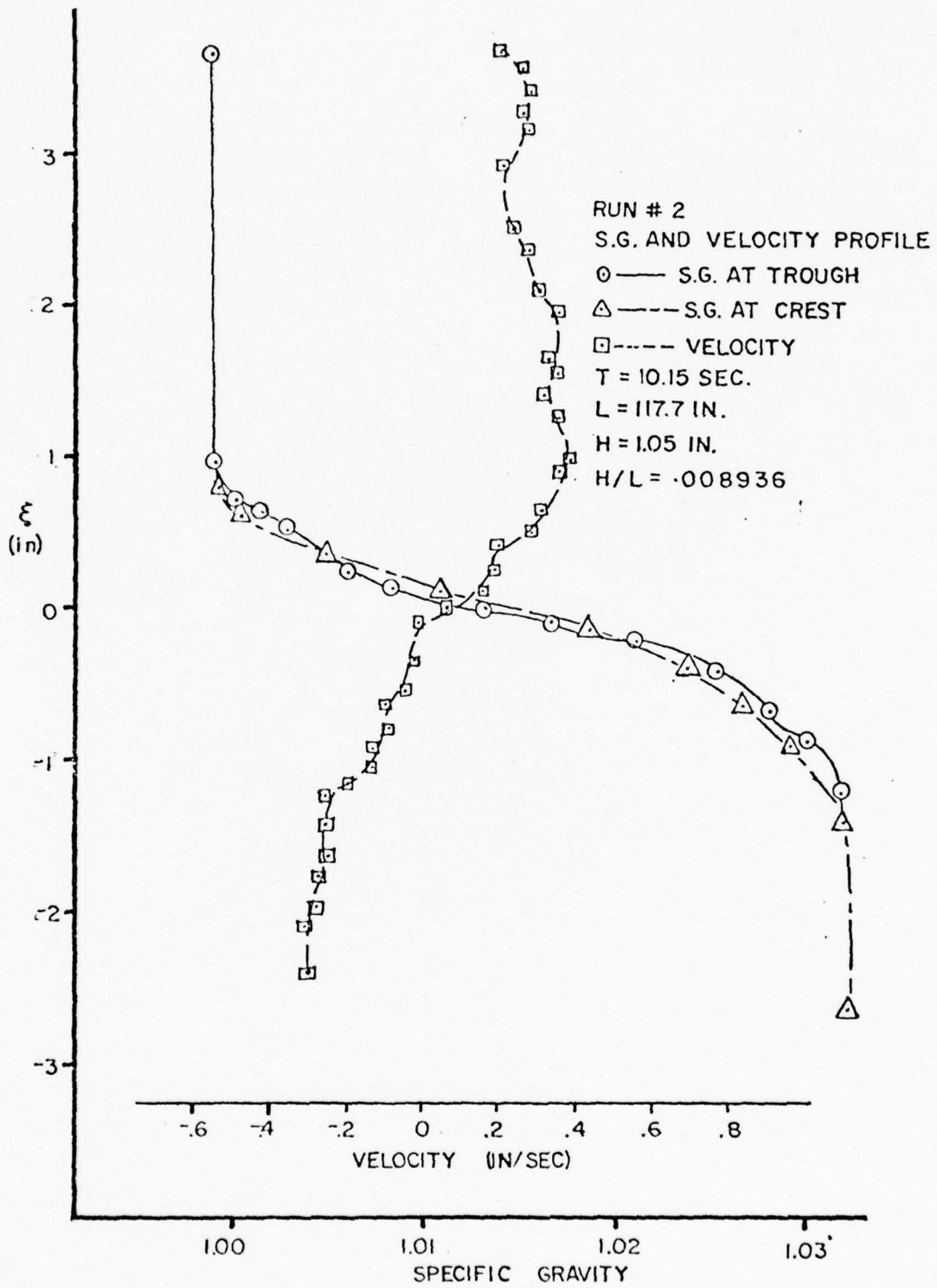


Figure 25. Comparison Between Wave Crest and Trough, Run #2

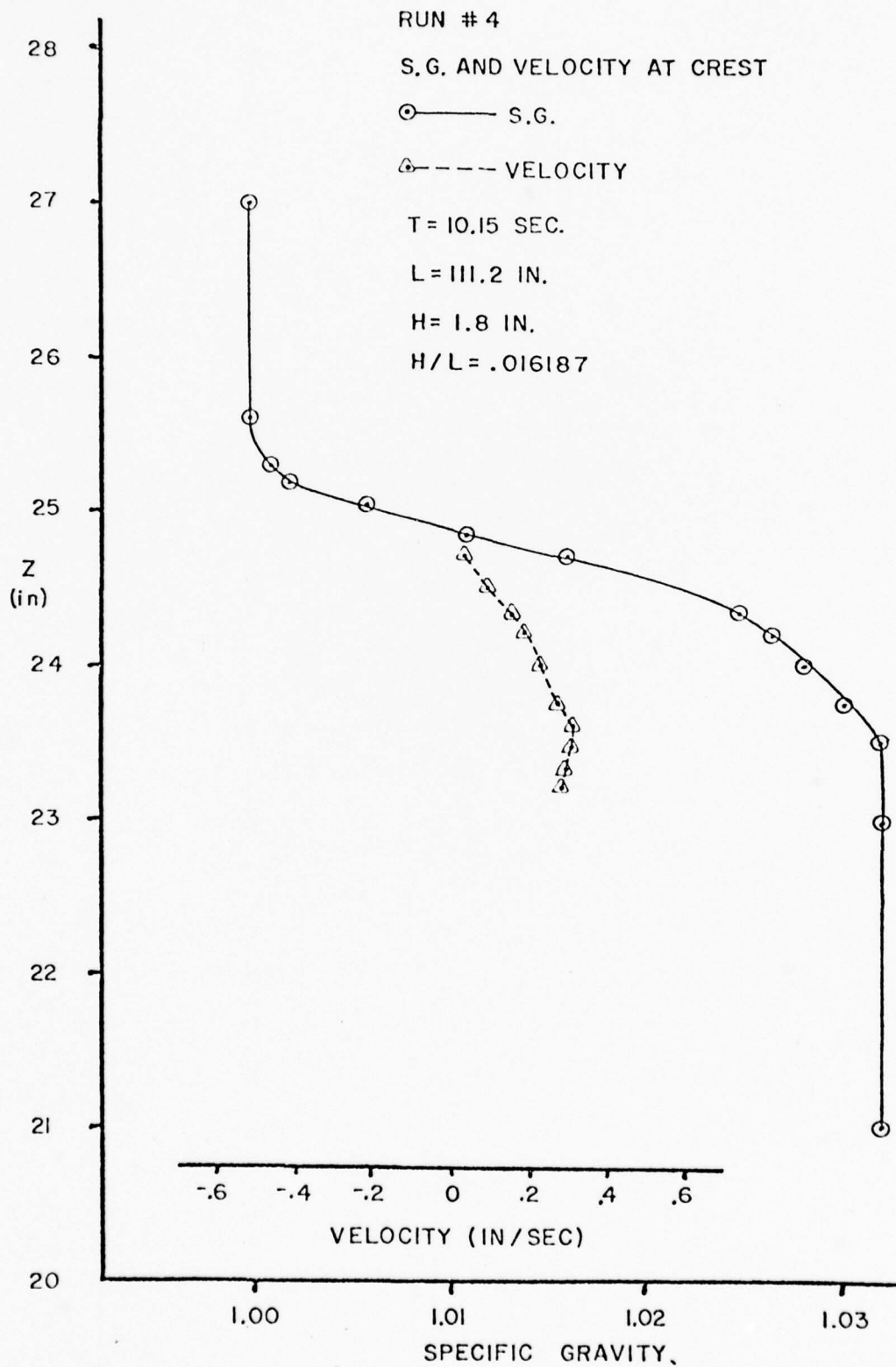


Figure 26. Density and Velocity Profiles at Wave Crest, Run #4

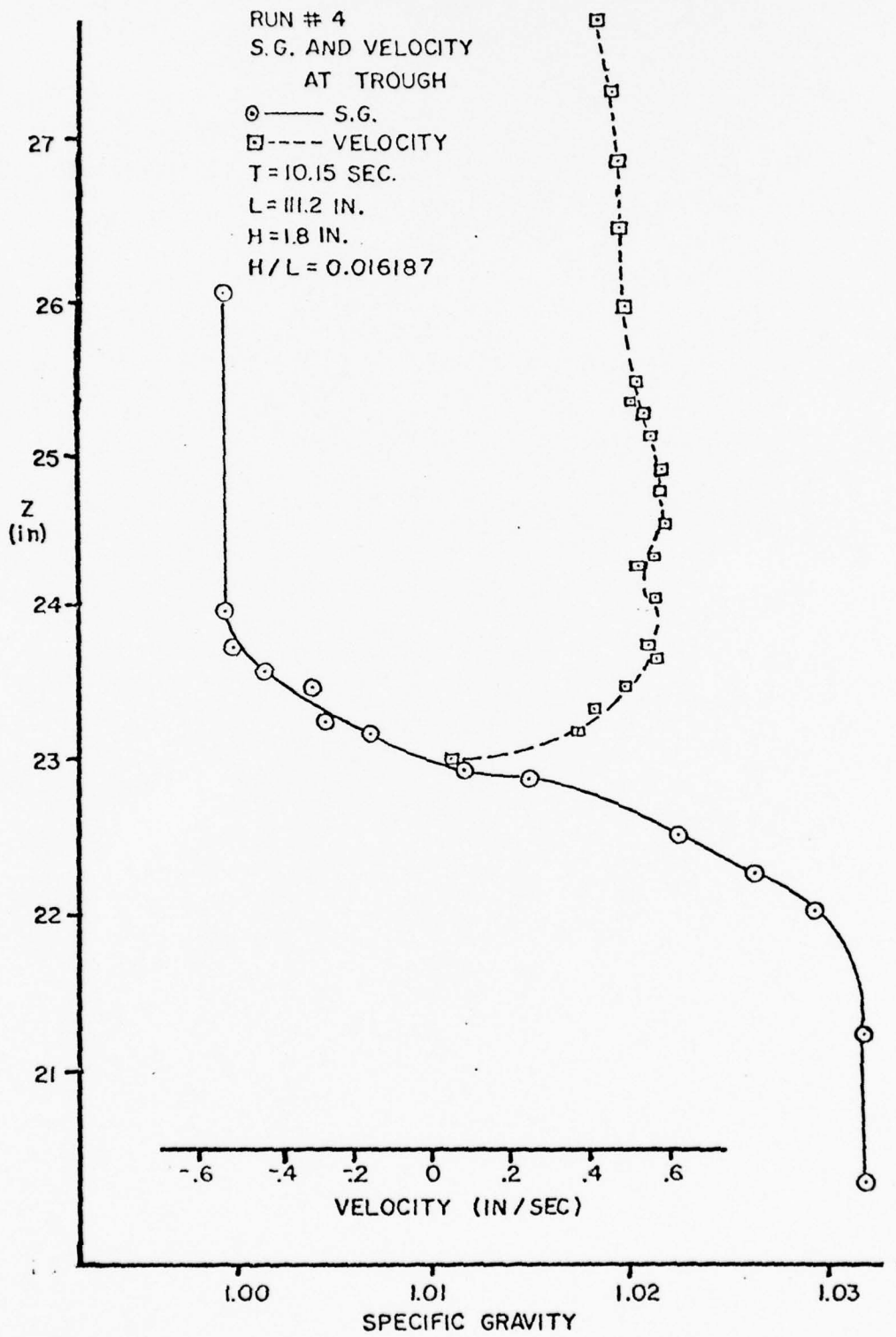


Figure 27. Density and Velocity Profiles at Wave Trough, Run #4

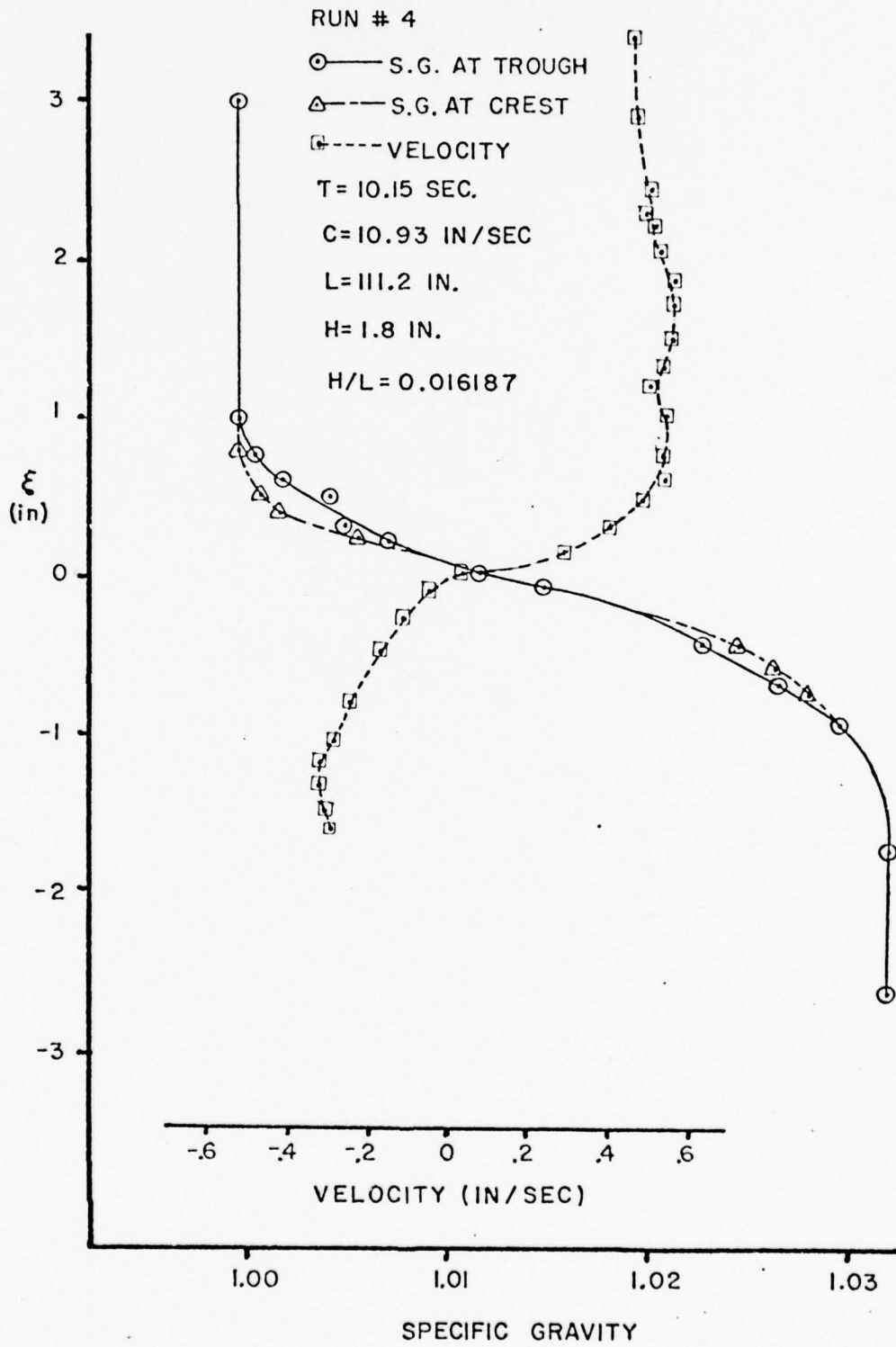


Figure 28. Comparison Between Wave Crest and Trough, Run #4

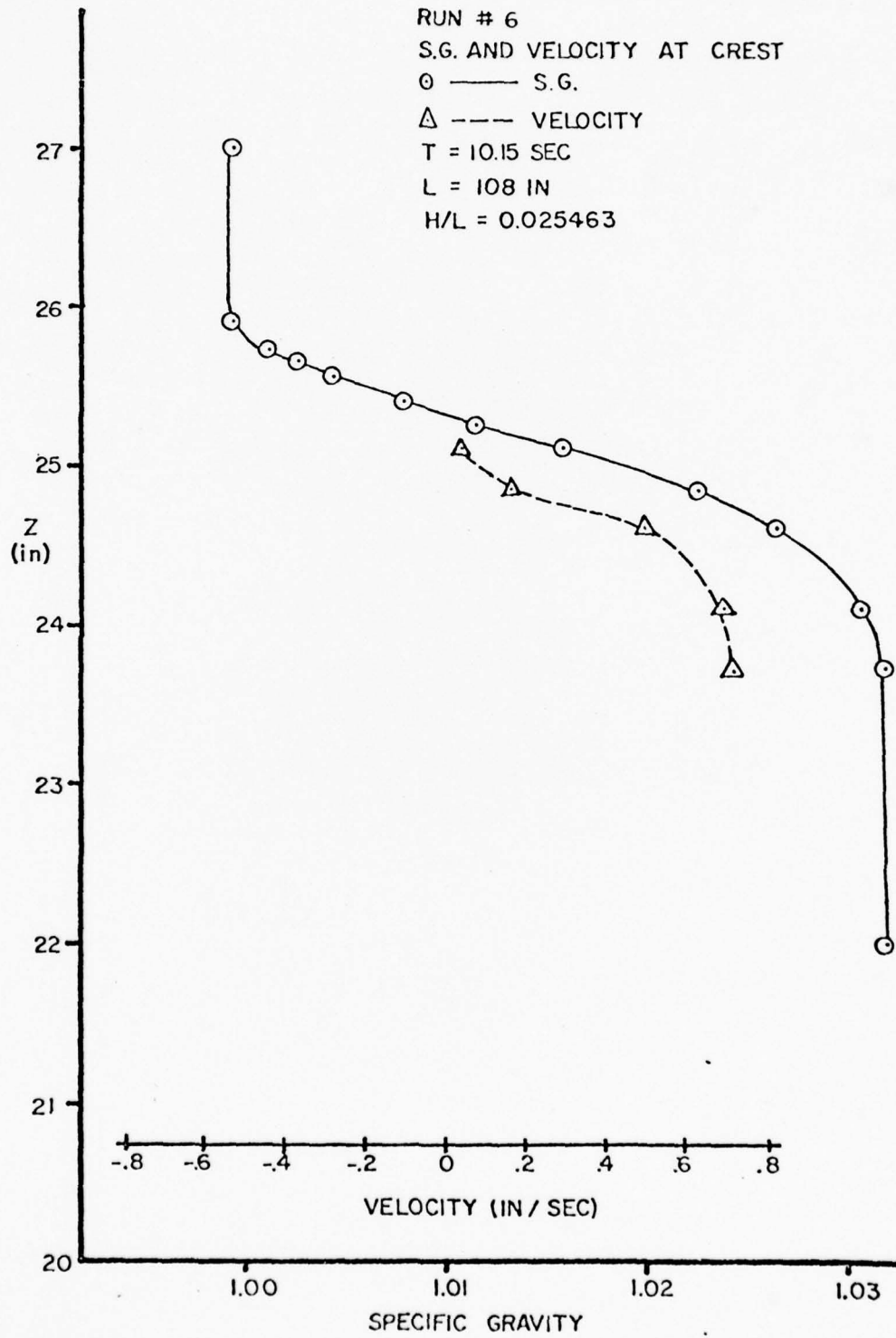


Figure 29. Density and Velocity Profiles at Wave Crest, Run #6

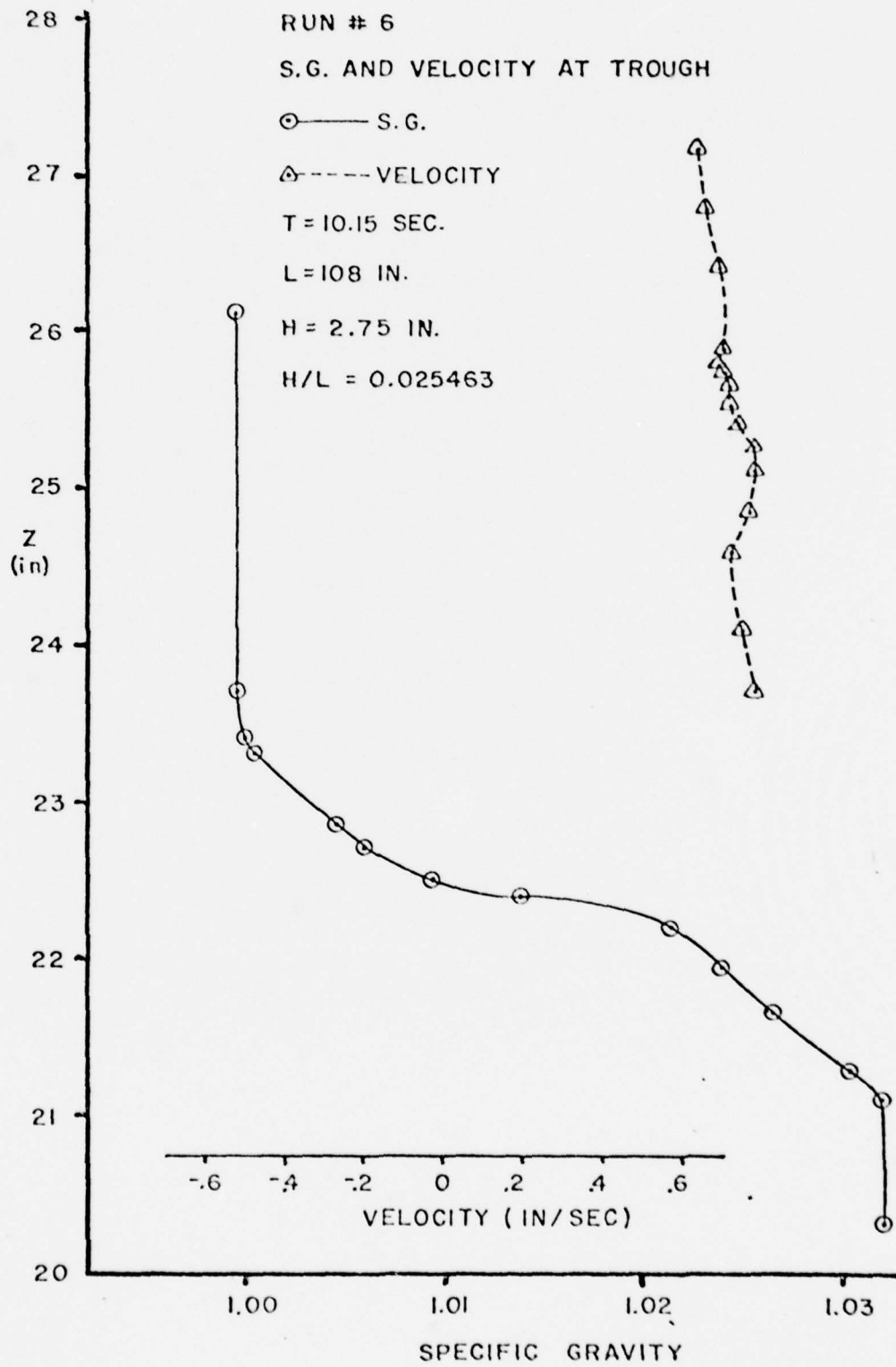


Figure 30. Density and Velocity Profiles at Wave Trough, Run #6

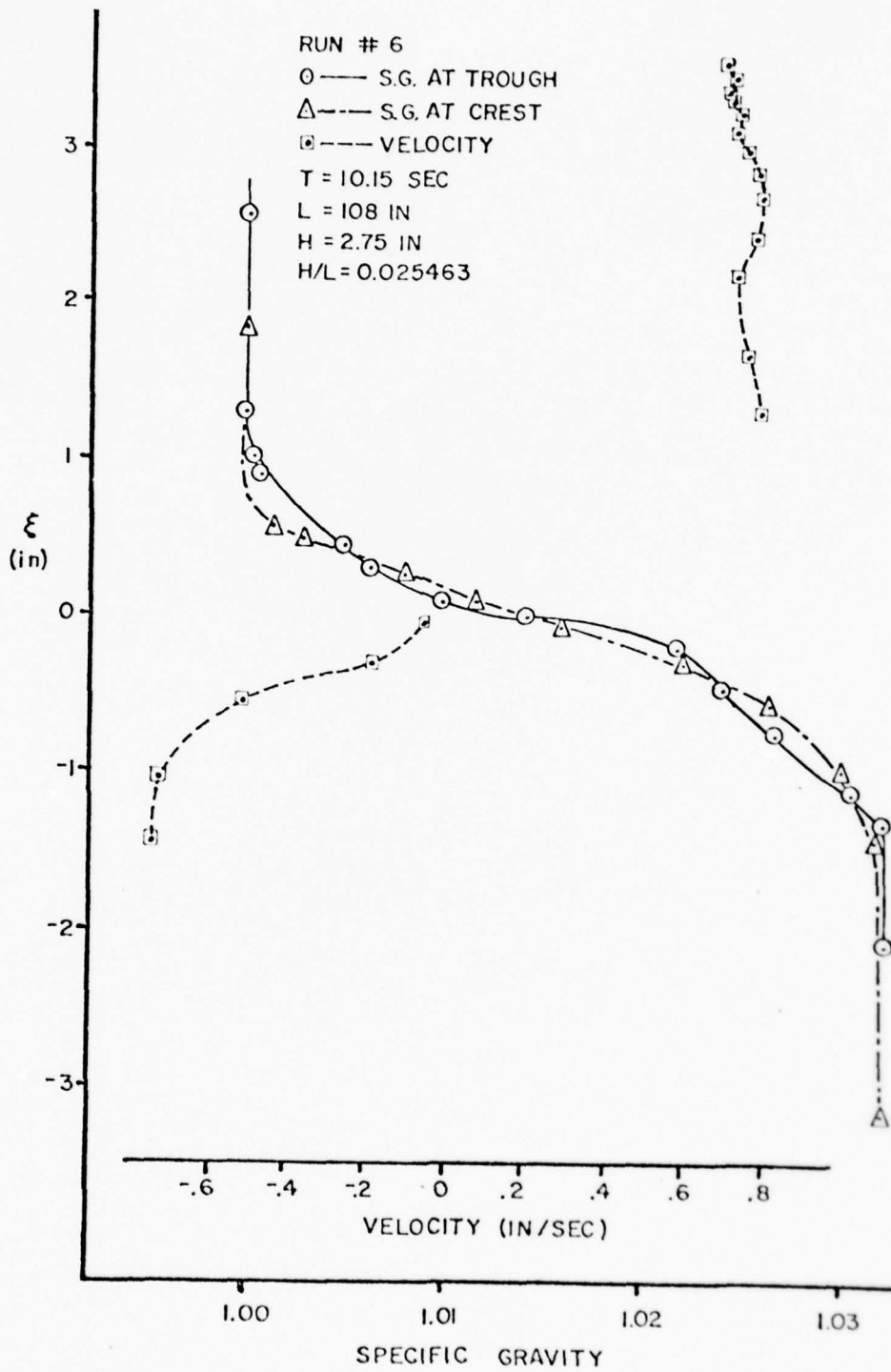


Figure 31. Comparison Between Wave Crest and Trough, Run #6

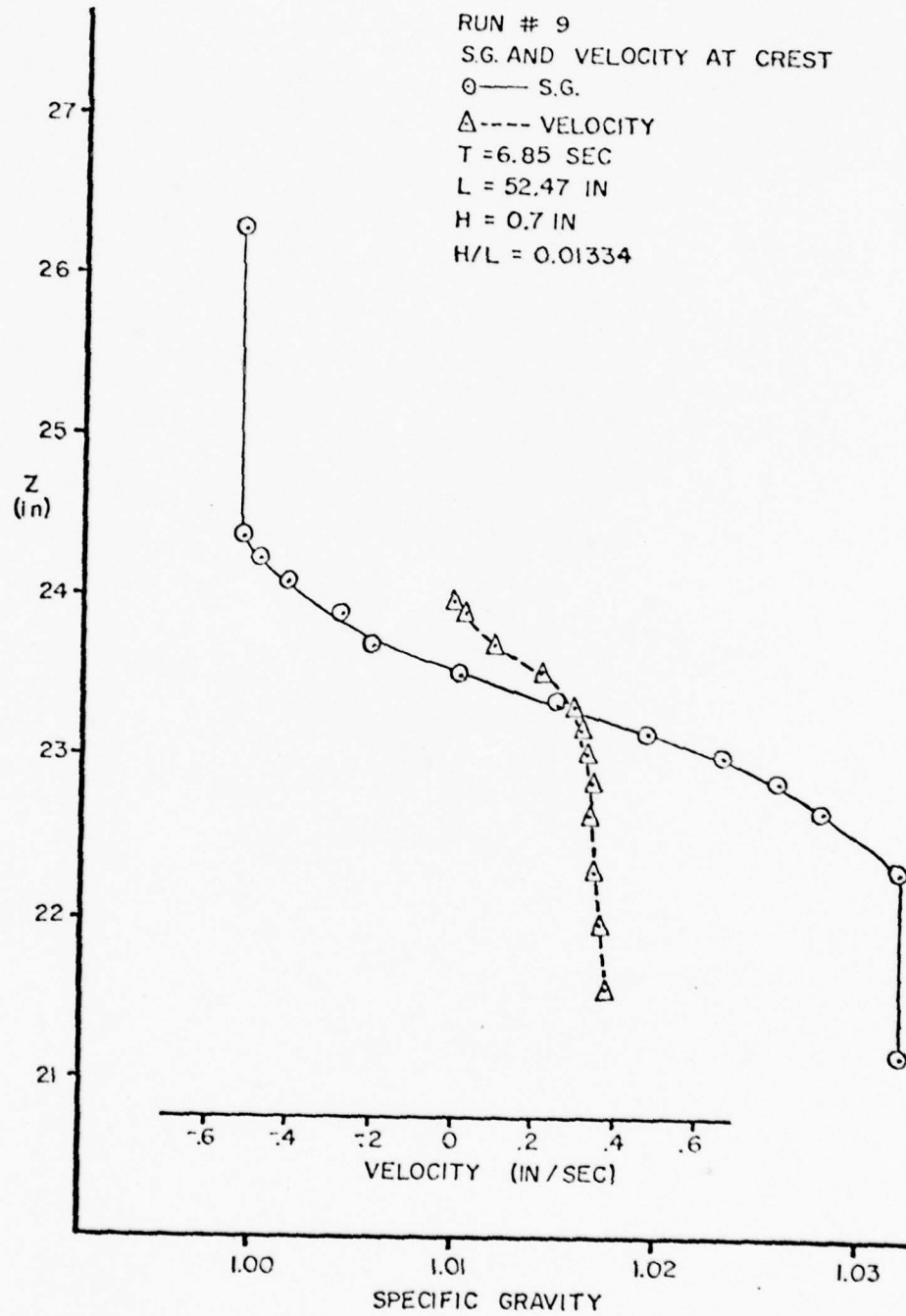


Figure 32. Density and Velocity Profiles at Wave Crest, Run #9

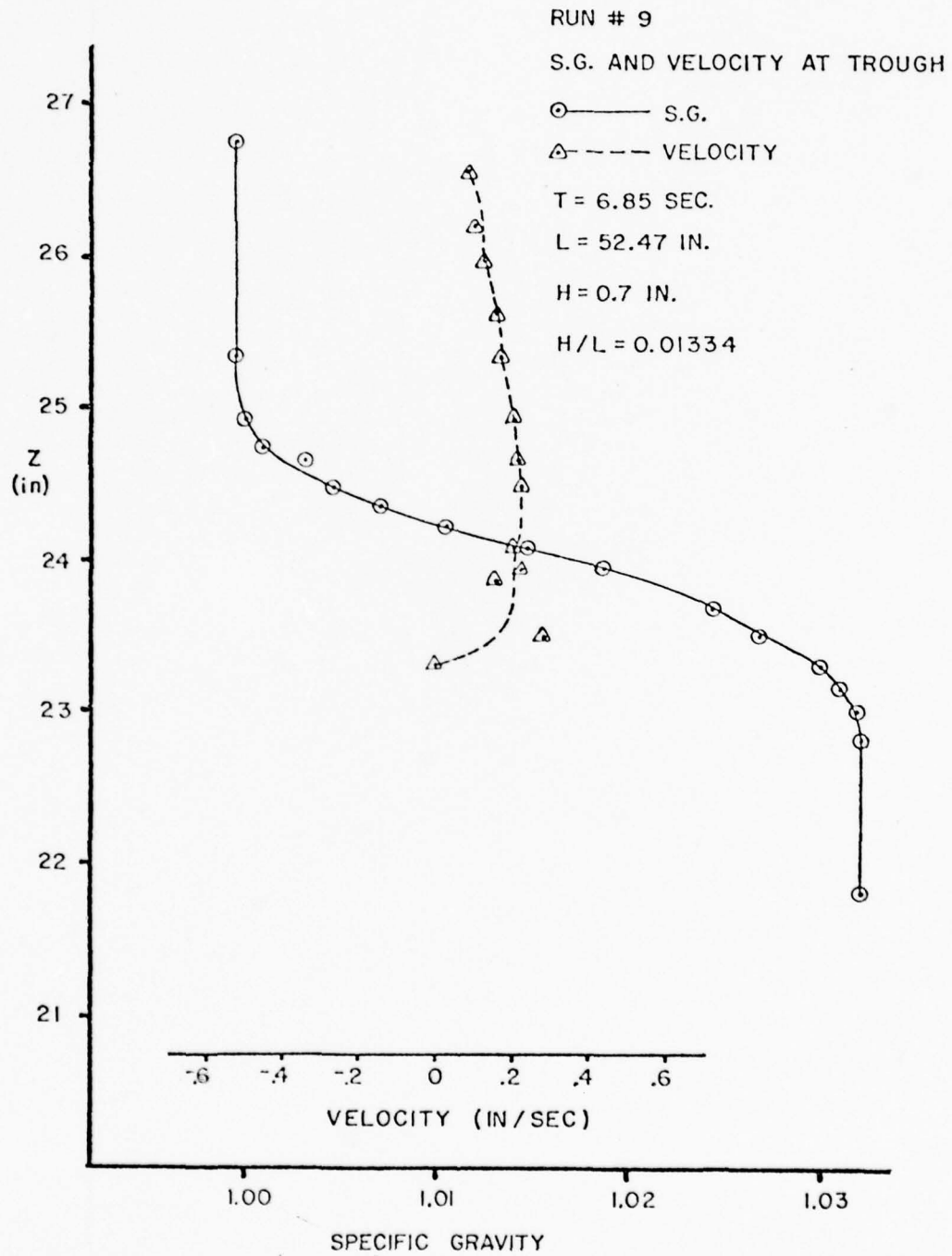


Figure 33. Density and Velocity Profile at Wave Trough, Run #9

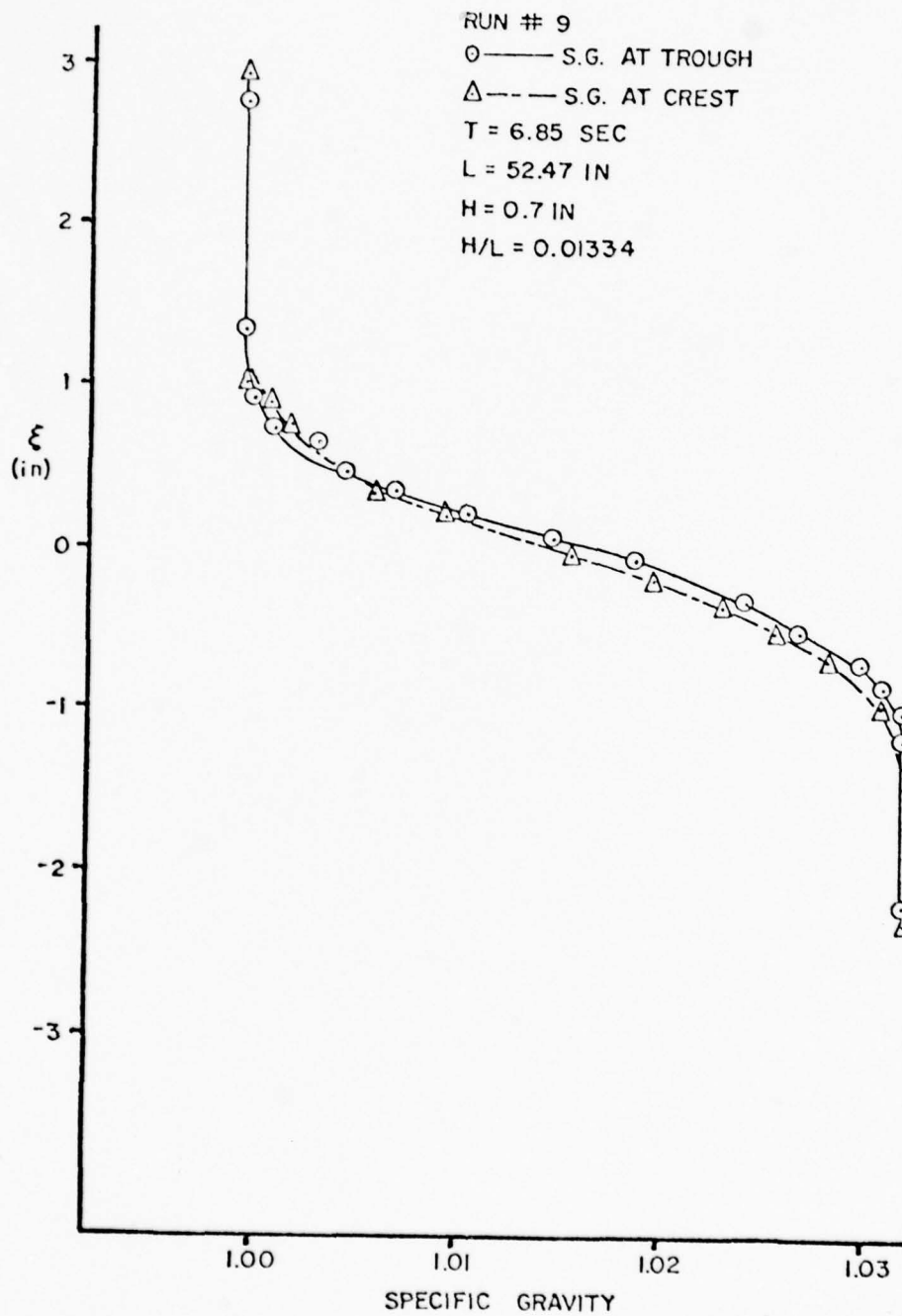


Figure 34. Comparison Between Wave Crest and Trough, Run #9

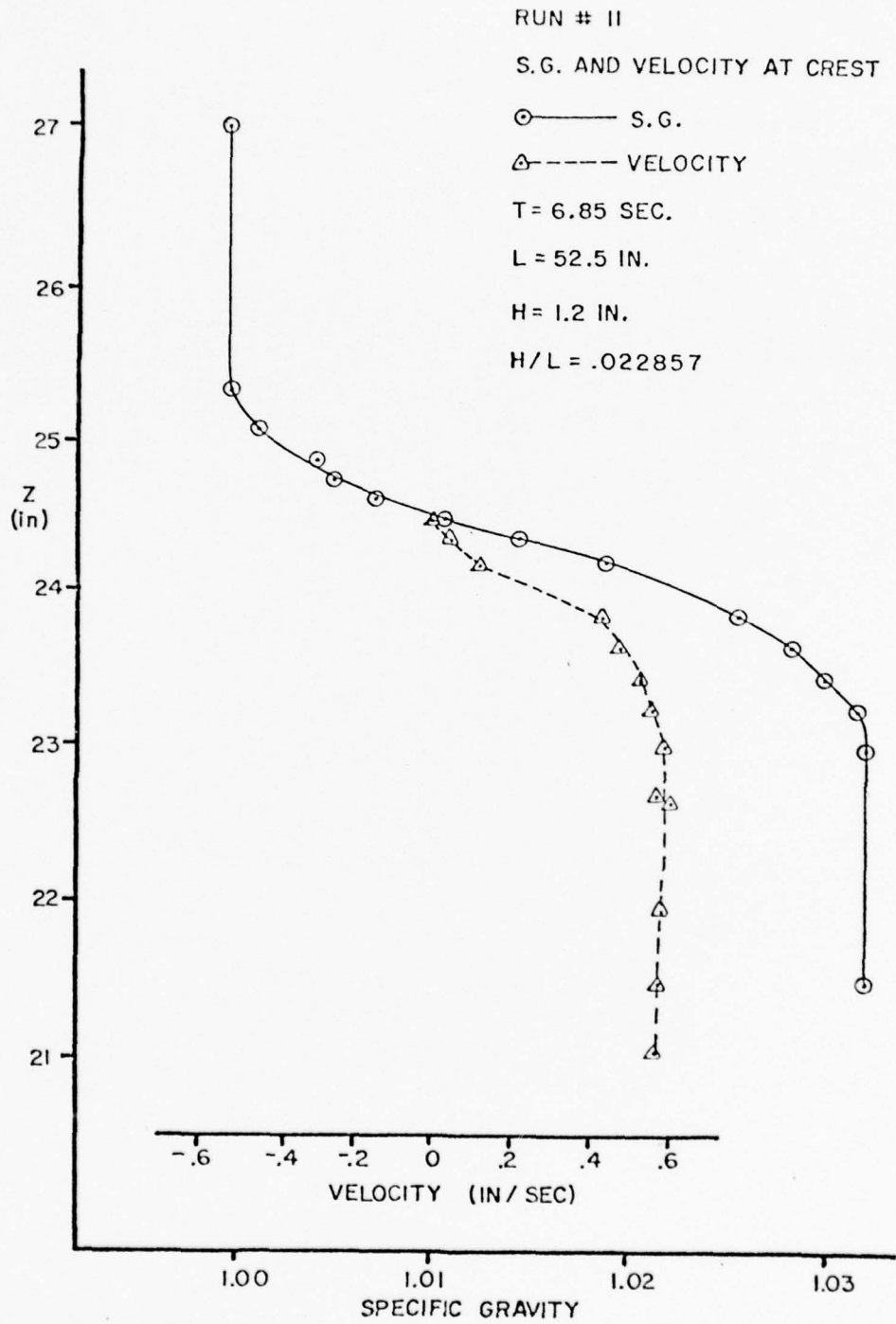


Figure 35. Density and Velocity Profiles at Wave Crest, Run #11

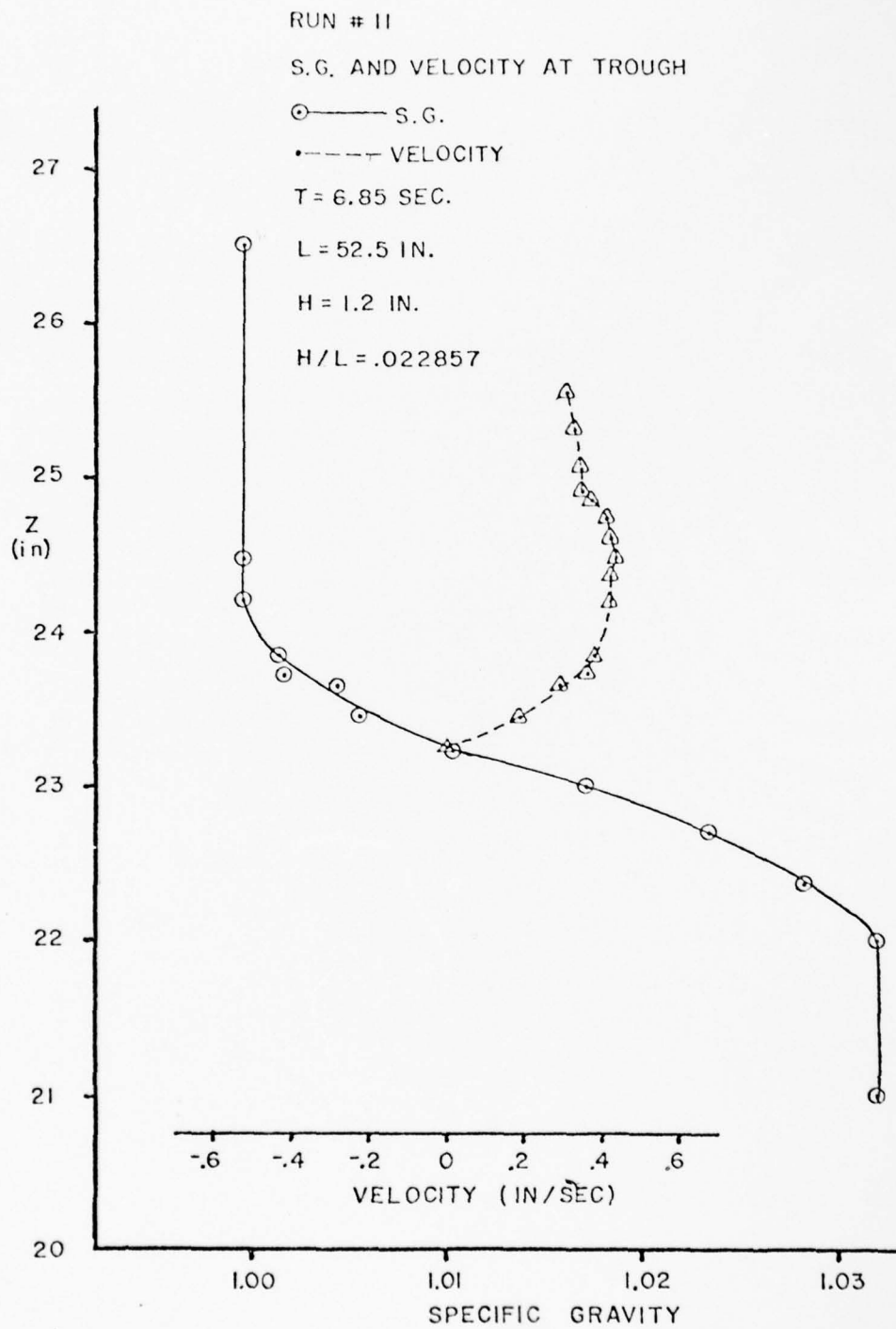


Figure 36. Density and Velocity Profiles at Wave Trough, Run #11

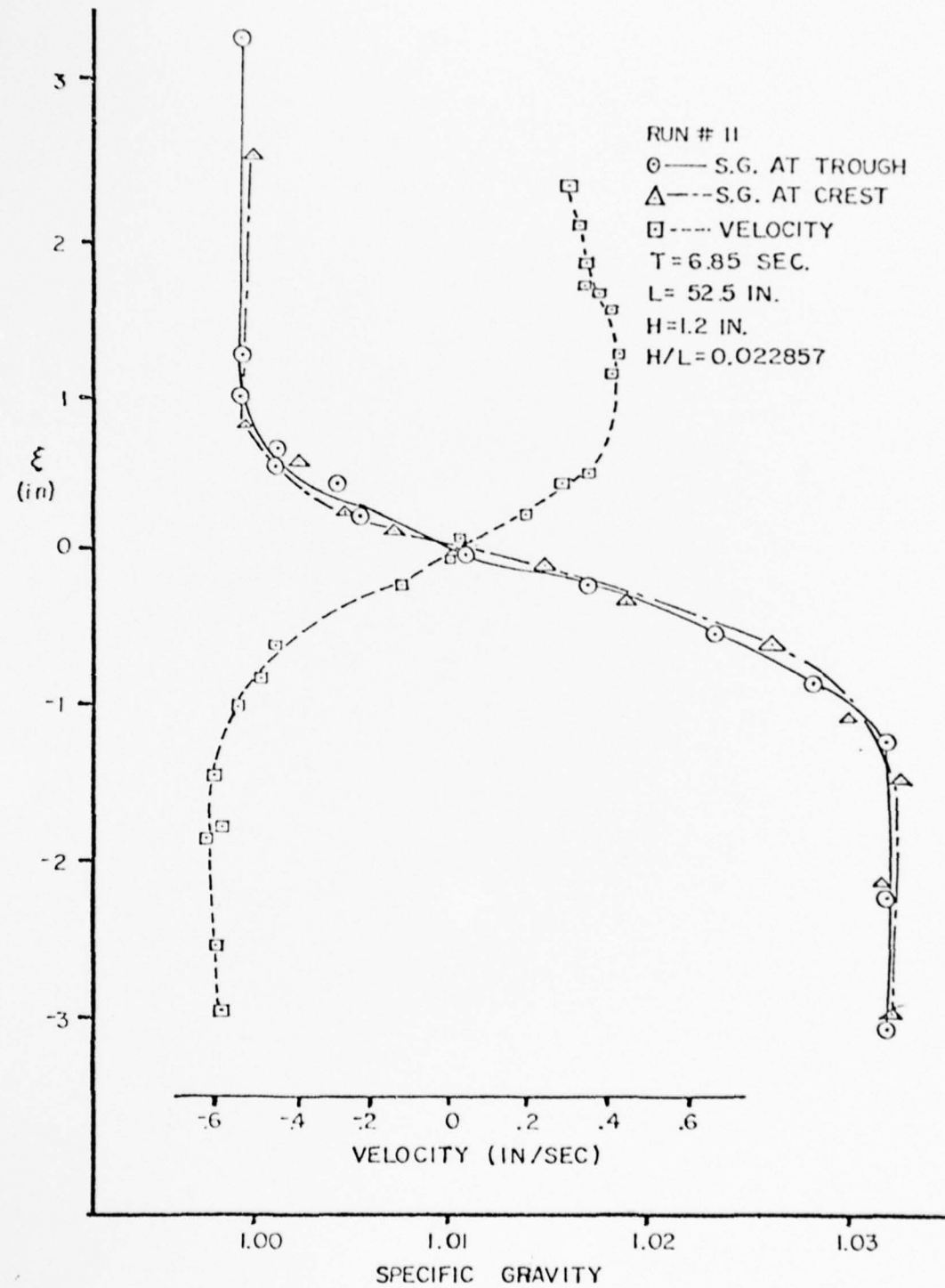


Figure 37. Comparison Between Wave Crests and Trough, Run #11

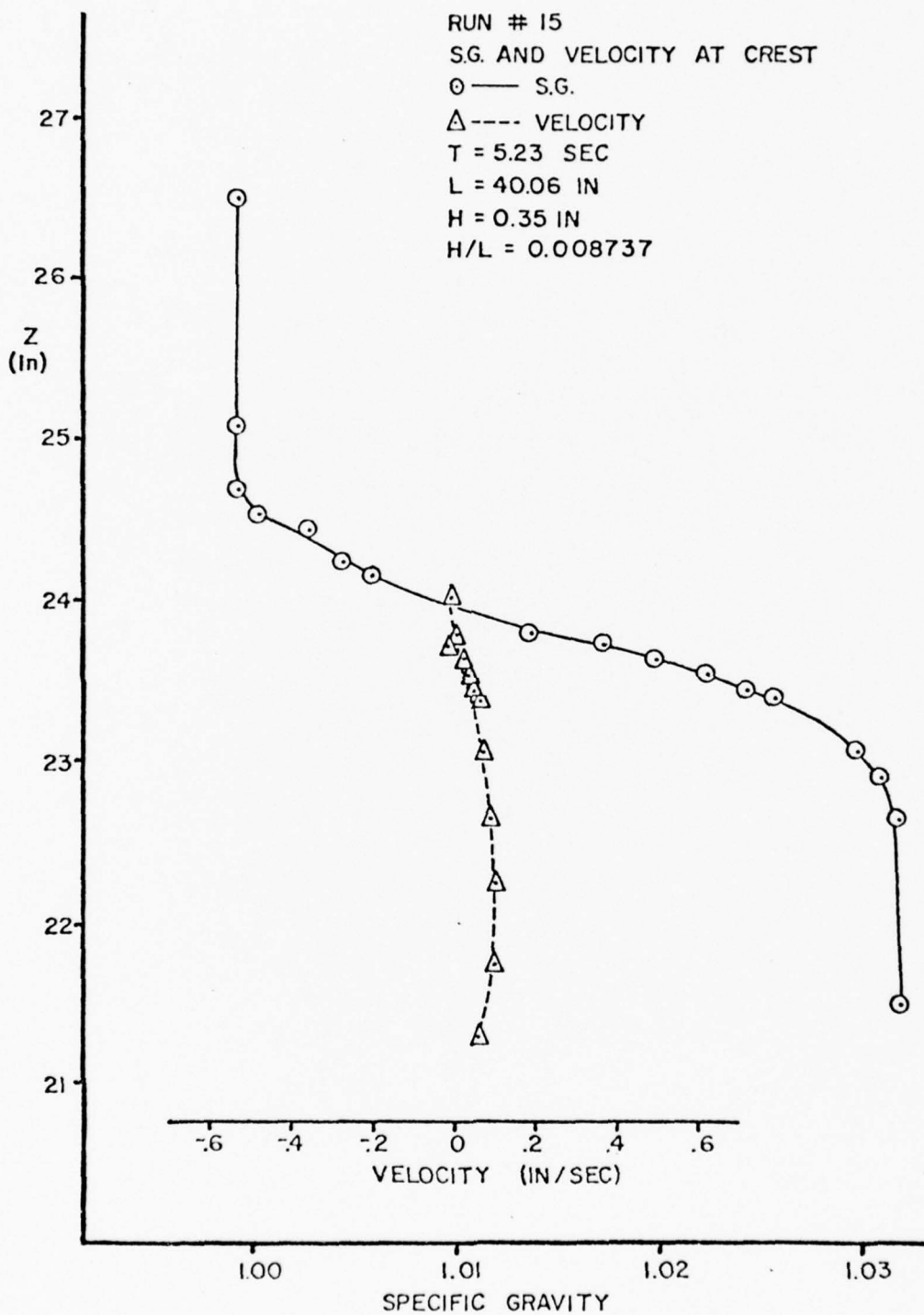


Figure 38. Density and Velocity Profiles at Wave Crest, Run #15

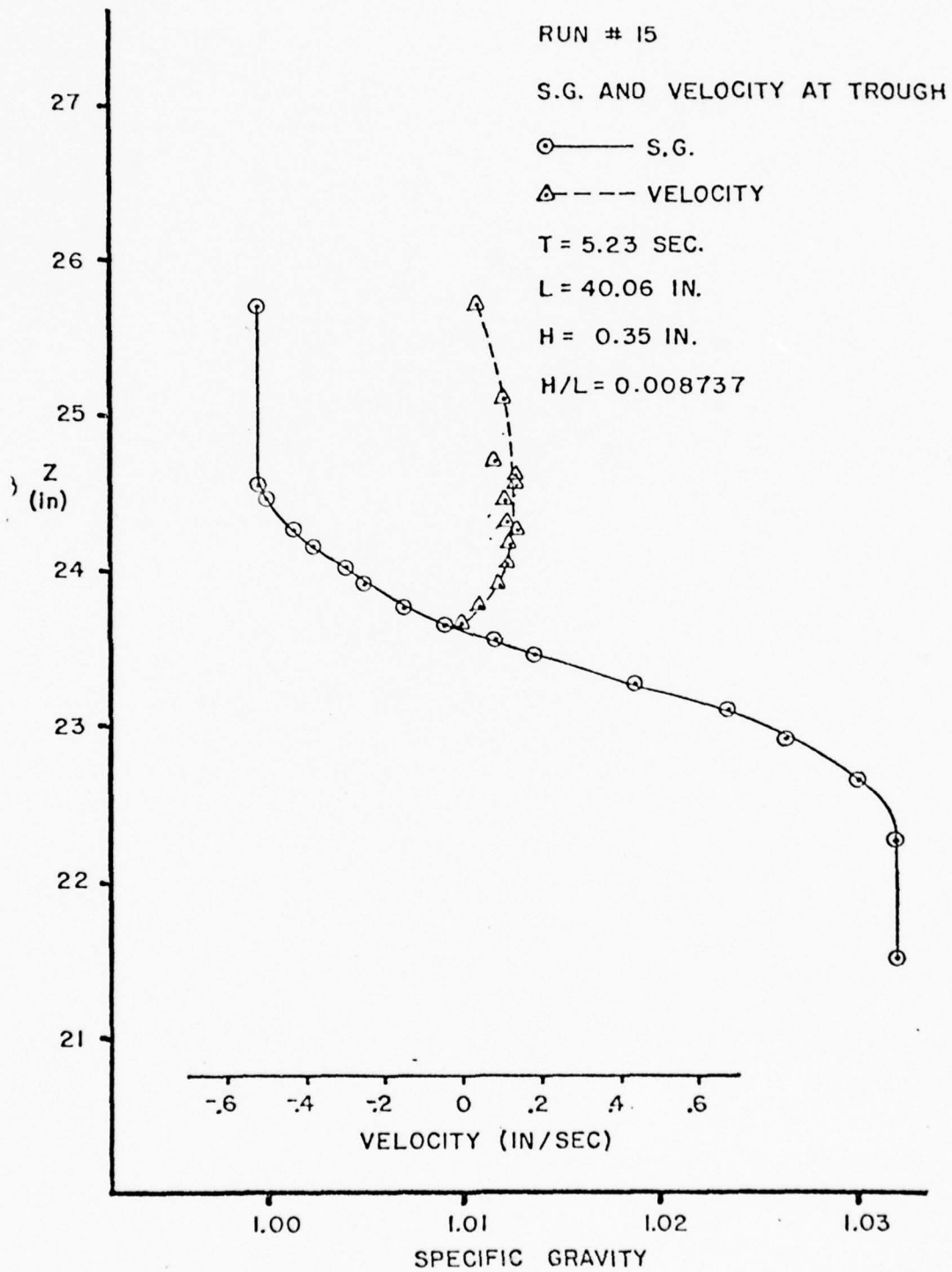


Figure 39. Density and Velocity Profiles at Wave Trough, Run #15

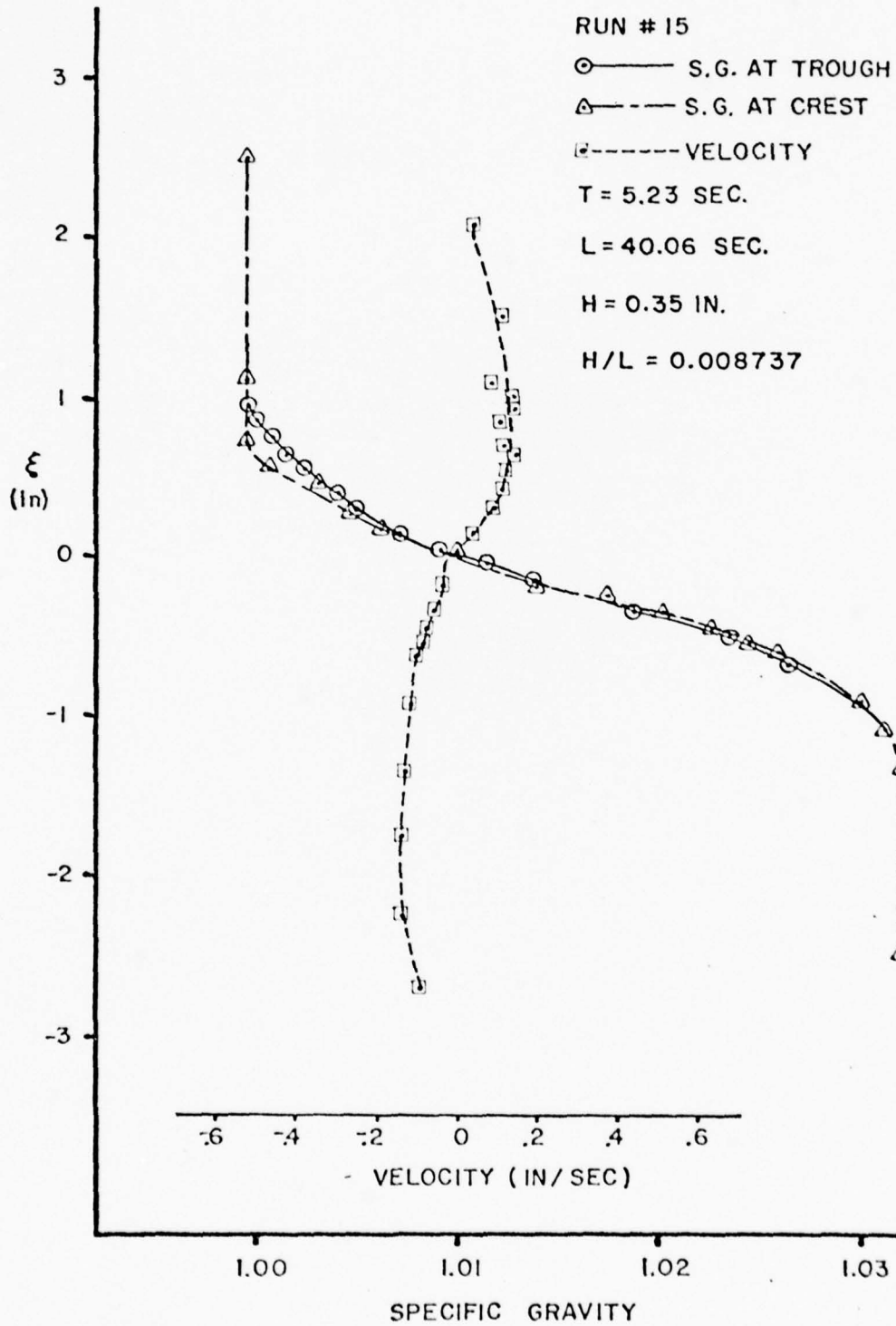


Figure 40. Comparison Between Wave Crest and Trough, Run #15

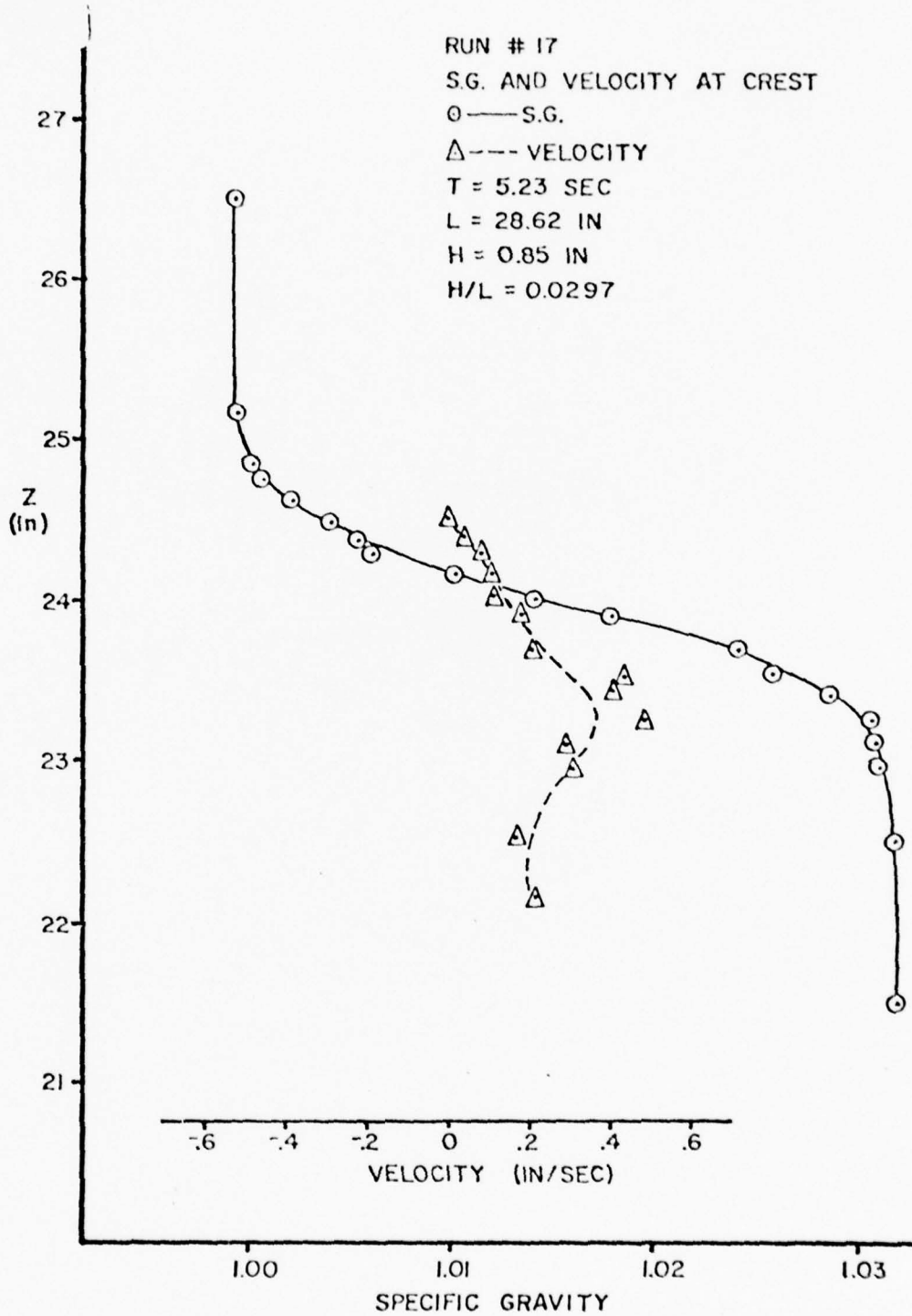


Figure 41. Density and Velocity Profiles at Wave Crest, Run #17

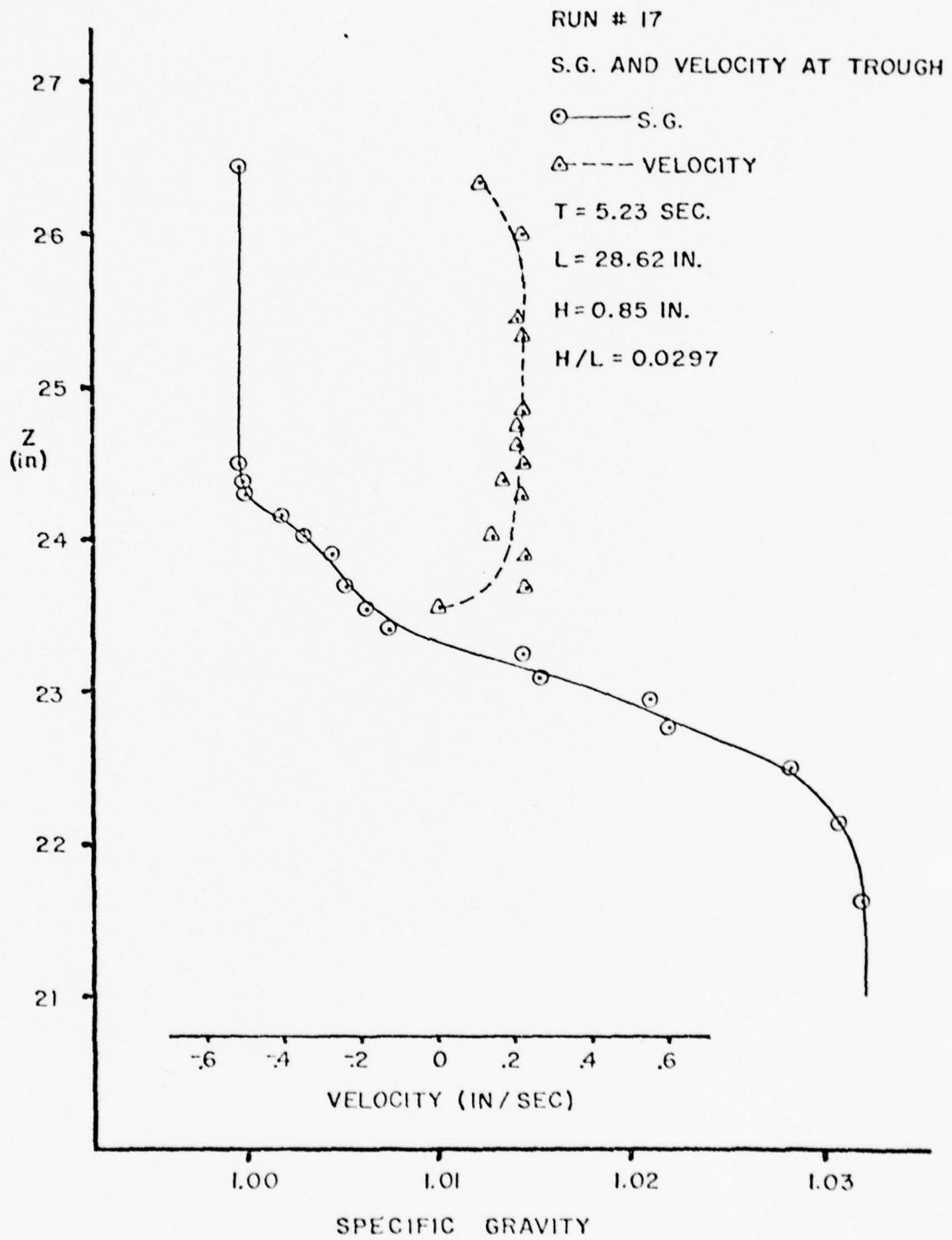


Figure 42. Density and Velocity Profiles at Wave Trough, Run #17

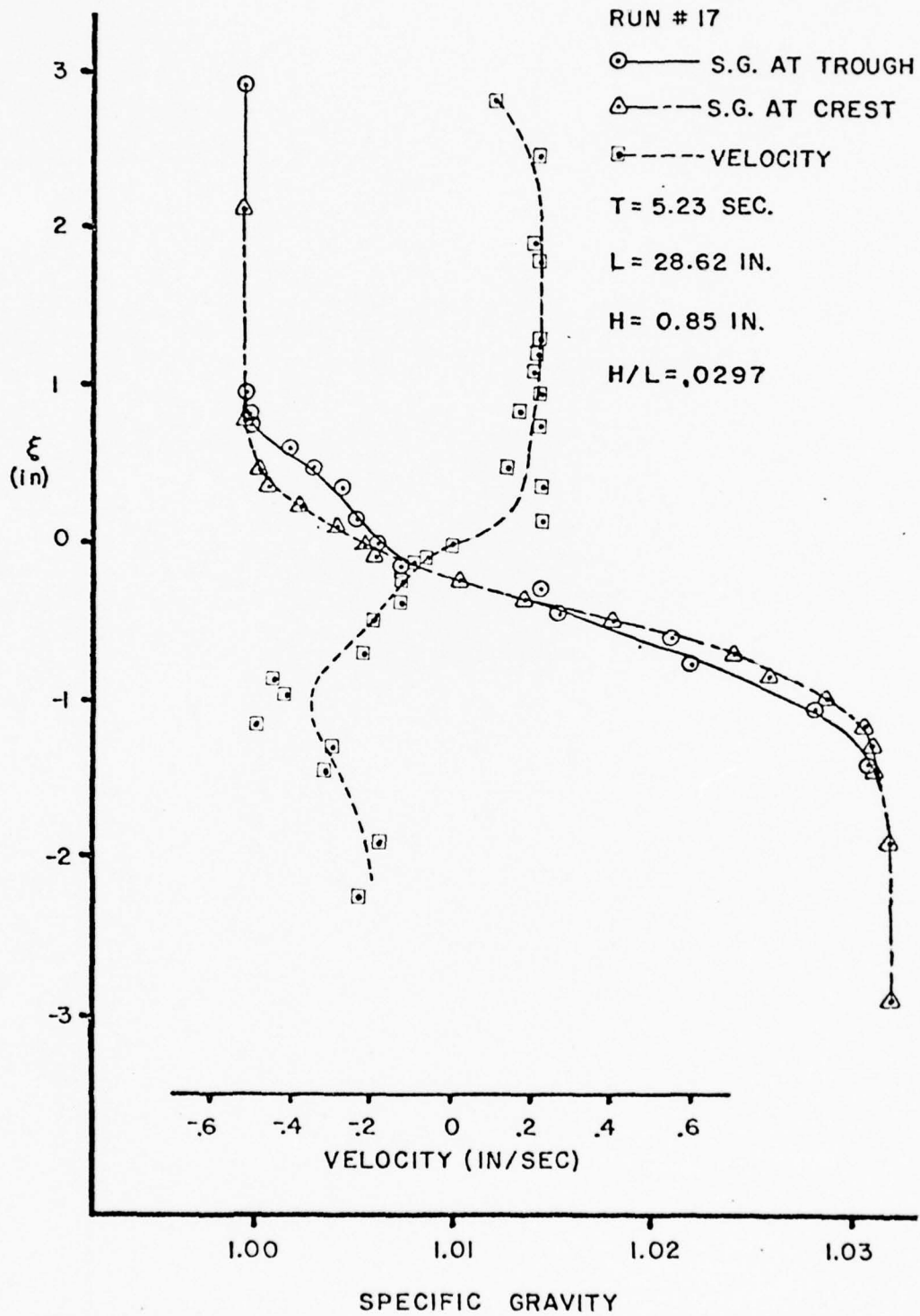


Figure 43. Comparison Between Wave Crest and Trough, Run #17

The wave height H_t can be determined by superimposing the density profiles at the wave crests and troughs. It could also be obtained from the conductivity position plots made by the X-Y plotter during the experiments (see Figure 72 in the Appendix). The wave heights H_t are compared with the initial wave heights H_0 in Table 3.

TABLE 3

Run No.	H_0 (in)	H_t (in)	ΔH (in)	Remark
2	1.06	1.05	0.01	Stable
4	2.25	1.8	0.45	Transition
6	3.25	2.75	0.50	Unstable
9	0.87	0.7	0.17	Stable
11	1.38	1.2	0.18	Transition
15	0.63	0.35	0.28	Transition
17	1.25	0.85	0.40	Unstable

A simple computer program was written to calculate the Richardson number. Richardson number and Brunt-Väisälä frequency profiles are presented in Figures 44 through Figure 58. The minimum value on the Richardson number profile for each experiment is tabulated in Table 4. These values will be denoted by R_{imin} . It should be noted that in Figures 44 through Figure 58, the Richardson number becomes zero at points above and below the interface. This results from the density gradient going to zero at these points. For a homogeneous fluid the Richardson number has no meaning and thus ceases to be a stability parameter.

Interfacial waves were not generated by waves with small steepness ratios. As the steepness ratio was increased the interfacial waves formed and the internal wave height was reduced. The energy in internal waves

is proportional to the square of the wave height. Since the wave maker constantly supplies energy to these waves, a reduction in wave height would indicate that energy is being dissipated or transferred to another part of the flow. From Table 3 it can be seen that every reduction in wave height was preceded by the formation of interfacial waves. It thus appears that energy is transferred from the long internal waves to the interfacial waves once unstable conditions are reached.

TABLE 4

Run No.	Min R_i	Remark
2	15.24	Stable
4	1.02	Transition
6	1.96	Unstable
11	5.55	Transition
15	3.19	Transition
17	2.34	Unstable

When the wave height was reduced the steepness ratio and thus the velocity gradient in the interfacial layer were reduced accordingly. This would have a stabilizing effect on the flow. As would be expected, the interfacial waves ceased to exist after a period of time (approximately 5 to 10 minutes) and the internal wave height increased. The stabilizing effect of the reduction in steepness ratio caused the interfacial waves to transfer their energy back to the internal waves. There was very little energy dissipated in turbulence as evidenced by the essentially constant density profile in the interfacial layer throughout the experiment (see Figure 19).

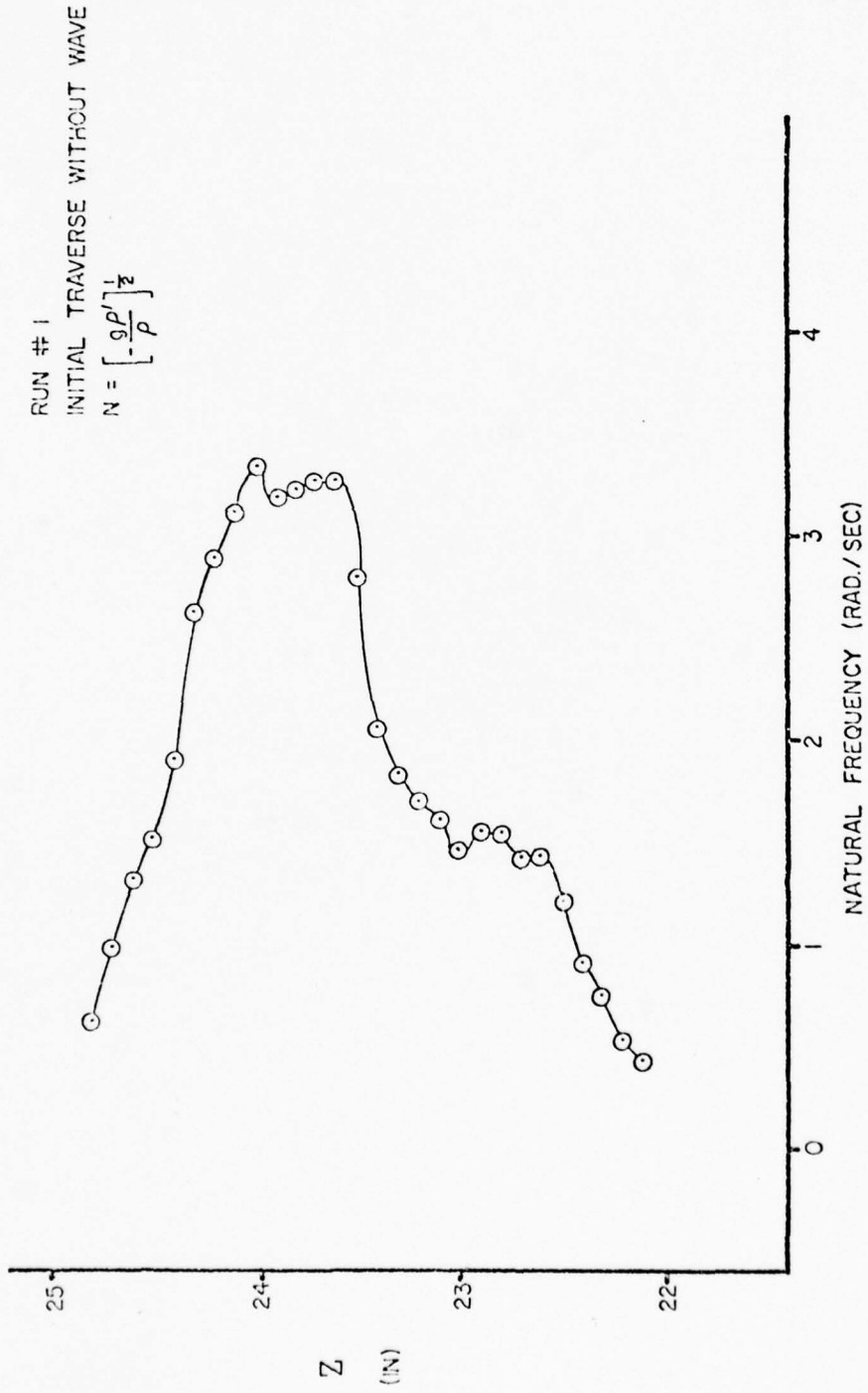


Figure 44. Natural Frequency Profile, Run #1

RUN #5
FINAL TRAVERSE WITHOUT WAVES

$$N = \left[-\frac{g\rho'}{\rho} \right]^{\frac{1}{2}}$$

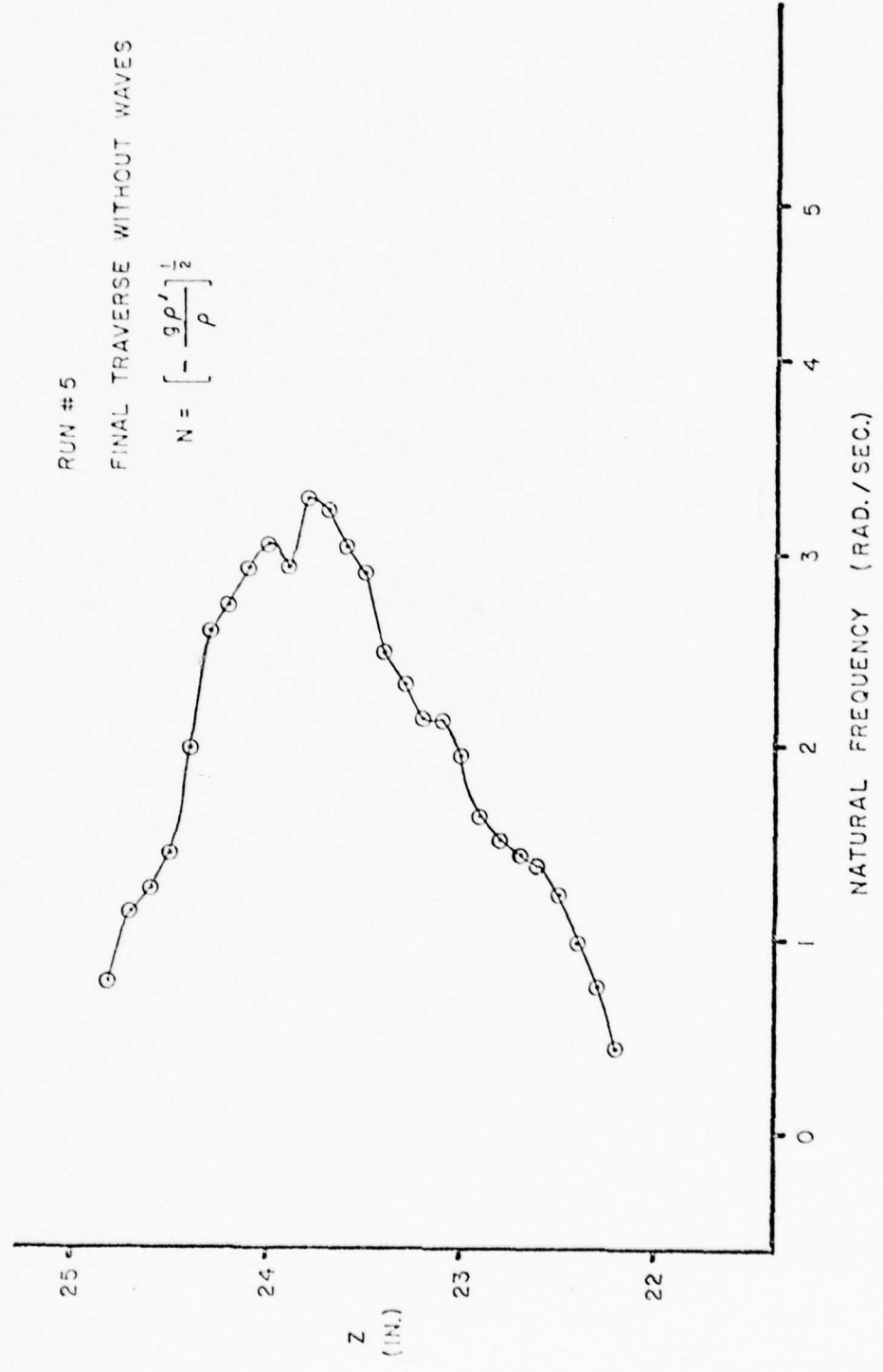


Figure 45. Natural Frequency Profile, Run #5

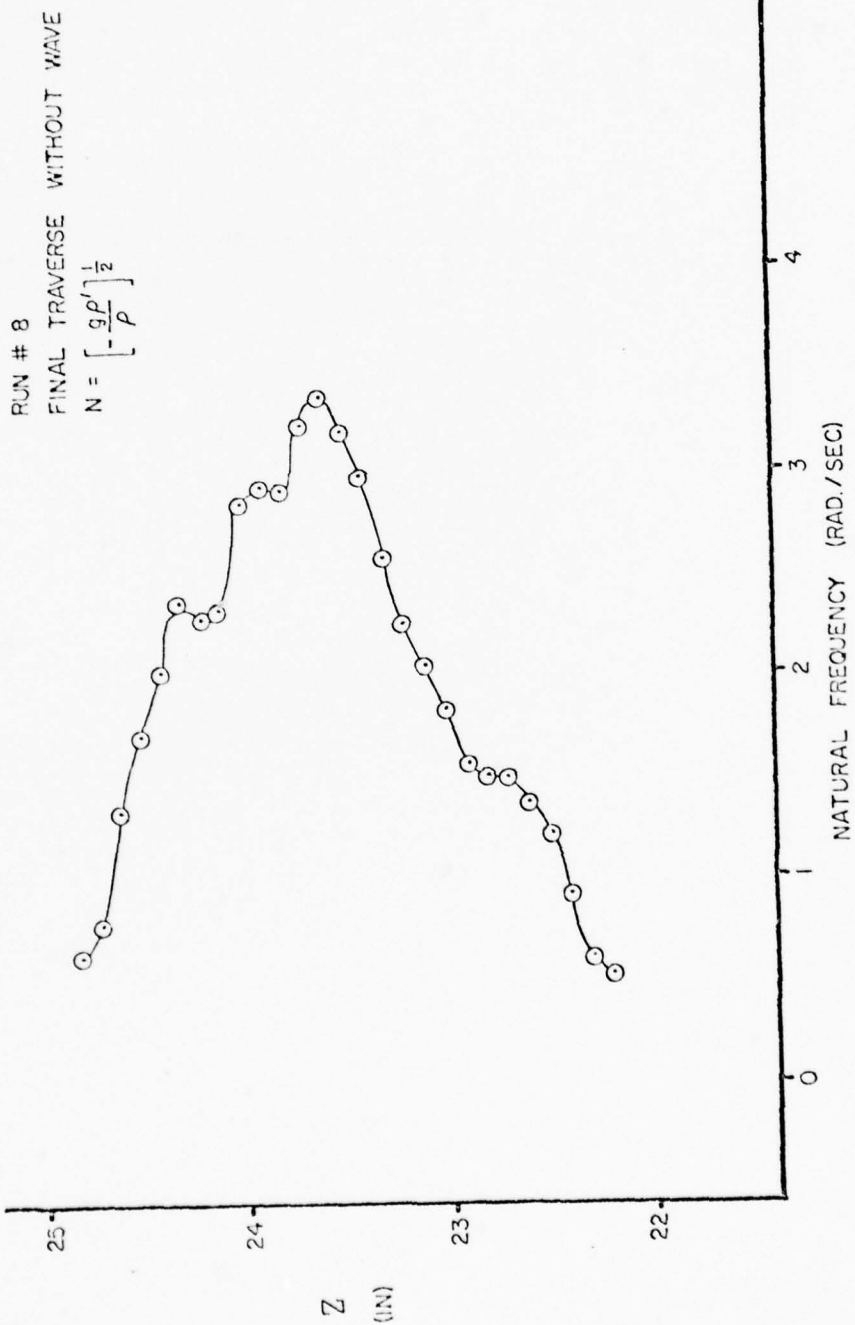


Figure 46. Natural Frequency Profile, Run #8

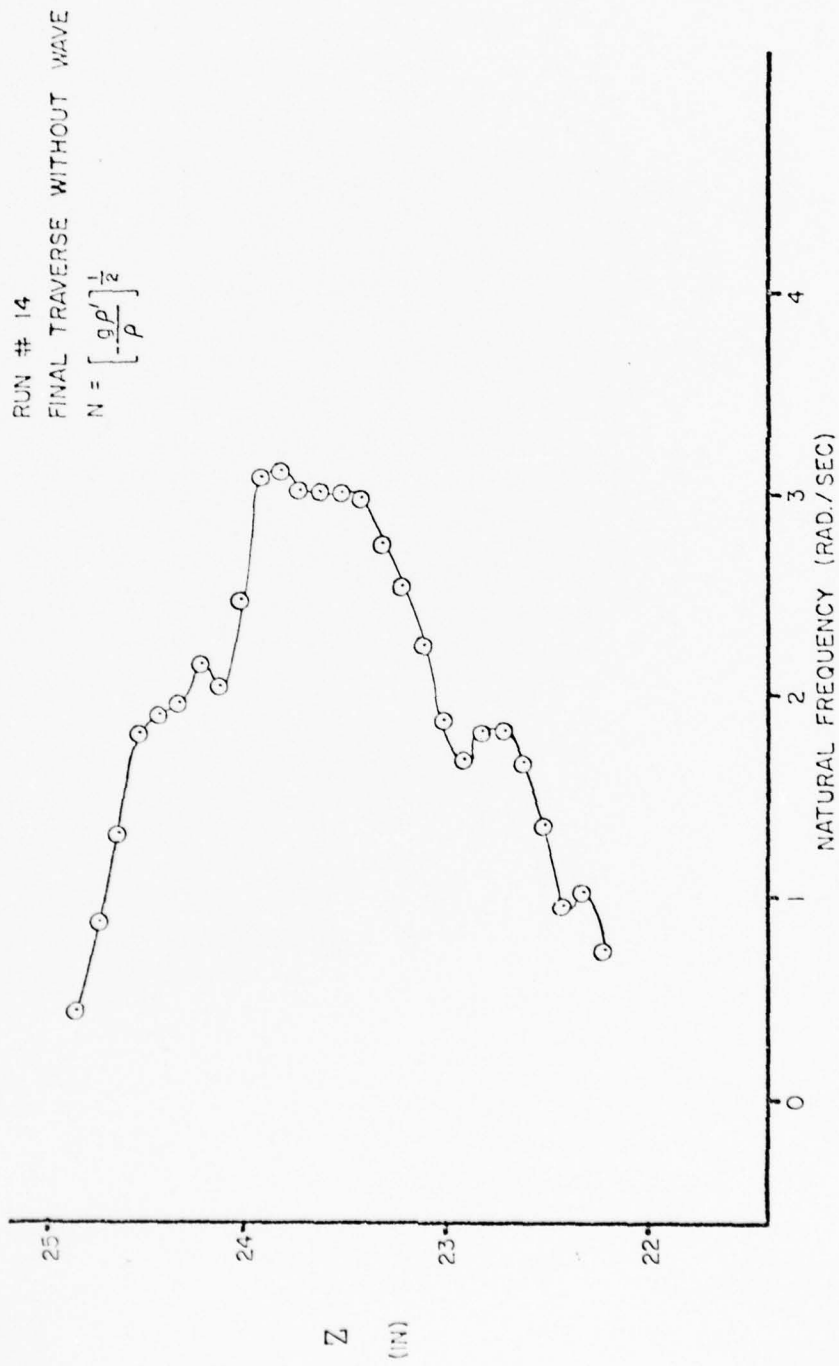


Figure 47. Natural Frequency Profile, Run #14

RUN # 19
 FINAL TRAVERSE WITHOUT WAVE

$$N = \left[-\frac{g\rho'}{\rho} \right]^{1/2}$$

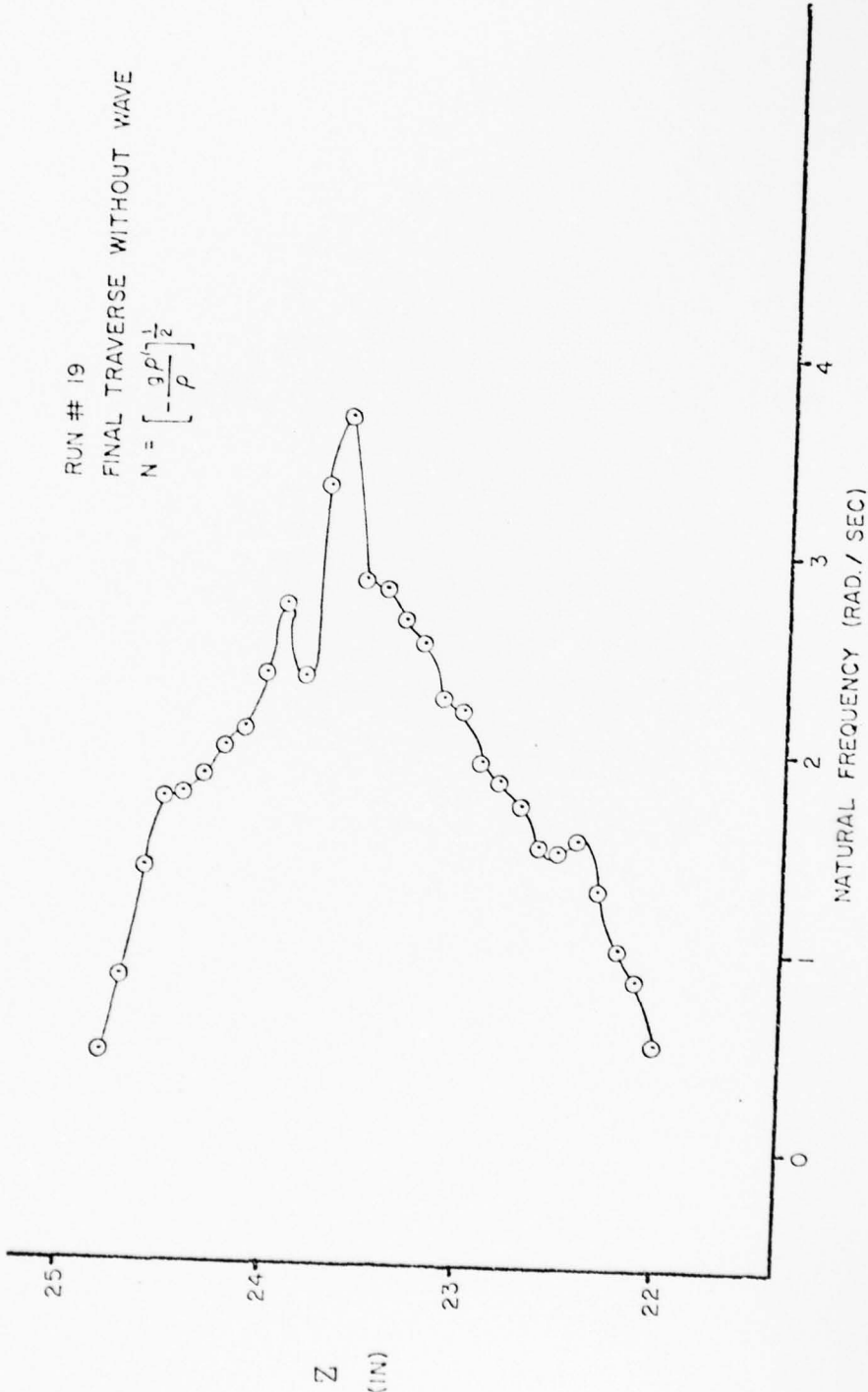


Figure 48. Natural Frequency Profile, Run #19

RUN # 2, AT CREST
 ○ — RICHARDSON NUMBER
 △ --- NATURAL FREQUENCY
 T = 10.15 SEC.
 L = 117.7 IN.
 H = 1.05 IN.
 H/L = 0.008936

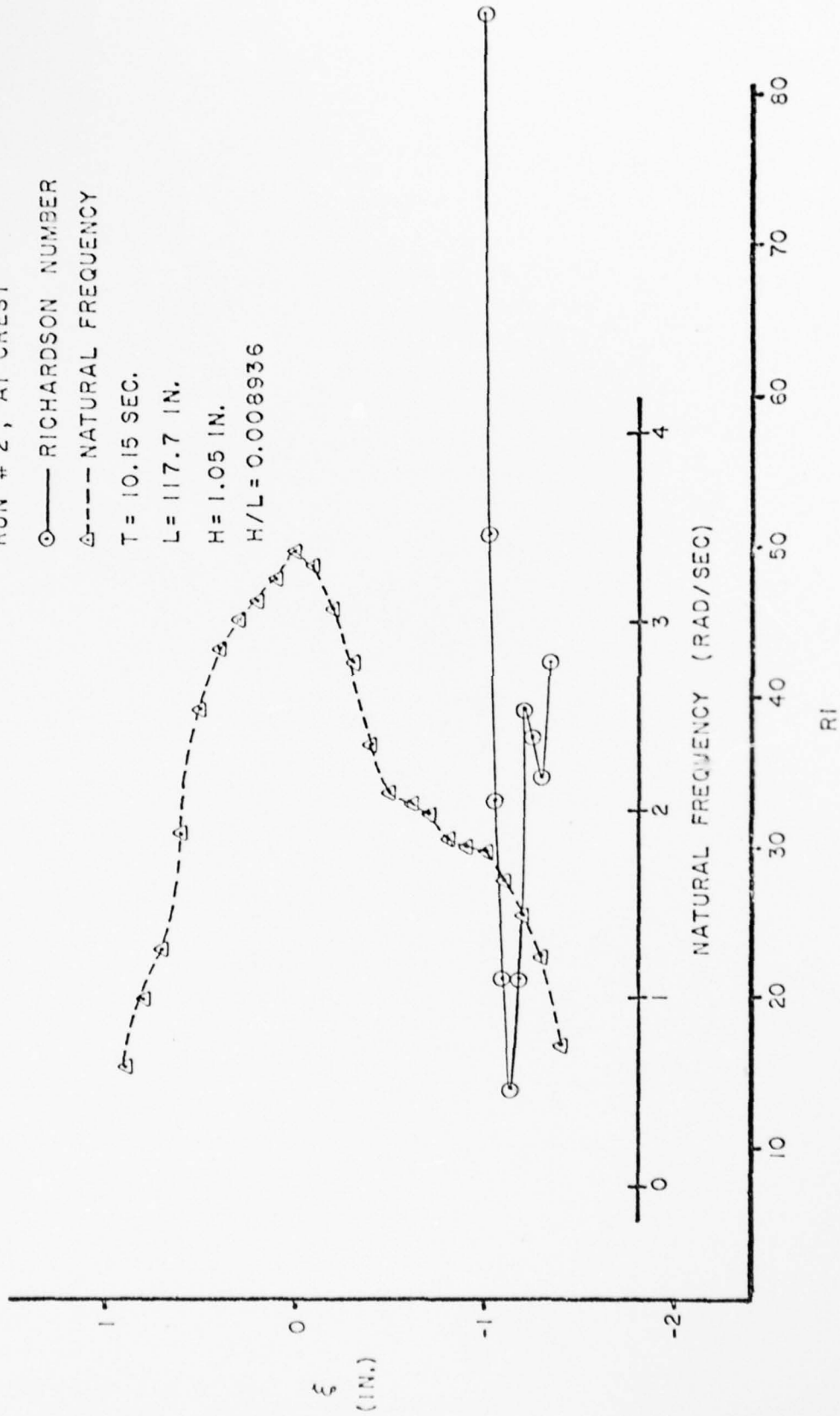


Figure 49. Richardson Number Profile at Wave Crest, Run #2

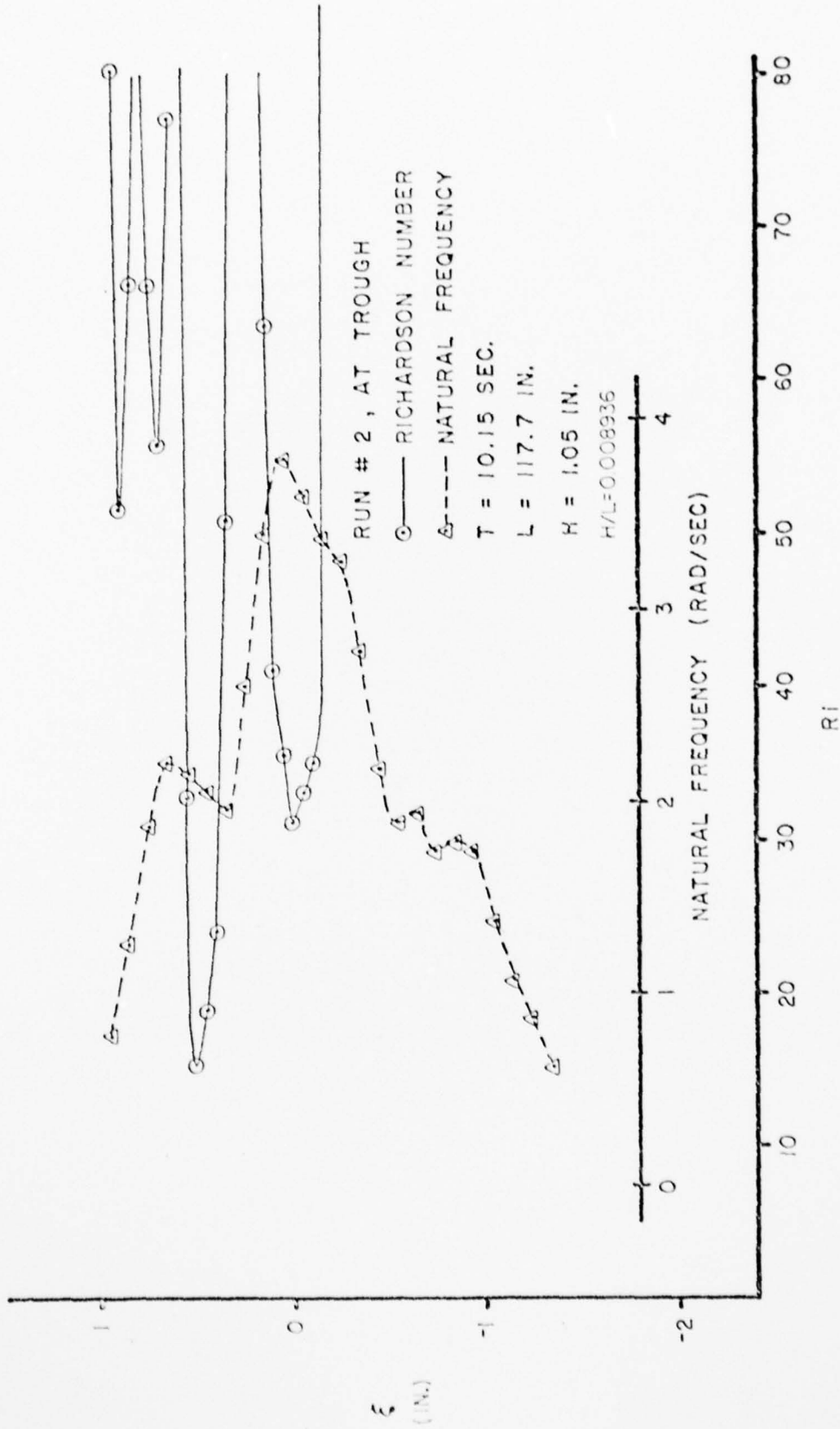


Figure 50. Richardson Number Profile at Wave Trough, Run #2

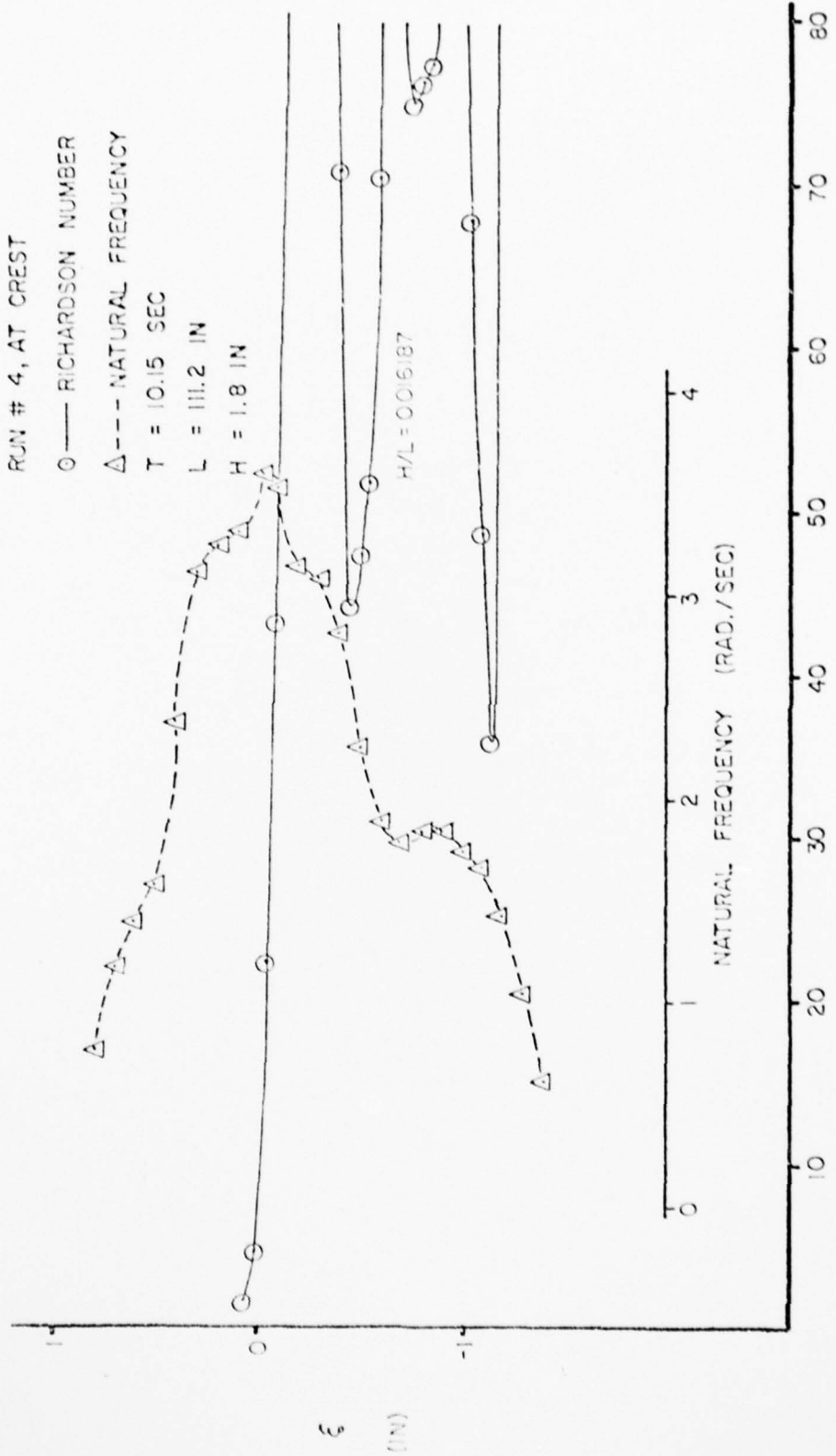


Figure 51 . Richardson Number Profile at Wave Crest, Run #4

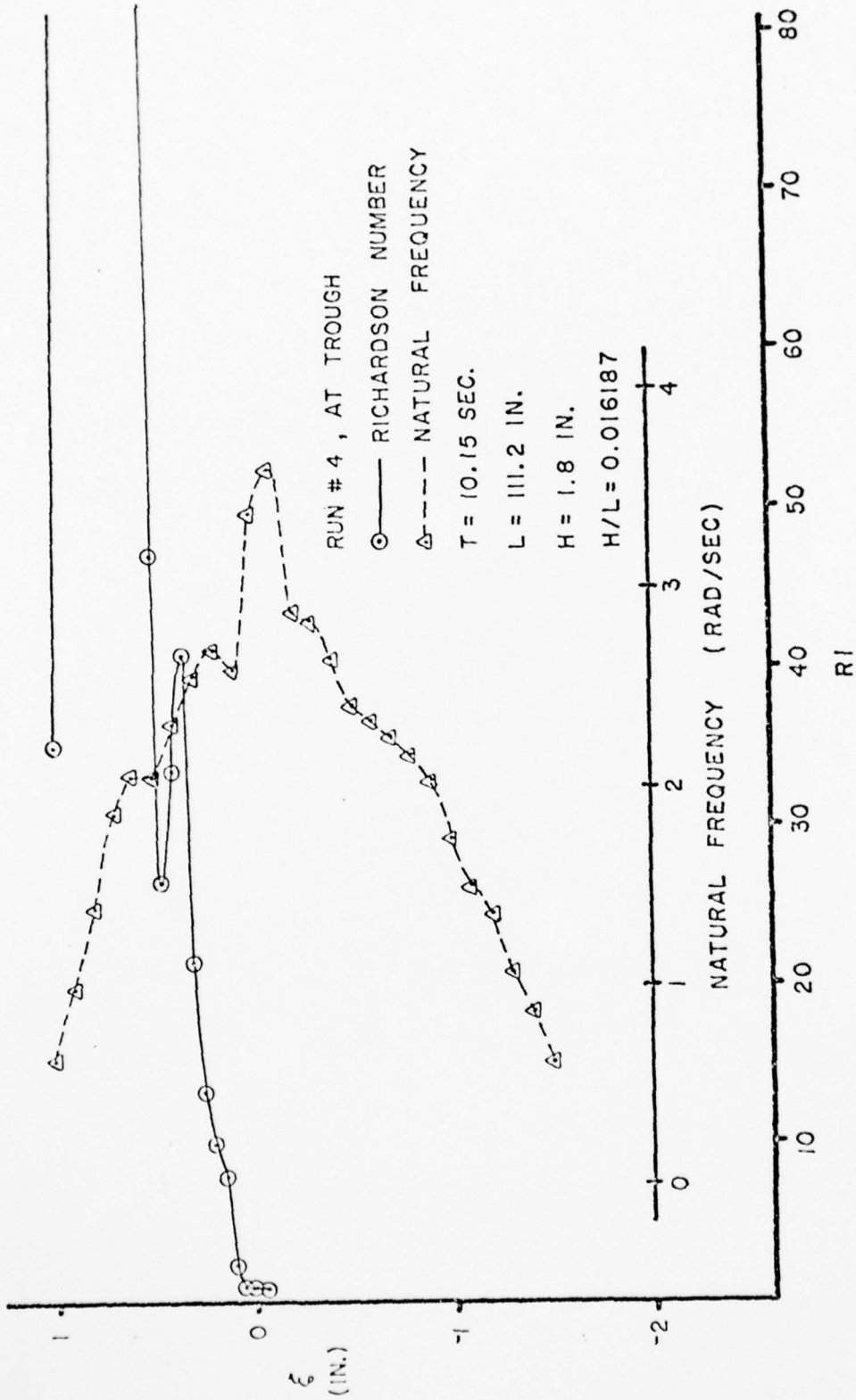


Figure 52 . Richardson Number Profile at Wave Trough, Run #4

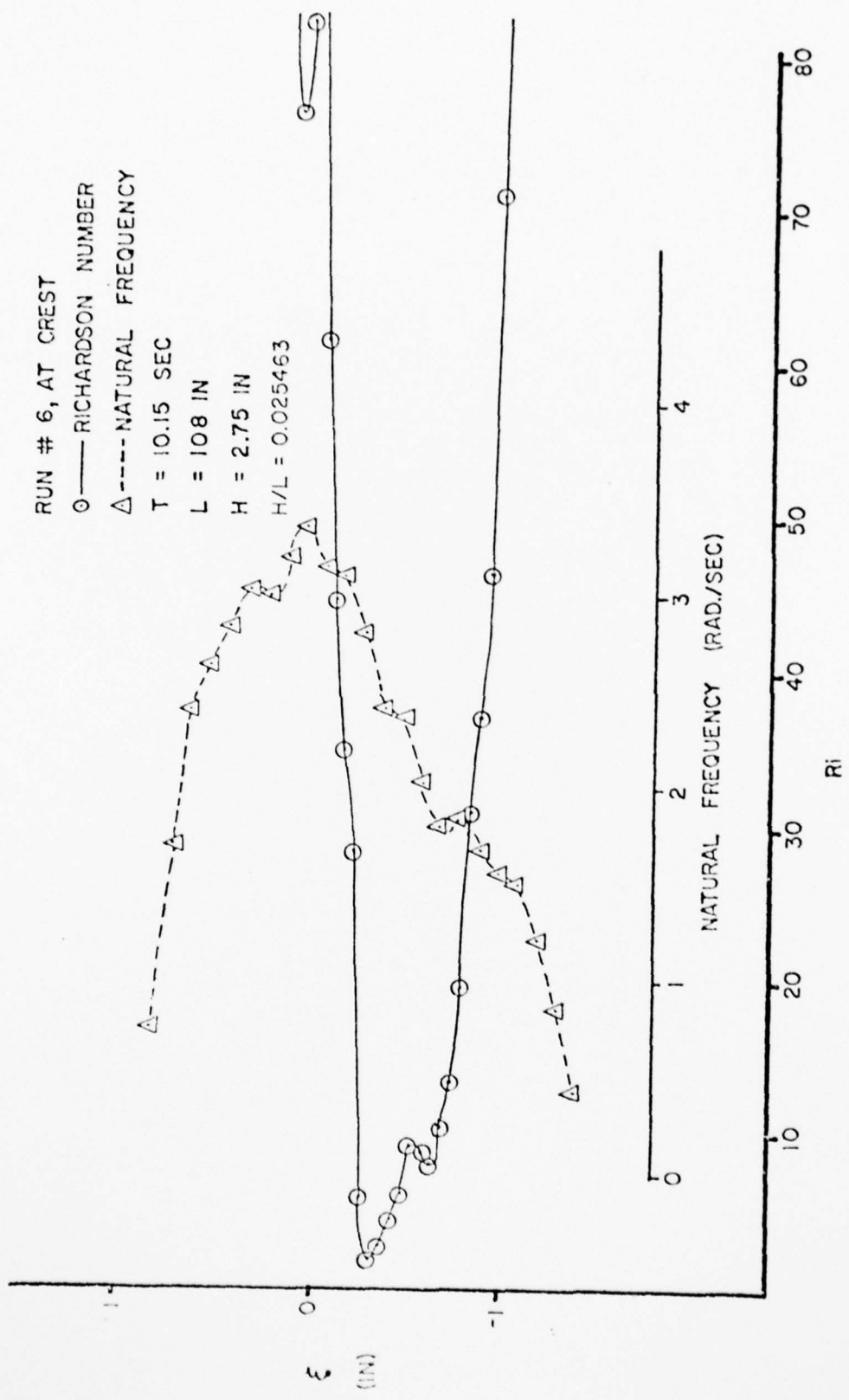


Figure 53 . Richardson Number Profile at Wave Crest, Run #6

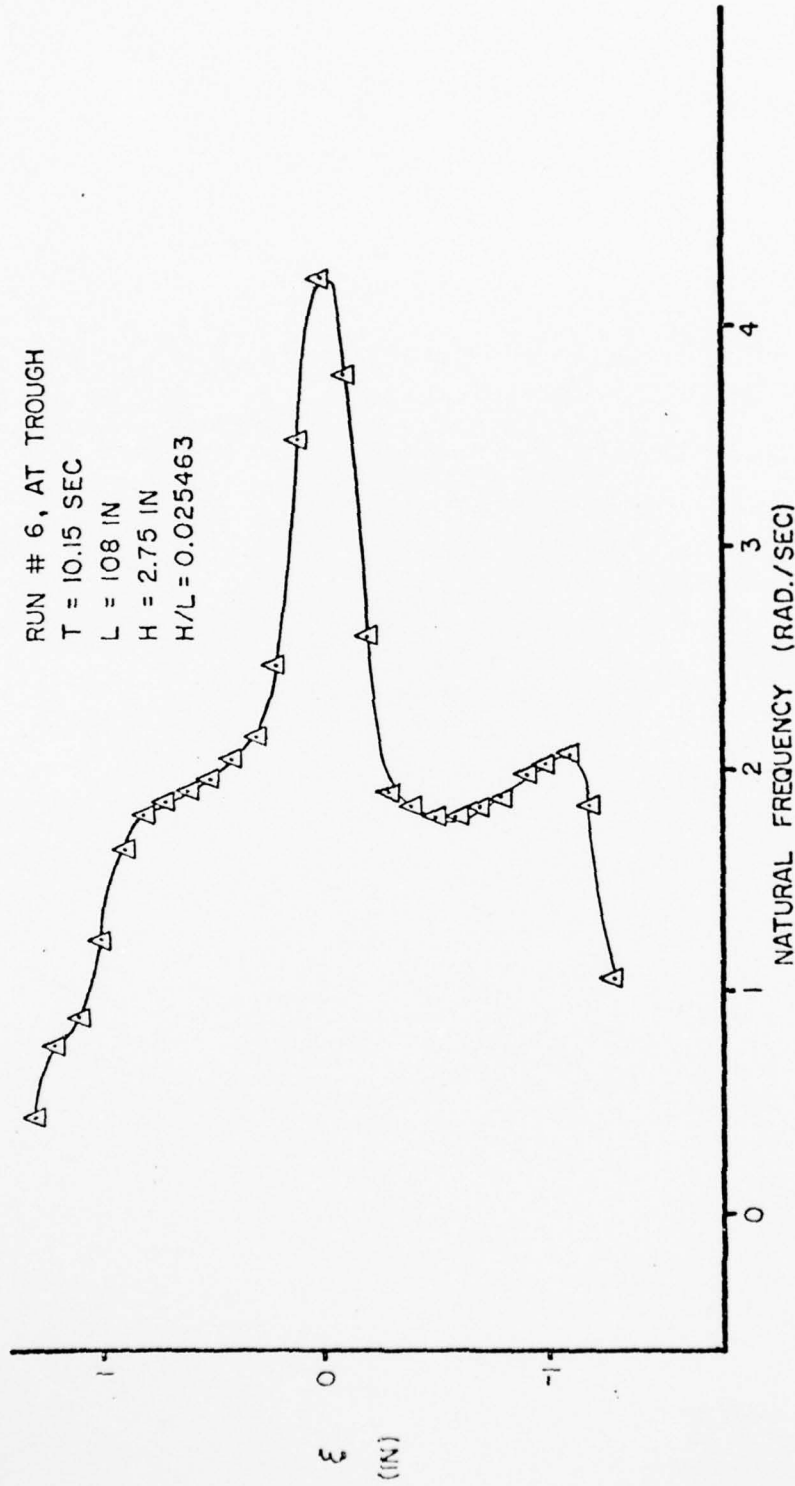


Figure 54. Natural Frequency Profile at Wave Trough, Run #6

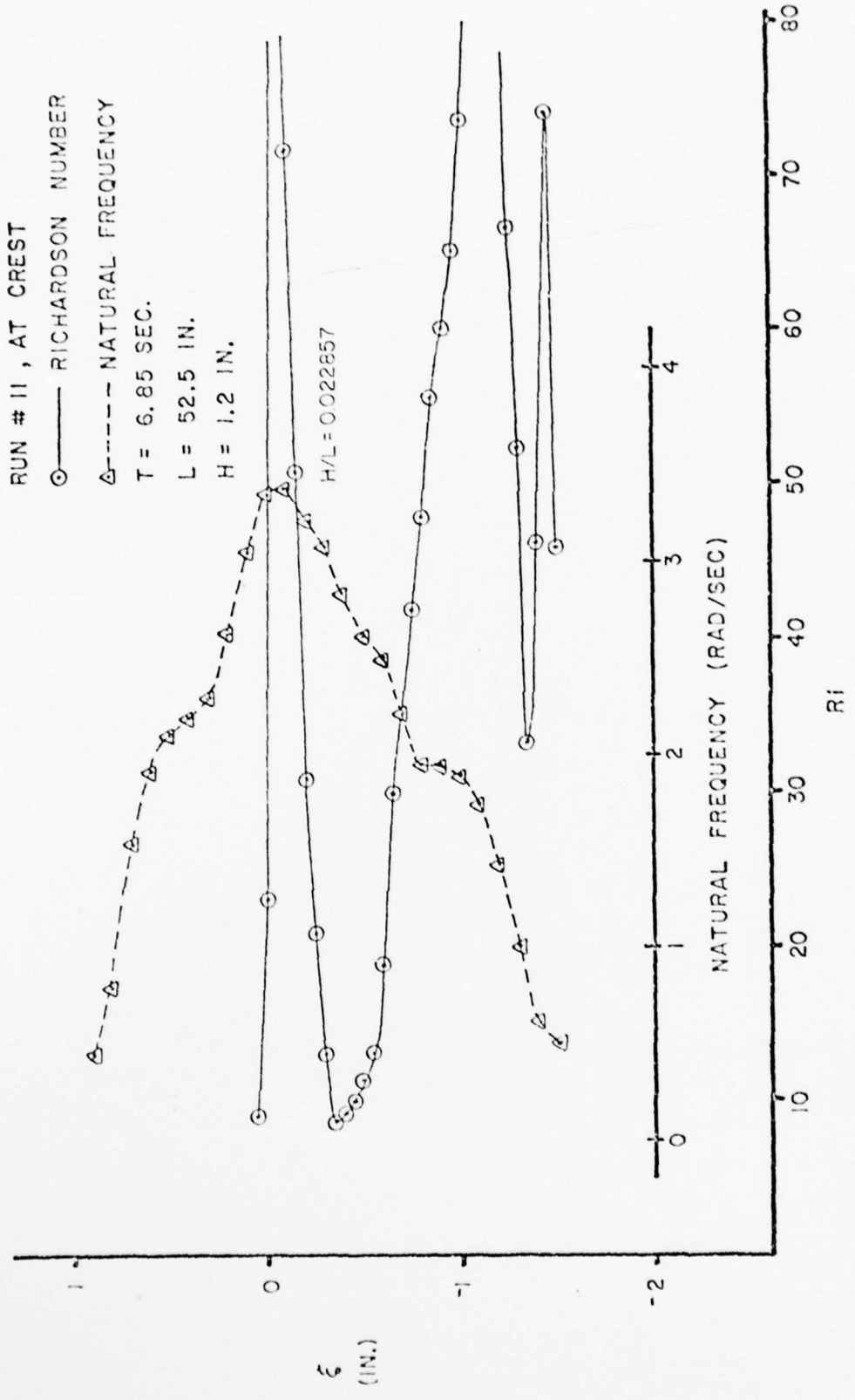


Figure 55. Richardson Number Profile at Wave Crest, Run #11

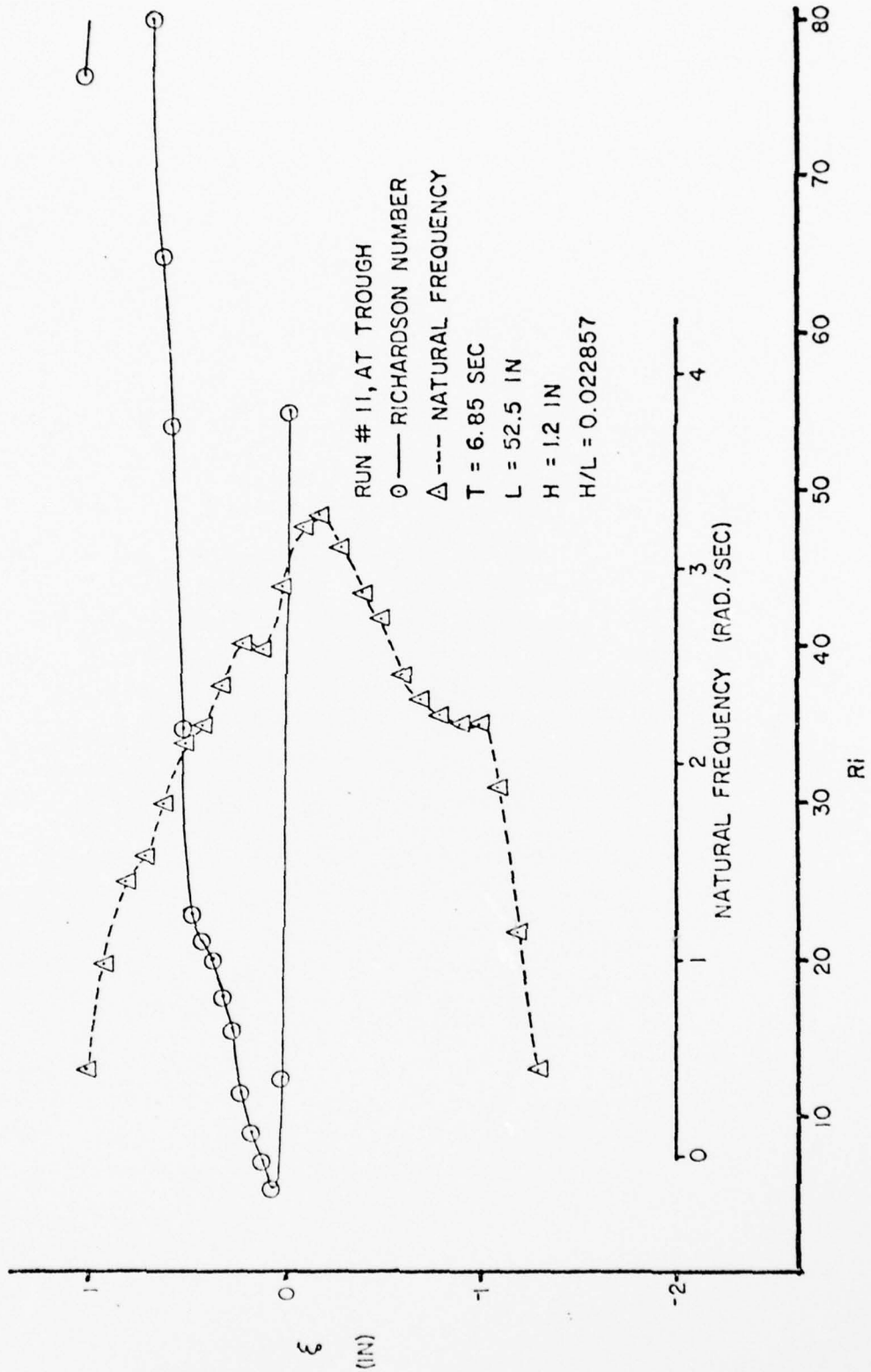


Figure 56. Richardson Number Profile at Wave Trough, Run #11

RUN # 15, AT CREST
 Δ --- NATURAL FREQUENCY
 Ri > 80, WHEN $\zeta < 0$
 T = 5.23 SEC
 L = 40.06
 H = 0.35
 H/L = 0.008737

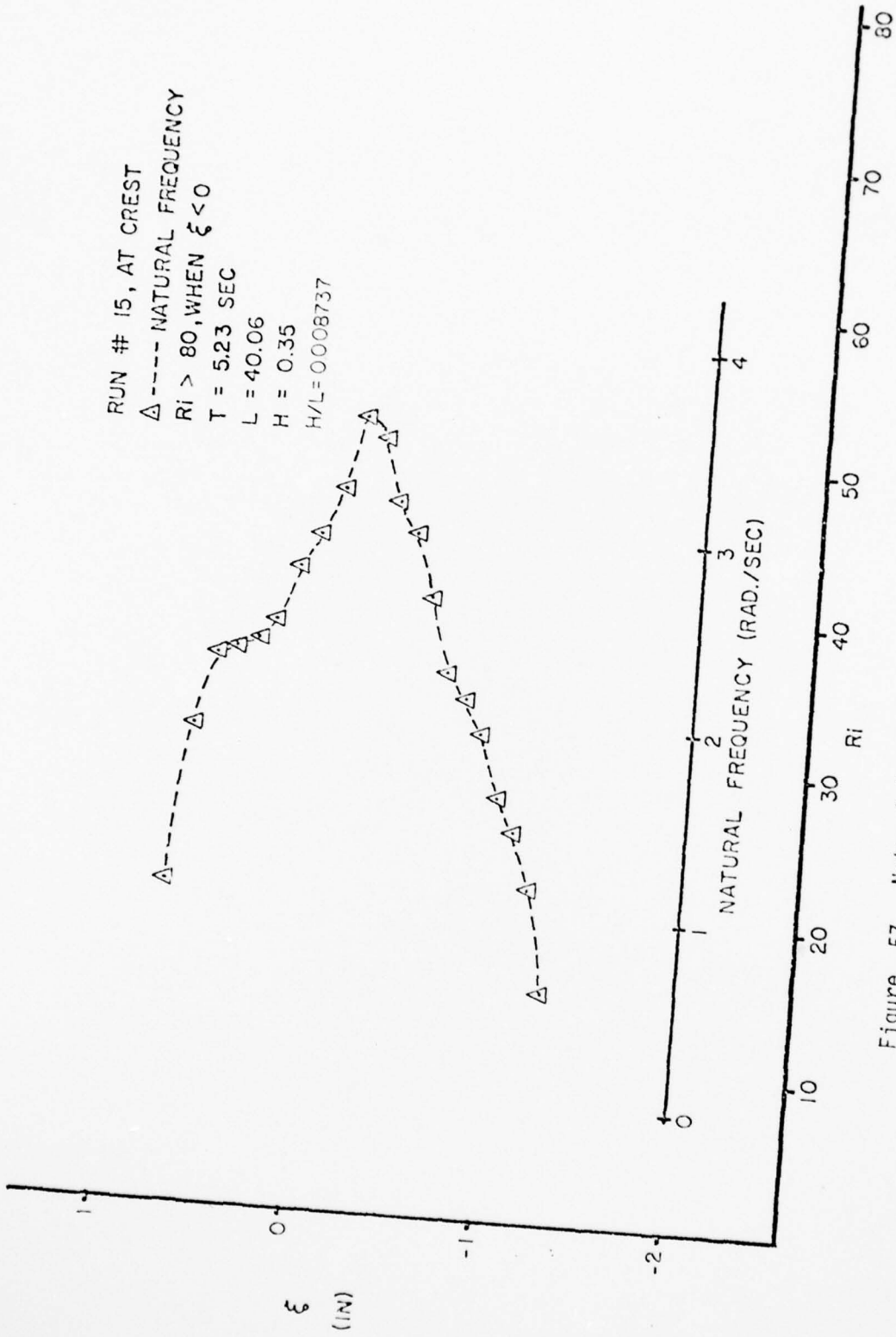


Figure 57. Natural Frequency Profile at Wave Crest, Run #15

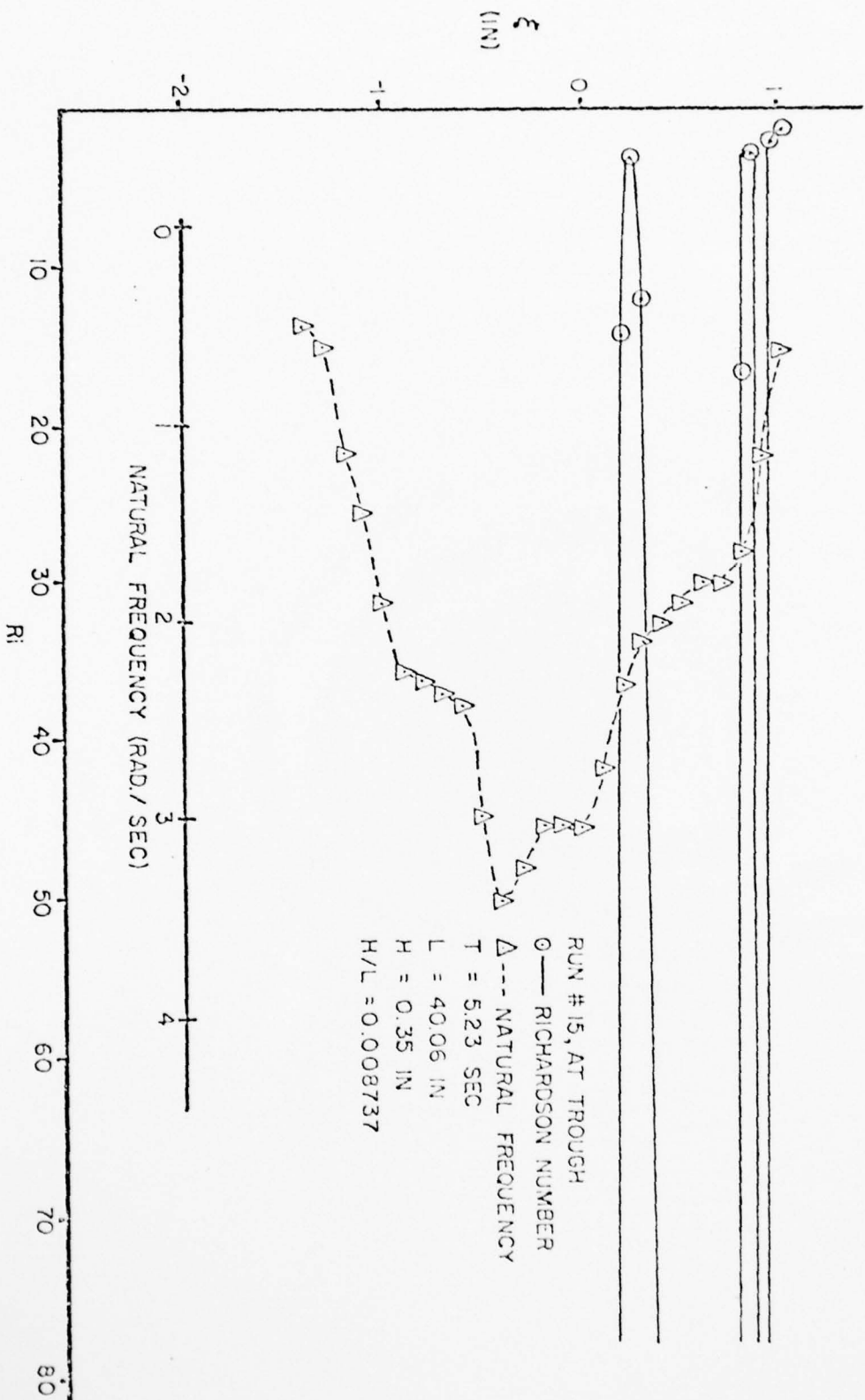


Figure 58. Richardson Number Profile at Wave Trough, Run #15

With the increased steepness the flow becomes unstable once again and the cycle is repeated. The energy transferred to the interfacial waves is proportional to $H_0^2 - H_t^2$. This energy transfer is plotted versus minimum Richardson number in Figure 59. It appears that $H_0^2 - H_t^2$ increases exponentially with the decreasing minimum Richardson number. Thus the minimum Richardson number in the flow appears to be an indicator of the conditions necessary for the transfer of energy to an interfacial disturbance. In other words, the minimum Richardson number appears to be a good indicator of the degree of instability.

Next, an explanation of why the high frequency waves are trapped in the interfacial layer is given. In order for a disturbance to grow, the Richardson number must be smaller than some critical value. In addition, only disturbances with frequencies less than the natural frequency (Brunt-Väisälä frequency) can exist in the fluid as pointed out in Chapter 1. Thus if the interfacial layer becomes unstable and internal waves of certain frequencies (less than natural frequency) result, these waves are confined to the region where the Brunt-Väisälä frequency is equal to or greater than these frequencies. A definition sketch is shown in Figure 60. It was also pointed out in Chapter 1 that disturbances propagating in a stratified fluid will have a vertical component of propagation until it reaches a level where the Brunt-Väisälä frequency coincides with its frequency. Thus disturbances with frequencies less than N_{\min} (see Figure 59) will propagate into the stable region and cease to exist. For this reason only waves with frequencies greater than n_{\min} and less than N_{\max} are believed to exist in the interfacial layer.

The critical value of the Richardson number as determined by these experiments is larger than that predicted by the linear, inviscid theory.

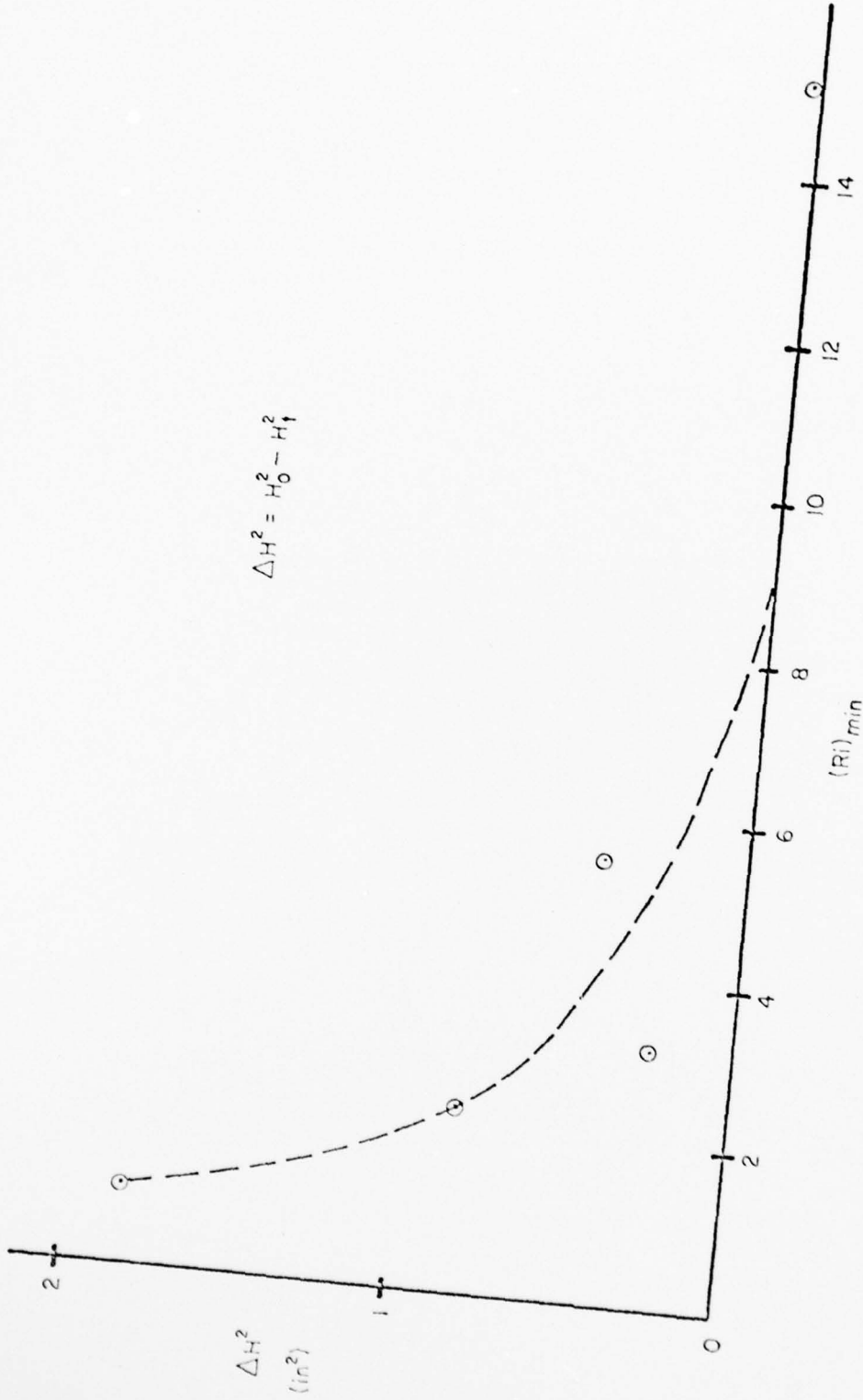


Figure 59. Energy Transfer vs. Minimum Richardson Number

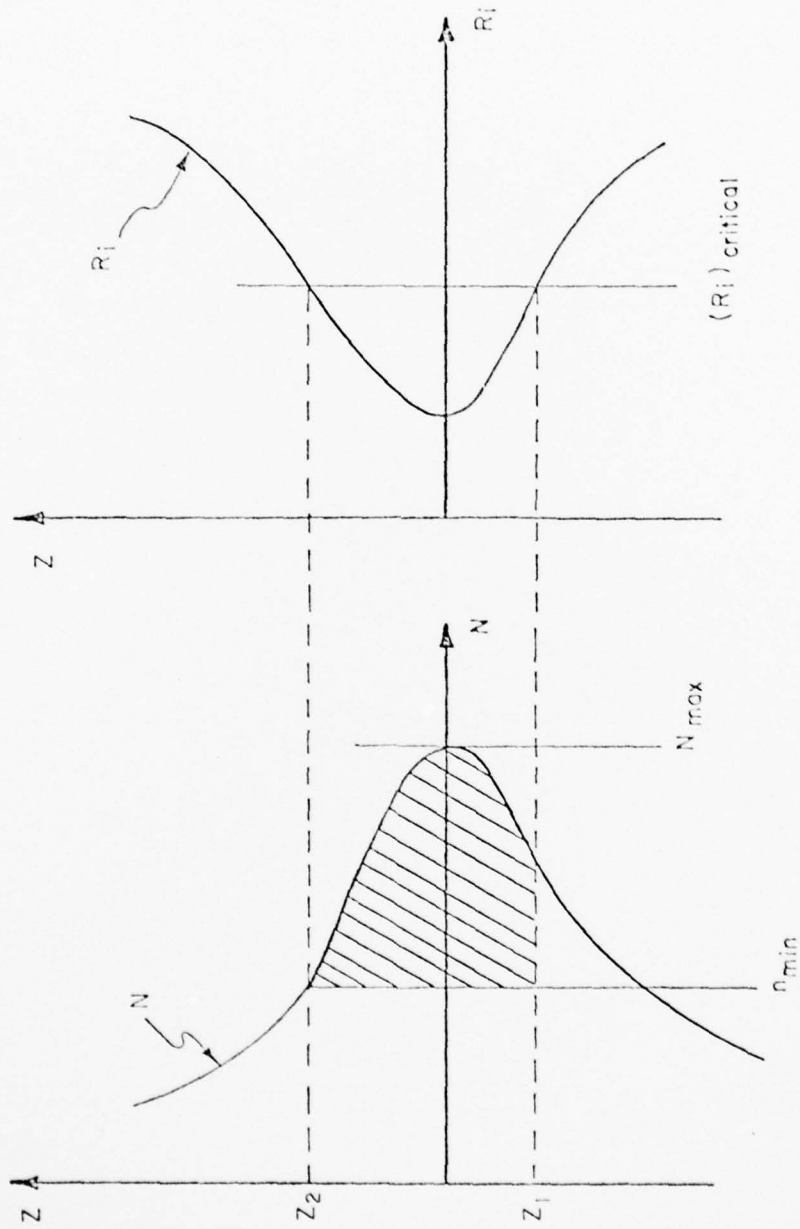


Figure 60 . Definition Sketch of Trapped Interfacial Waves

This is probably due to nonlinear effects caused by the finite size of the waves. From Figure 59 the critical value of Richardson number (R_{icr}) is approximately 10.

The changes in temperature in the interfacial region were small, as can be seen in the temperature profiles presented in Figure 61. This coupled with the fact that the conductivity readings were found to be only slightly dependent on temperature (see Figure 62) made temperature correction of the conductivity unnecessary.

Unfortunately the attempt to analyze the frequency spectrum failed. The frequencies of the disturbances were expected to be near the natural frequencies in the interfacial layer. From the Brunt-Väisälä frequencies plots in Figures 44 through 49, it can be seen that the maximum natural frequency is 0.54 Hz. From the visicorder recording of velocity (see Figure 73 and 74 in the Appendix), the frequency of the disturbance was estimated to be between 0.5 and 0.67 Hz, which is very close to the range of natural frequencies.

In these experiments, the wave steepness was not excessively high. It is expected that if the wave steepness is much larger, the disturbances will be in the turbulent subrange and significant changes in the density profile will occur. The periodic exchange of energy between the internal and interfacial waves should no longer occur when this happened.

AD-A070 183

FLORIDA UNIV GAINESVILLE COASTAL AND OCEANOGRAPHIC --ETC F/6 8/10
AN EXPERIMENTAL INVESTIGATION OF INTERFACIAL WAVES GENERATED BY--ETC(U)
1975 I B CHOU

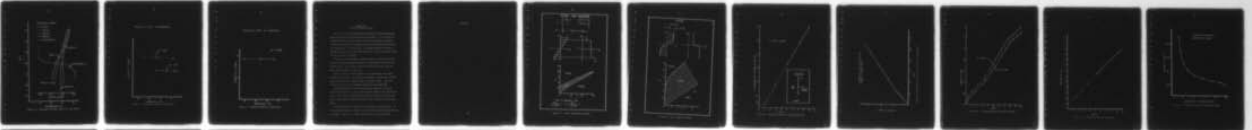
N00014-68-A-0173

NL

UNCLASSIFIED

2 OF 2

AD
A070183



END
DATE
FILMED
7-79
DDC

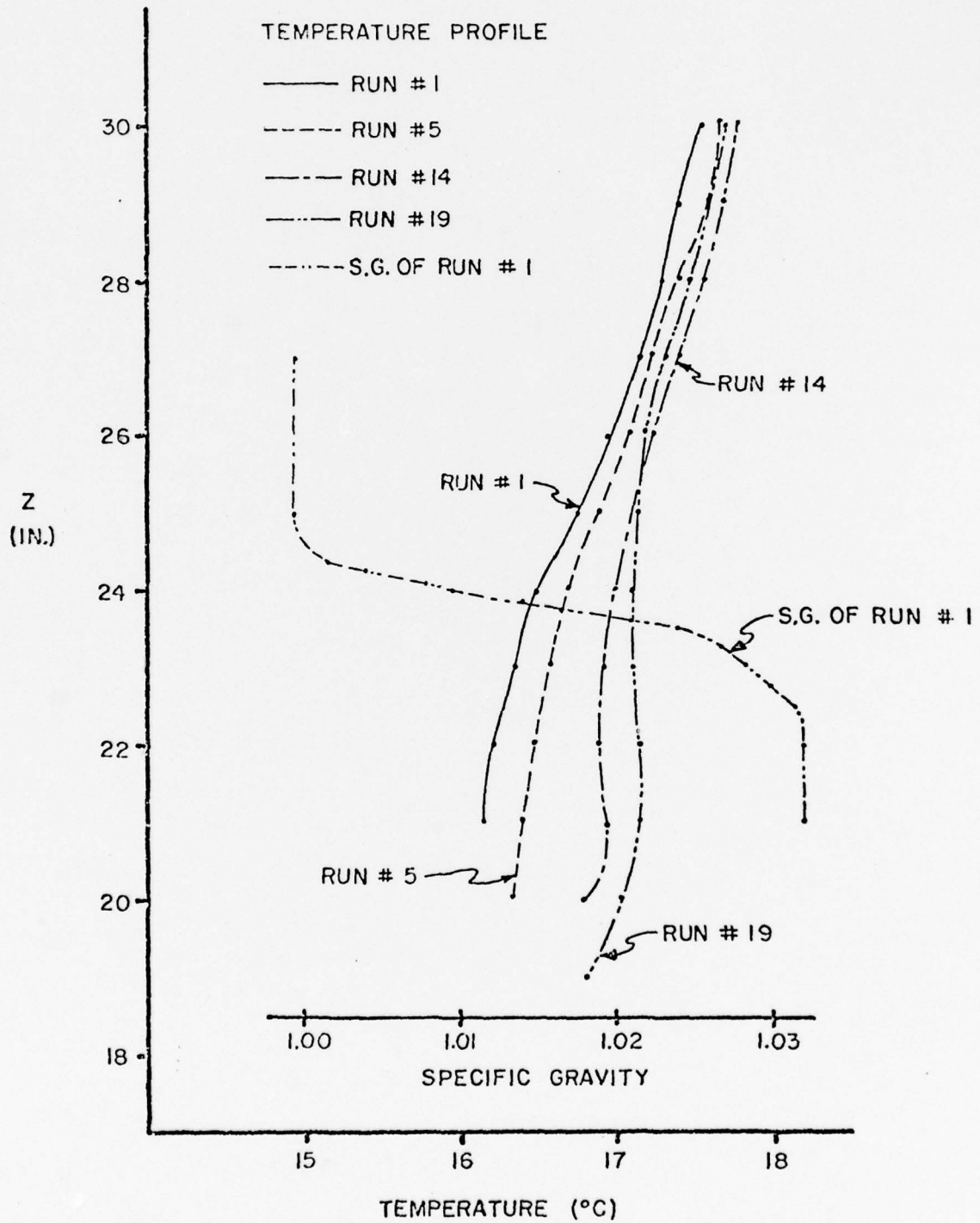


Figure 61. Temperature Profiles, Runs #1, 5, 14, and 19

TEMPERATURE EFFECT ON CONDUCTIVITY

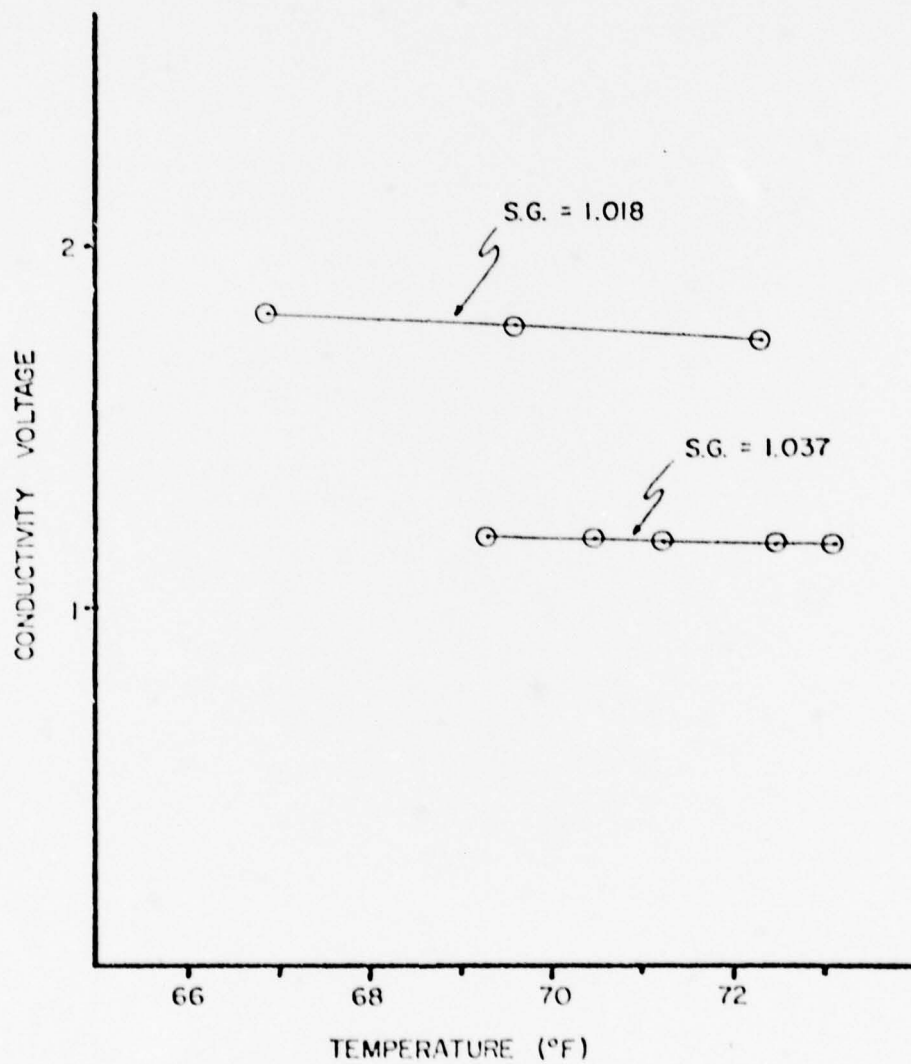


Figure 62. Temperature Effect on Conductivity

TEMPERATURE EFFECT ON CONDUCTIVITY

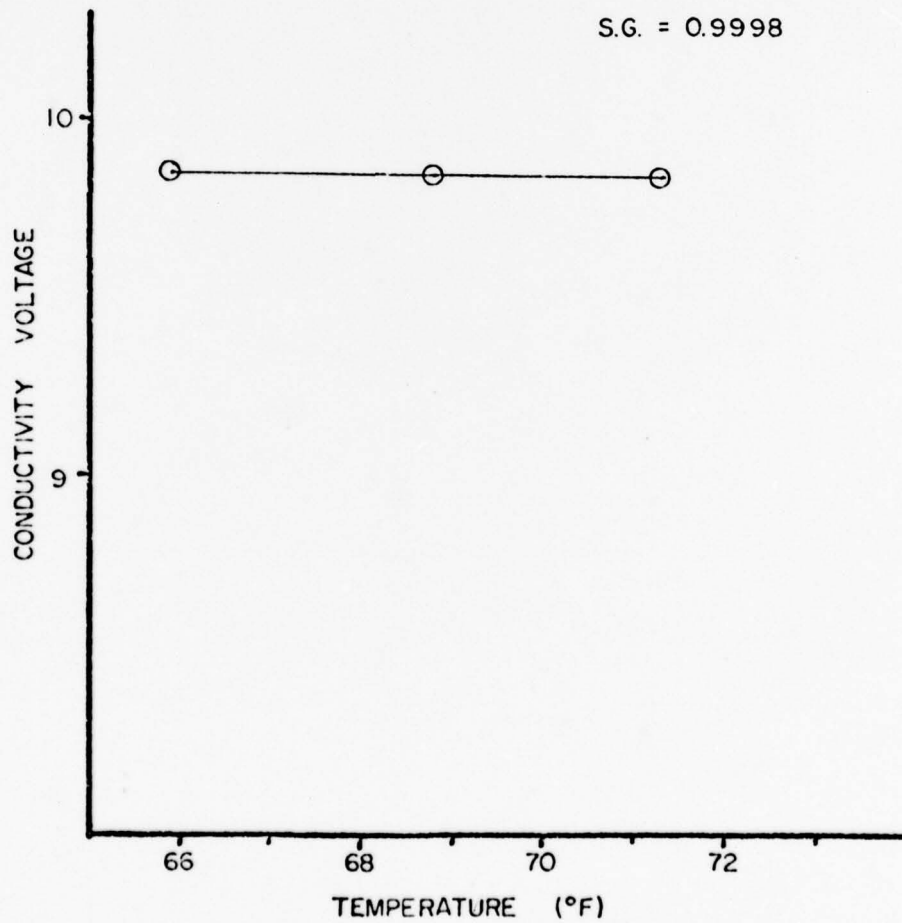


Figure 63. Temperature Effect on Conductivity

CHAPTER VII
ASPECTS OF FUTURE STUDIES

This thesis only investigated the initiation of the high frequency interfacial waves generated by long internal waves. It is highly recommended that the interfacial wave spectrum be measured and analyzed in order to determine the frequencies that exist and the energy level of the disturbances. To achieve this, a cylinder-type hot-film probe is needed for measuring very low fluid velocities. Also, a low noise level FM tape recorder is required.

In this set of experiments, complete velocity profiles were absent because the wedge-type hot-film probe can only measure the velocity in one direction. The cylinder-type hot-film probe will also allow complete velocity profiles to be made.

There were only a limited number of wave frequencies and heights examined in this work. This should be expanded to include more internal wave frequencies and a greater range of steepness ratios. With sufficient data, a critical Richardson number will be established.

The growth and decay of the internal waves should be studied by measuring the spatial as well as the temporal changes in the interfacial waves. This can be accomplished by moving the traverse along the wave tank and by monitoring the wave heights at more stations using the wave gages. 100

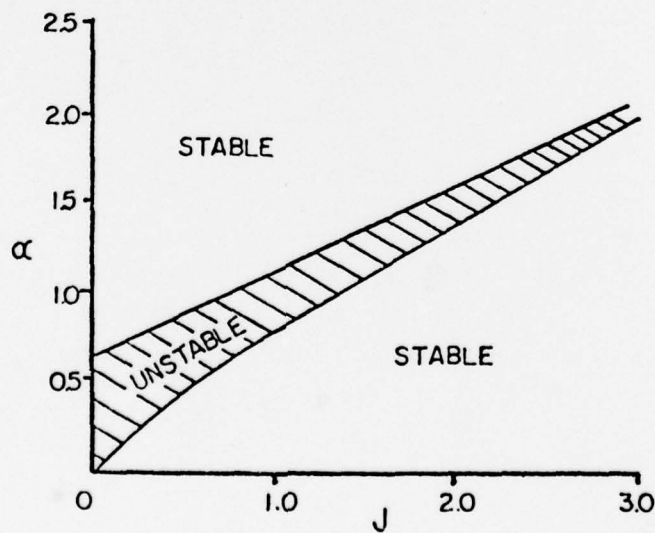
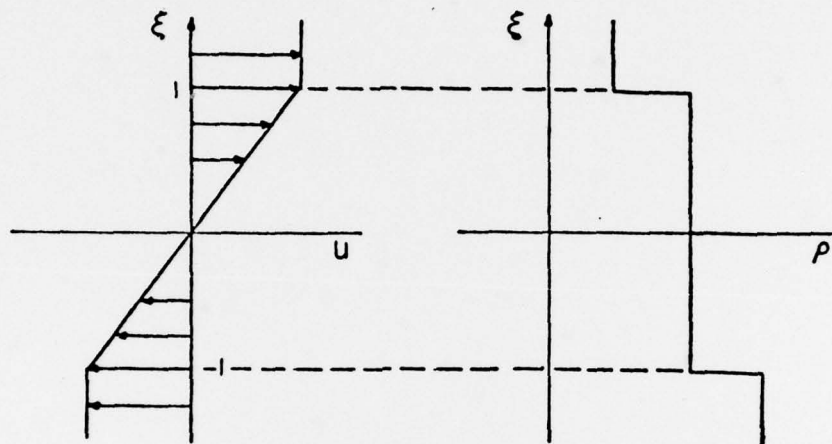
In these studies, the transition to turbulence is not examined. It is recommended that the steepness ratio be increased and the transition investigated. Hopefully, a transition parameter can be established.

APPENDIX

TAYLOR AND GOLDSTEIN

$$u = \begin{cases} \text{Sgn } \xi & (|\xi| > 1) \\ \xi & (|\xi| \leq 1) \end{cases}$$

$$\beta = \frac{p'}{p} = \delta(\xi+1) + \delta(\xi-1)$$



FLOW IS UNSTABLE FOR:

$$\frac{2\alpha}{1+e^{-2\alpha}} - 1 < J < \frac{2\alpha}{1-e^{-2\alpha}} - 1$$

Figure 64 . Taylor and Goldstein's Model

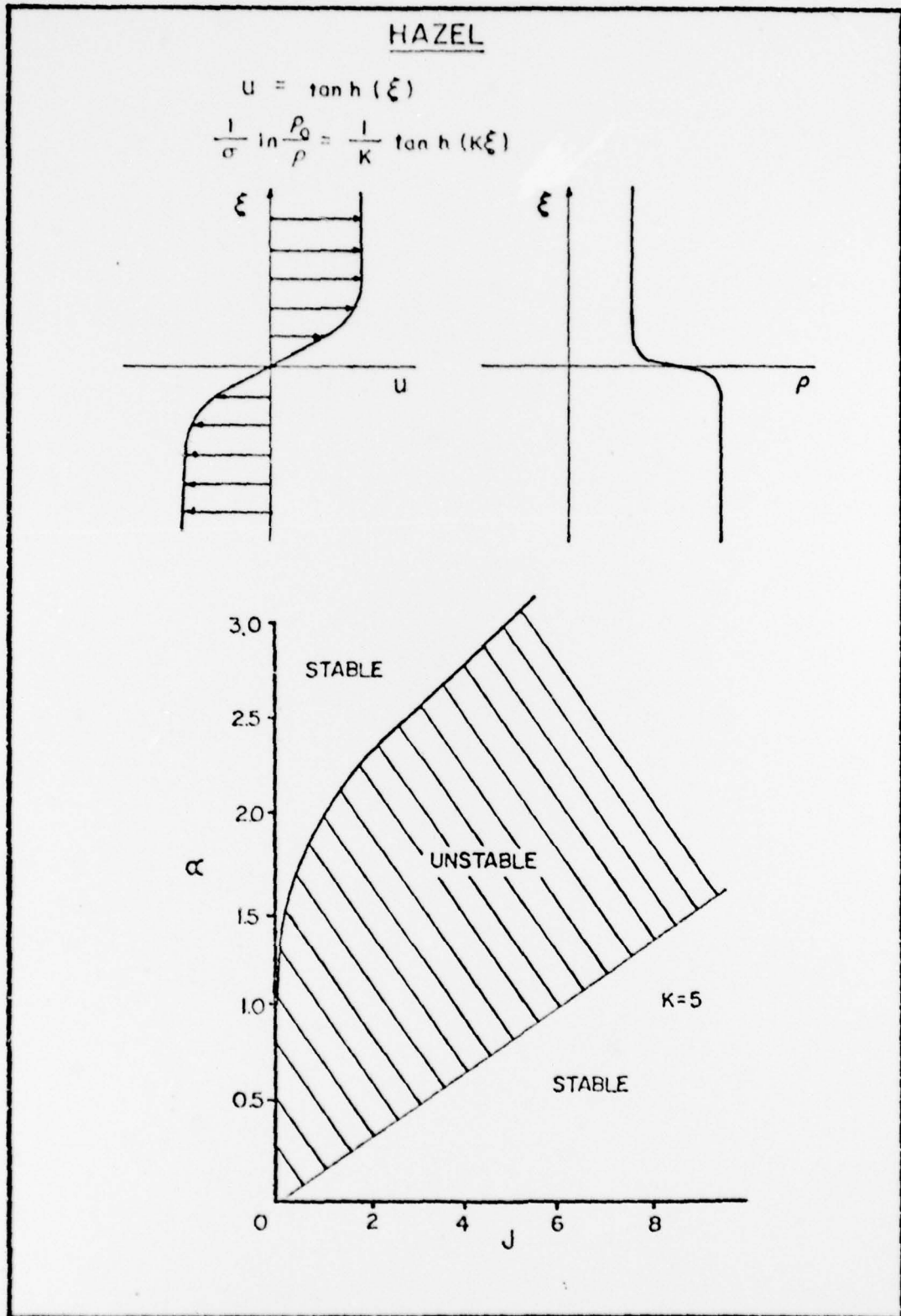


Figure 65. Hazel's Numerical Model

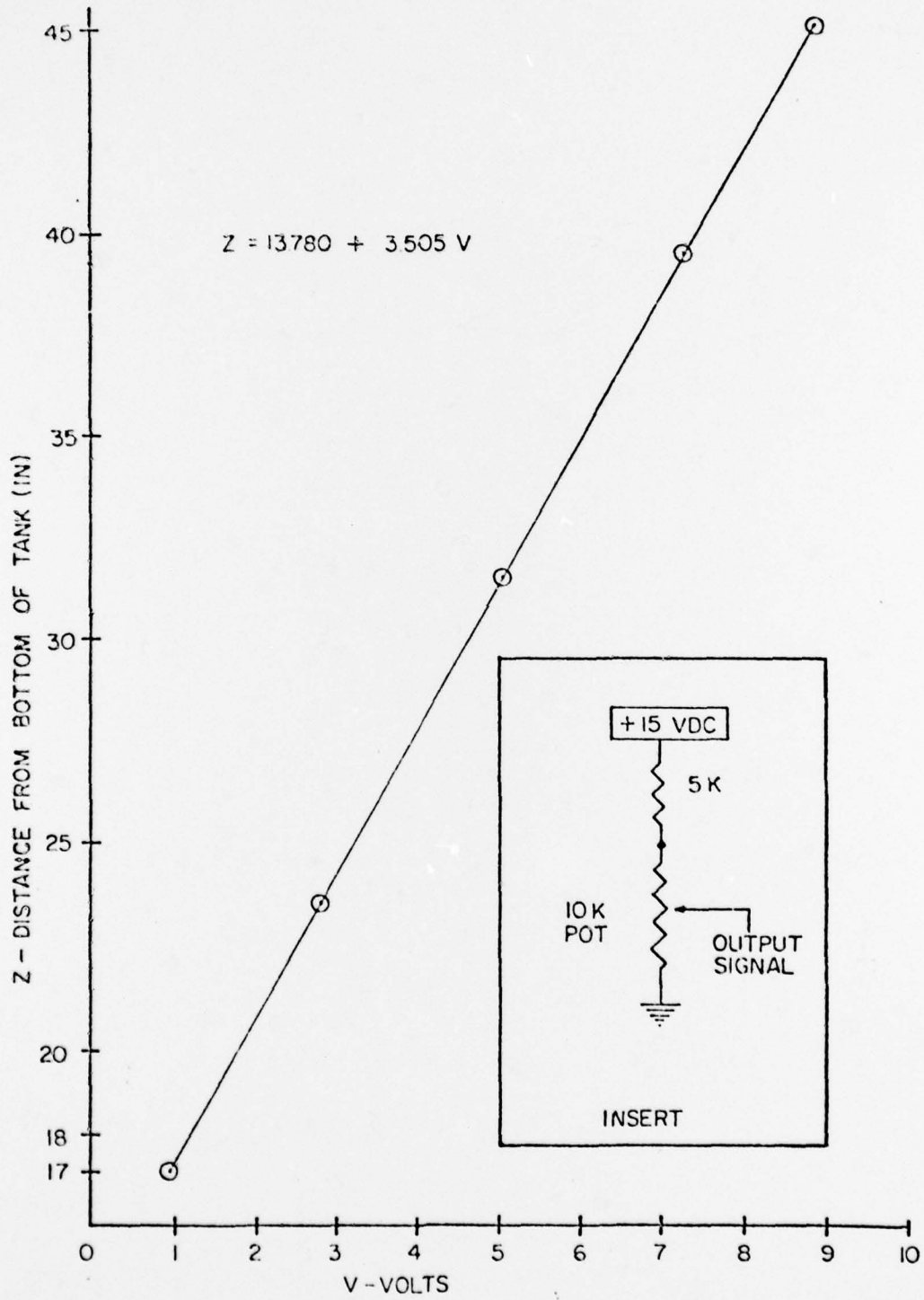


Figure 66. Calibration Curve for Position Indicator

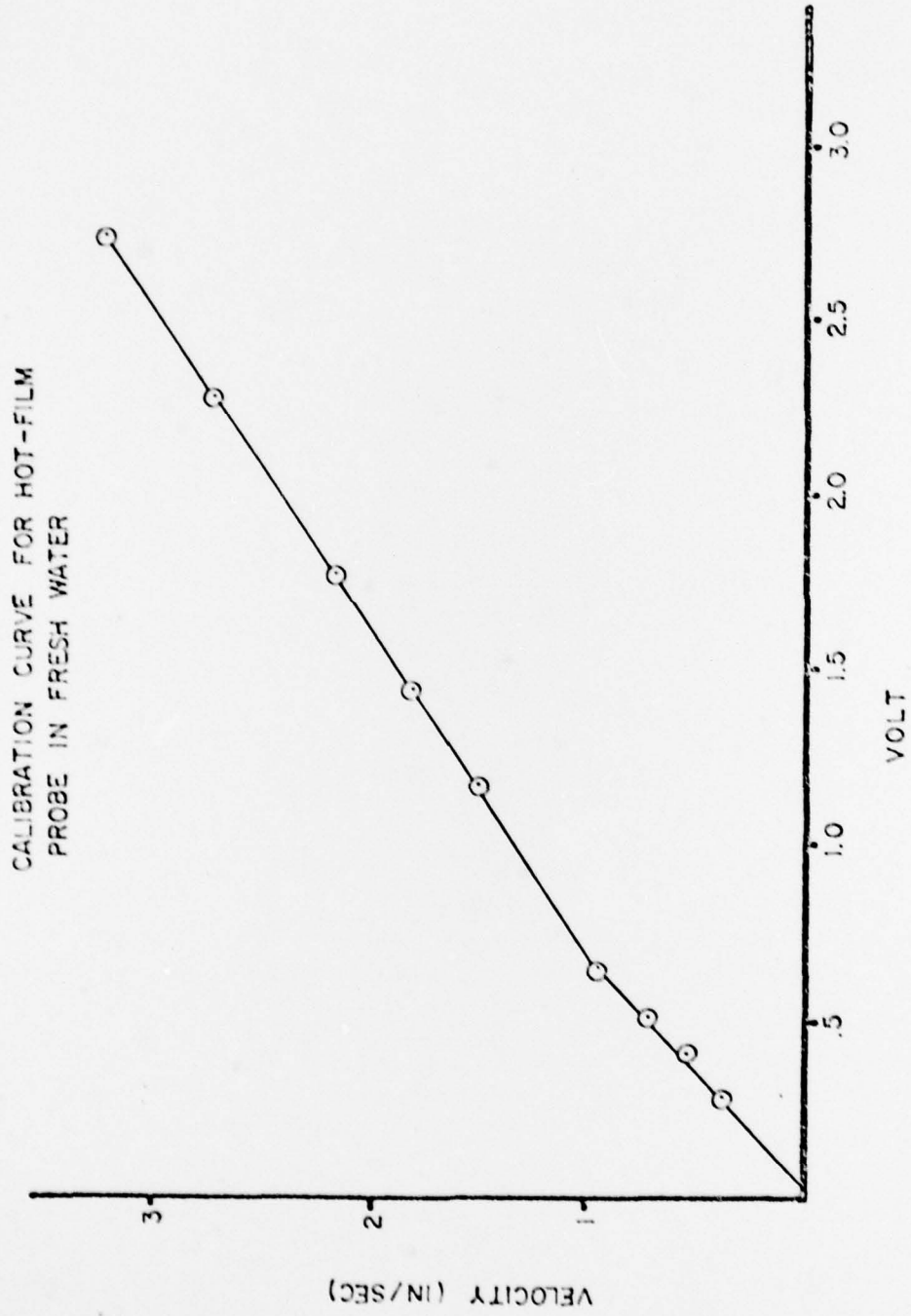


Figure 67. Calibration Curve for Hot-Film Probe in Fresh Water

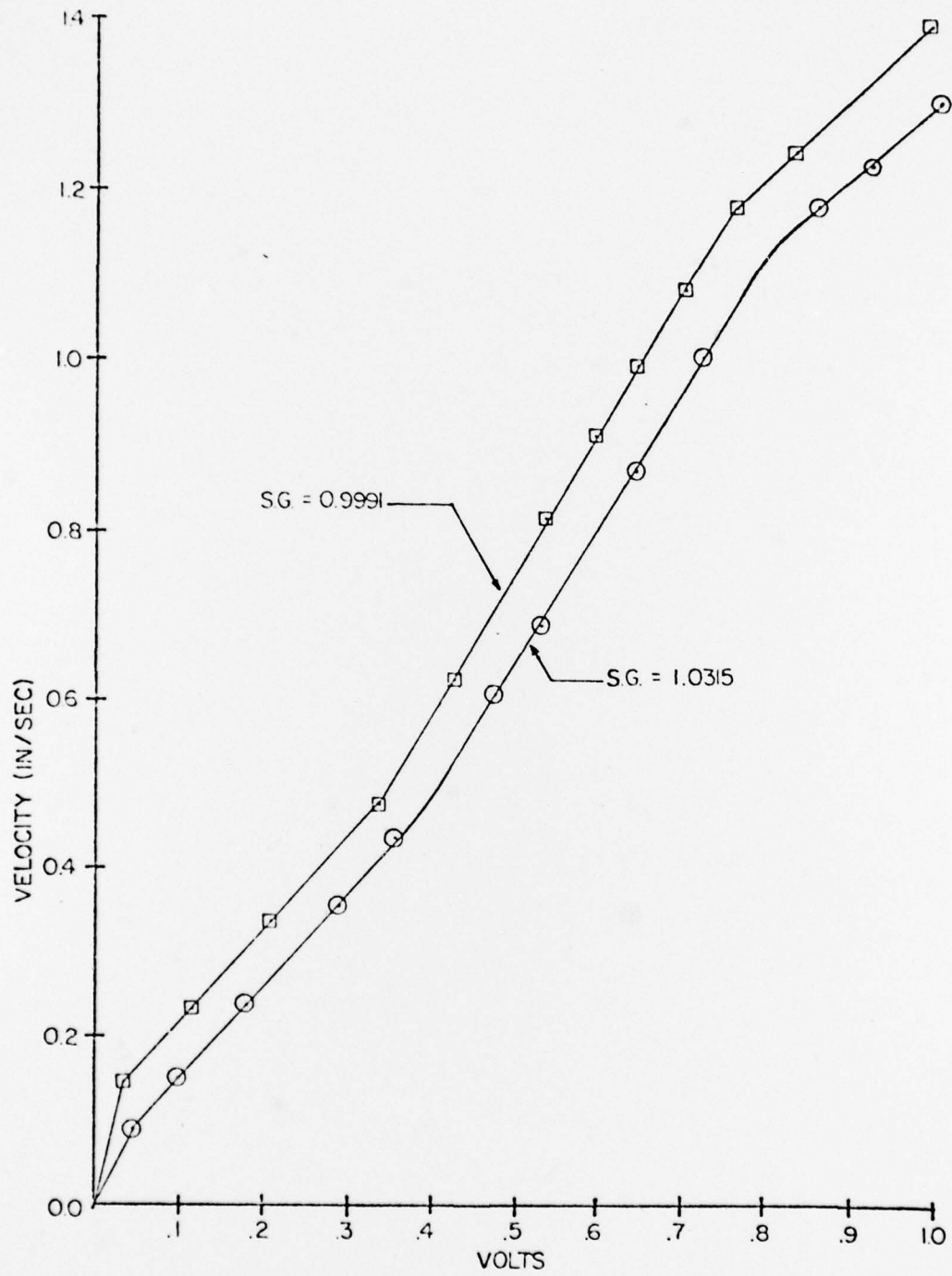


Figure 68 . Calibration Curves for Hot-Film Probe

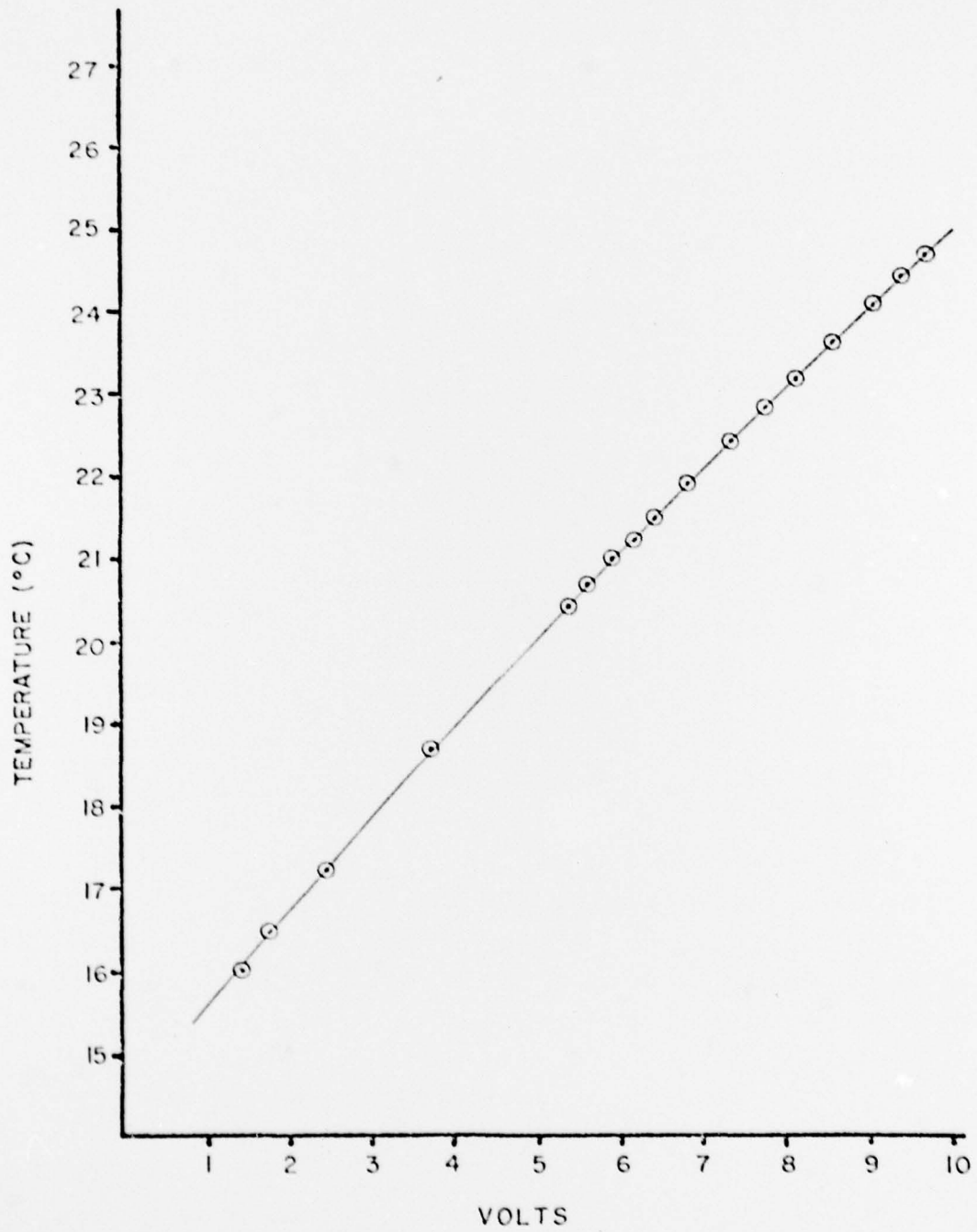


Figure 69. Calibration Curve for Thermistor

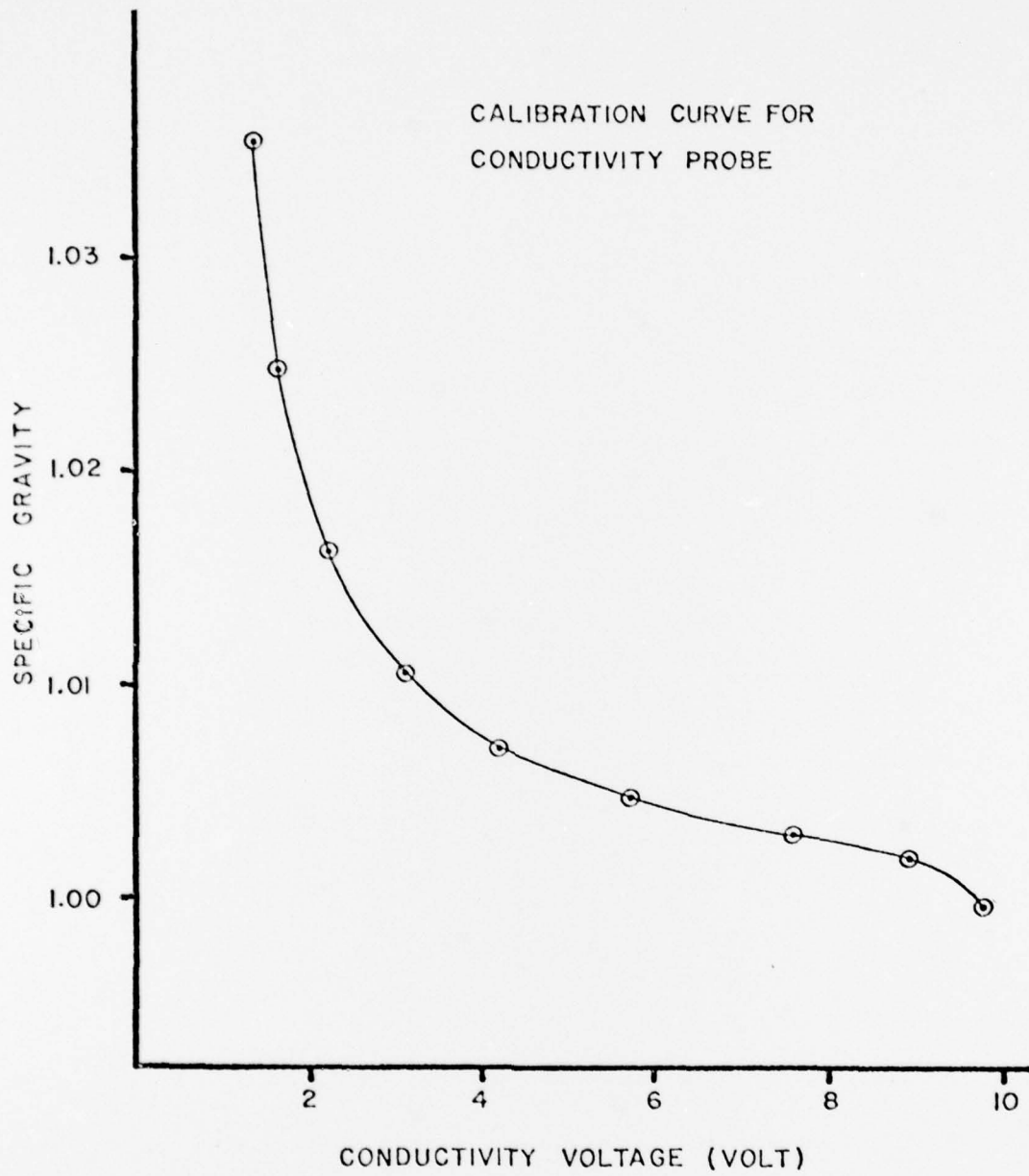
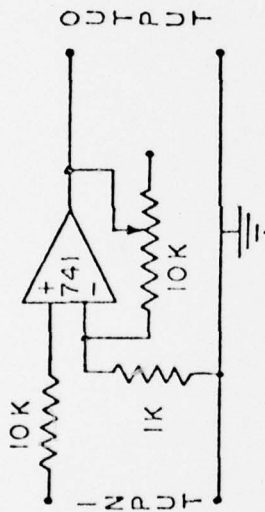
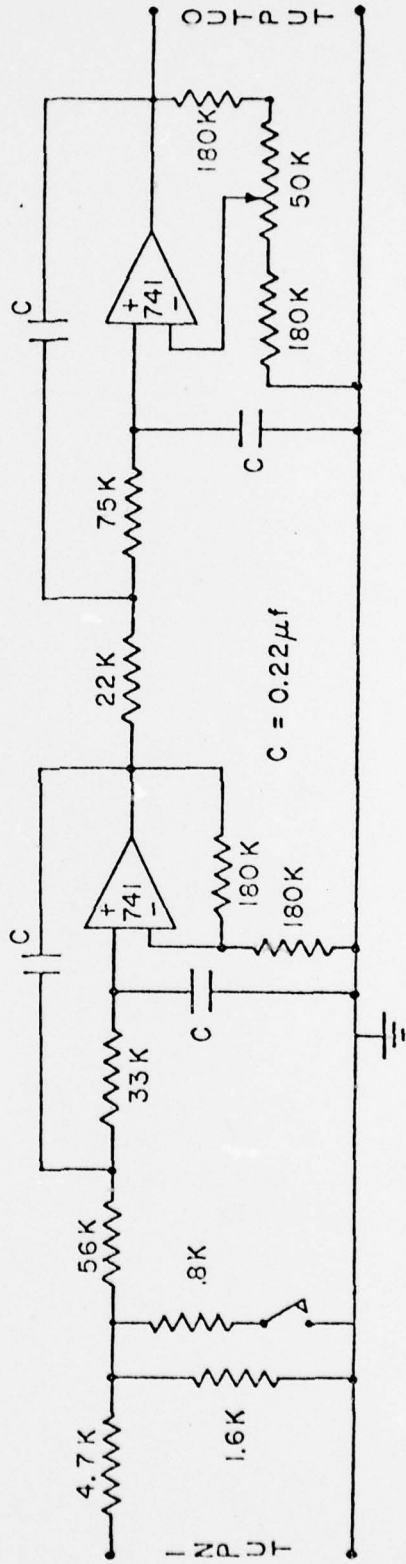


Figure 70. Calibration Curve for Conductivity Probe



PRE-AMP CIRCUIT



LOW-PASS FILTER CIRCUIT

Figure 71 . Pre-amplifier and Low-Pass Filter Circuit

X-Y PLOTTER · GRAPH PAPER

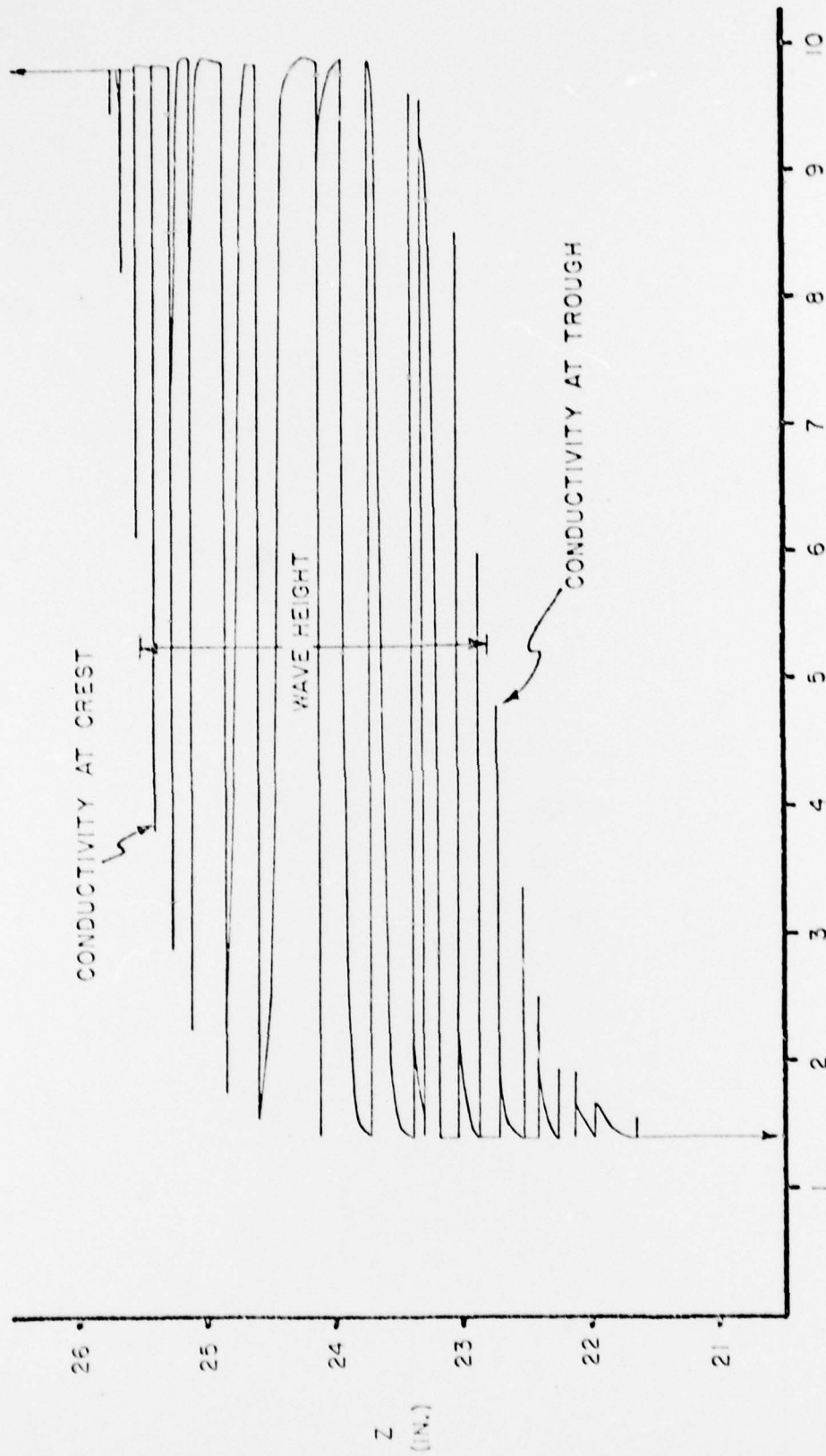


Figure 72. Determination of Wave Height from X-Y Plotter Graph Paper

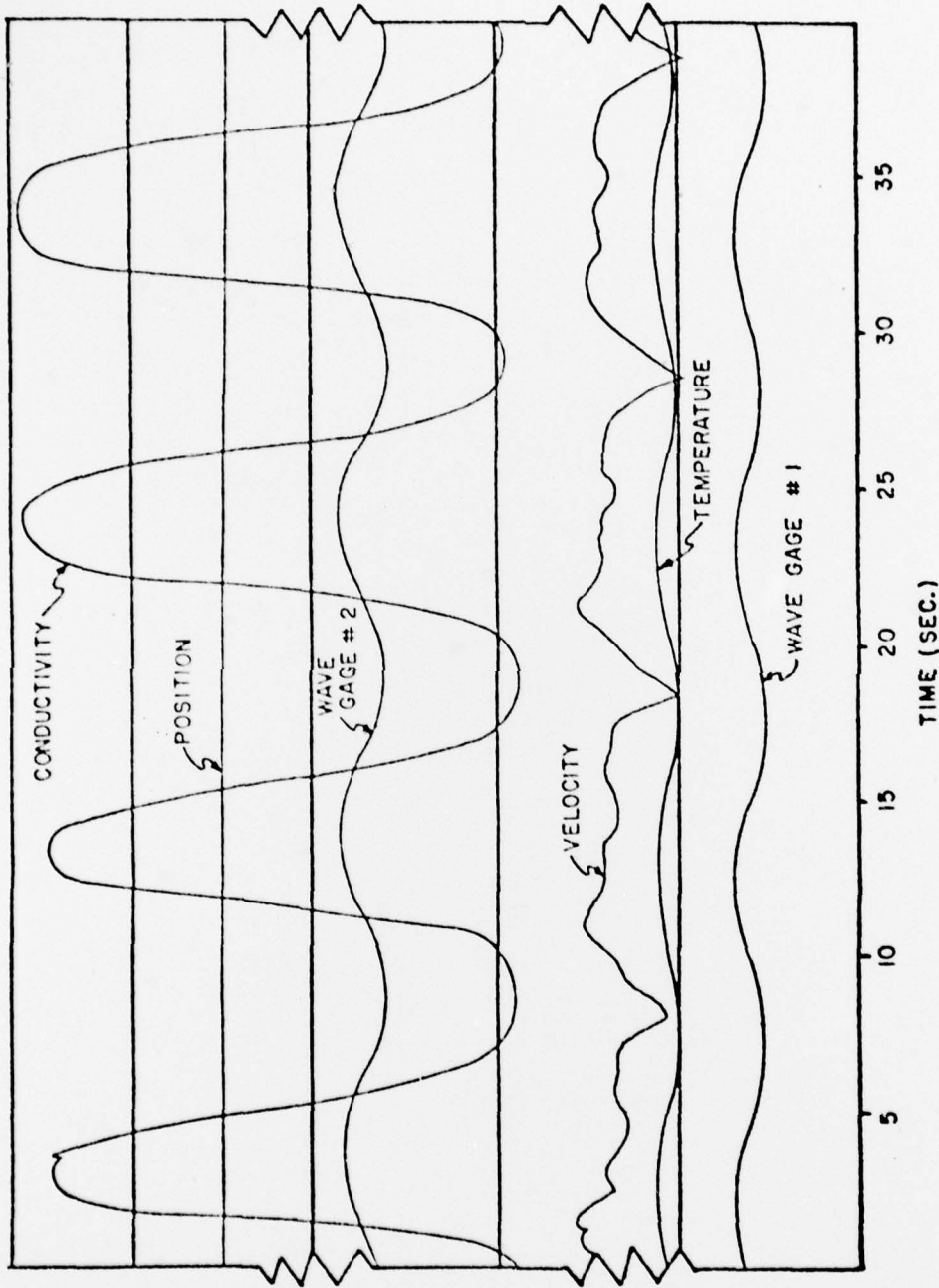


Figure 73. Visicorder Chart Paper, Run #4

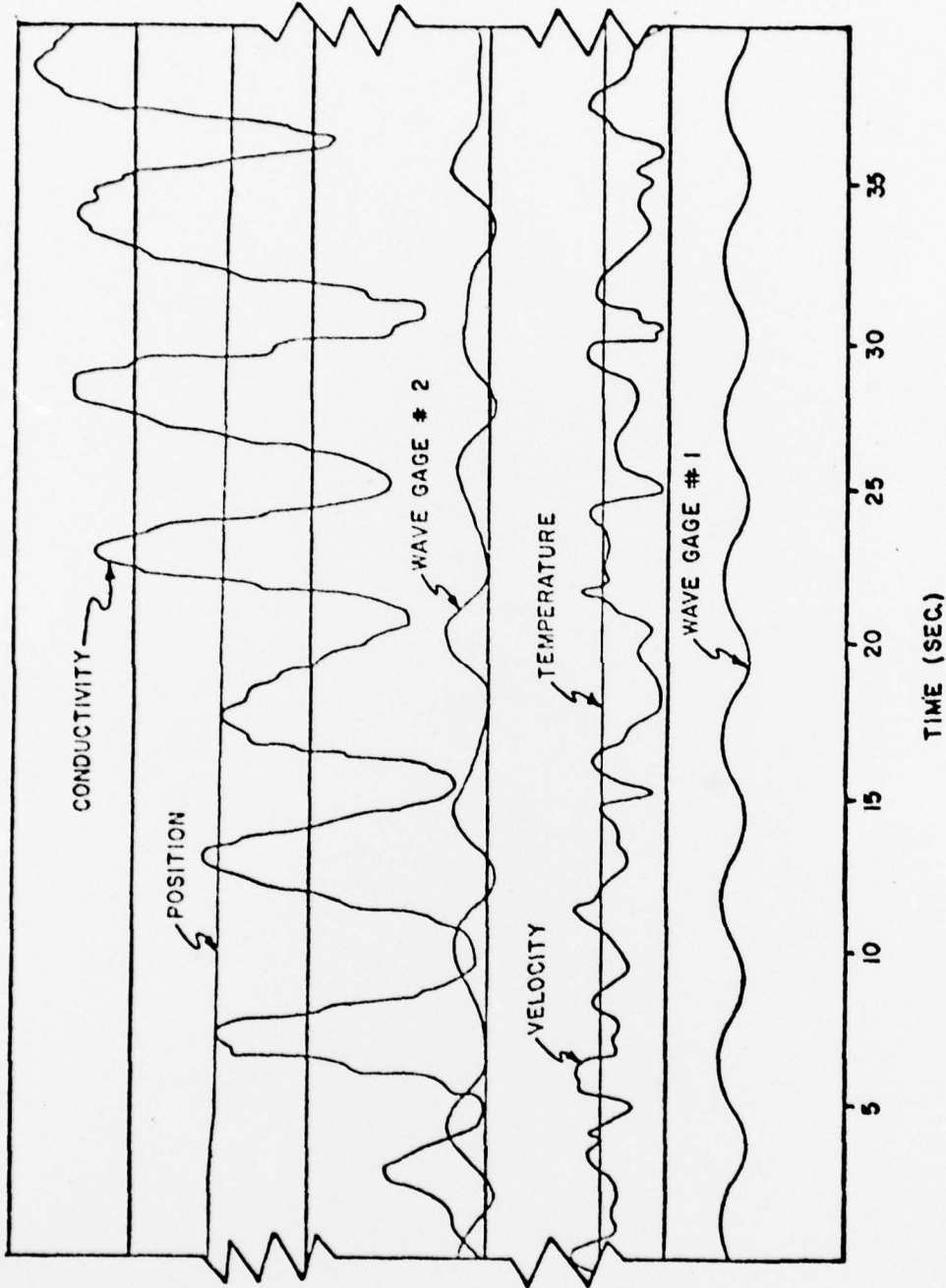


Figure 74. Visicorder Chart Paper, Run #11

BIBLIOGRAPHY

- Benjamin, T. Brooke, (1963), "The Threefold Classification of Unstable Disturbances in Flexible Surfaces Bounding Inviscid Flows," J. Fluid Mech., Vol. 16, Part 3, pp. 417 - 450.
- Browand, F.K. and C. D. Winant, (1973), "Laboratory Observations of Shear-Layer Instability in a Stratified Fluid," Boundary-Layer Meteorology, Vol. 5, pp. 67 - 77.
- Doddington, H.W. and D.M. Sheppard, (1974), "A Laboratory Instrument for Measuring Electrical Conductivity in Stratified NaCl Solution," Submitted to the Editorial Office of the Review of Scientific Instruments.
- Drazin, P.G. and L.N. Howard, (1966), "Hydrodynamic Stability of Parallel Flow of Inviscid Fluids," Trans. Amer. Soc. Civil Engineering, Vol. 128, pp. 849 - 869.
- Pao, Yih-Ho, (1969), "Spectra of Internal Waves and Turbulence in Stratified Fluid, 1. General Discussion and Indications from Measurements in Stably Stratified Atmosphere and Ocean," Radio Science, Vol. 4, Number 12, pp. 1315 - 1320.
- Phillips, O.M., (1969), The Dynamics of the Upper Ocean, Cambridge University Press.
- Powell, G.M. and D.M. Sheppard, (1974), "A Laboratory Optical Internal Wave Gage," College of Engineering, University of Florida, July, 1974.
- Scotti, R.S. and G.M. Corcos, (1972), "An Experiment on the Stability of Small Disturbances in a Stratified Free Shear Layer," J. Fluid Mech., Vol. 52, part 3, pp. 499 - 528.
- Sheppard, D.M., O. H. Shemdin, and Y.H. Wang, (1973), "A Multipurpose Internal Wave Facility," Department of Coastal and Oceanographic Engineering, Technical Report No. 19, University of Florida, June, 1973.
- Thorpe, S.A., (1973), "Experiments on Instability and Turbulence in a Stratified Shear Flow," J. Fluid Mech., Vol. 61, part 4, pp. 731 - 751.
- Turner, J.S., (1973), Buoyancy Effects in Fluids, Cambridge University Press.
- Wang, Y.H., (1972), "An Experimental Study of a Discontinuously Stratified Shear Layer," Ph.D. Dissertation, University of Southern California.
- Woods, J.D., (1968), "Wave-Induced Shear Instability in the Summer Thermocline," J. Fluid Mech., Vol. 32, part 4, pp. 791 - 800.

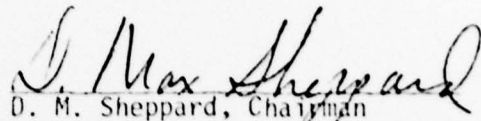
Woods, J.D., (1969), "On Richardson's Number as a Criterion for Laminar-Turbulent-Laminar Transition in the Ocean and Atmosphere," Radio Science, Volume 4, Number 12, pp. 1289 - 1298.

BIOGRAPHICAL SKETCH

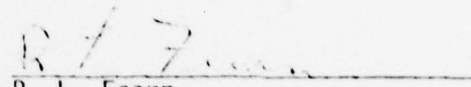
Ivan Bei Zu Chou was born November 18, 1948 in Hankow, China. In June, 1967, he graduated from Cheng Kuo High School in Taipei, Taiwan. He received the degree of Bachelor of Science with a major in River and Harbor Engineering from the Taiwan Provincial College of Marine and Oceanic Technology.

He came to the United States in August, 1973, to continue his studies at the University of Florida. He has worked as a graduate assistant while pursuing the degree of Master of Engineering in the field of Coastal and Oceanographic Engineering.

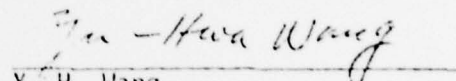
I certify that I have read this study and that in my opinion it conforms to acceptable standards of scholarly presentation and is fully adequate, in scope and quality, as a thesis for the degree of Master of Engineering.


D. M. Sheppard, Chairman
Assistant Professor of
Engineering Sciences

I certify that I have read this study and that in my opinion it conforms to acceptable standards of scholarly presentation and is fully adequate, in scope and quality, as a thesis for the degree of Master of Engineering.


R. L. Fearn
Assistant Professor of
Engineering Sciences

I certify that I have read this study and that in my opinion it conforms to acceptable standards of scholarly presentation and is fully adequate, in scope and quality, as a thesis for the degree of Master of Engineering.


Y. H. Wang
Assistant Professor of
Engineering Sciences

This thesis was submitted to the Dean of the College of Engineering and to the Graduate Council, and was accepted as partial fulfillment of the requirements for the degree of Master of Engineering.

March, 1975

Dean, College of Engineering

Dean, Graduate School